Technische Universität München

Max-Planck-Institut für Biochemie

Abteilung Strukturforschung

Biologische NMR-Arbeitsgruppe

Molecular architecture of Spire-actin complexes and its implication for actin filament assembly

Anna Magdalena Ducka

Vollständiger Abdruck der von der Fakultät für Chemie der Technischen Universität München zur Erlangung des akademischen Grades eines

Doktors der Naturwissenschaften

genehmigten Dissertation.

Vorsitzender: Univ.-Prof. Dr. M. Groll

Prüfer der Dissertation: 1. apl. Prof. Dr. Dr. h.c. R. Huber, i. R.

2. Univ.-Prof. Dr. J. Buchner

Die Dissertation wurde am 15.06.2011 bei der Technischen Universität München eingereicht und durch die Fakultät für Chemie am 29.07.2011 angenommen.

To my Family and Friends

“The important thing is not to stop questioning.
Curiosity has its own reason for existing…”

A. Einstein

Acknowledgements

I would like to thank everyone who contributed to this work.

First of all, I would like to thank my supervisor Dr. Tad Holak, for giving me the opportunity to work in his group, interesting discussions and encouragement.

I am grateful to Professor Robert Huber for his precious advices and for being my "Doktorvater".

I would like to express my gratitude to my labmates, for creating a friendly atmosphere. Especially to Linda, Weronika and Michal, for all their friendship and help.

My special thanks go to Steffi and her family for their kindness, friendship and all wonderful moments spent together.

I am indebted to my family, for their love, constant support, motivation and understanding.

Most importantly, I would like to thank my husband Tomek, who helped me to complete this thesis, for his love, patience and care. Thank you…

Publications

Ducka AM, Joel P, Popowicz GM, Trybus KM, Schleicher M, Noegel AA, Huber R, Holak TA and Sitar T (2010) Structures of actin-bound Wiskott-Aldrich syndrome protein homology 2 (WH2) domains of Spire and the implication for filament nucleation. *Proc. Natl. Acad. Sci. USA* 107:11757-11762.

Sitar T, Gallinger J, **Ducka AM**, Ikonen T, Wohlhoefler M, Schmoller KM, Bausch AR, Joel P, Trybus KM, Noegel AA, Schleicher M, Huber R and Holak TA (2011) Molecular architecture of the Spire-actin nucleus and its implication for actin filament assembly. Manuscript under preparation.

Contents

1 Introduction

1.1 The cytoskeleton

The living cell is an incredibly complex system with the ability to organize itself in space and time. The organization of the cells is maintained by a three-dimensional network of fibrous structures known as cytoskeleton. It was thought that cytoskeleton is unique to eukaryotic cells, but recent research has identified an equivalent in prokaryotic organisms (Michie and Löwe, 2006; Shih and Rothfield, 2006).

The cytoskeleton plays a crucial role in many cellular processes such as: spatial organization of the cell content, connection of the cell, both physically and chemically to the external environment, and coordination of the movement and shape changing. It is a dynamic entity with some cytoskeletal components being assembled and disassembled to meet the changing needs of the cell.

In eukaryotic cells, various functions of the cytoskeleton are dependent on three families of filamentous assemblies, which are: actin filaments, microtubules and a group of polymers known collectively as intermediate filaments. Together, these polymers control the shape and mechanics of eukaryotic cells. All three are organized into networks that resist deformation but can reorganize in response to externally applied forces, and they have important roles in arranging and maintaining the integrity of intracellular compartments. Those three components are present in various proportions and geometry. Actin filaments provide mechanical structure and motility for amoeboid and animal cells. Microtubules are responsible for separating chromosomes and long range transport of large particles in all eukaryotes. Intermediate filaments in vertebrates function as intracellular ligaments and tendons to resist mechanical forces.

1.1.1 Actin

Actin is the most abundant intracellular protein in a eukaryotic cell. It was discovered together with myosin in 1940s by Straub (Straub, 1942). In muscle cells actin comprises about 20 percent of the total mass of cell protein; even in

non-muscle cells, actin makes up 1-5 percent of the cellular proteins (Holmes, 2009; Pollard and Borisy, 2003). A typical cytosolic concentration of actin in non-muscle cells is 0.5 mM; in special structures like microvilli, however, the local actin concentration can be tenfold higher. For comparison, a typical liver cell which has about 20,000 insulin receptor molecules, contains approximately half a billion (0.5×10^9) actin molecules (Lodish et al., 2000). This predominance of actin compared with other cell proteins is a common feature of all cytoskeletal proteins. Actin together with actin-binding proteins form structures that cover large spaces in a cell. Therefore these proteins are among the most abundant proteins in a cell.

Actin is a moderate-sized (41-42 kDa) protein consisting of approximately 375 residues, encoded by a large, highly conserved gene family. Some single-celled eukaryotes, like yeasts and amoebas, have a single actin gene, whereas many multicellular organisms contain multiple actin genes. For instance, humans have six actin genes, which encode isoforms of the protein, and some plants have as many as 60. Sequencing of these actins has revealed that they are one of the most conserved proteins in a cell, comparable with histones, the structural proteins of chromatin. Actin residues from amoebas and from animals are identical at 80 percent of the positions. In vertebrates three isoforms of actin called α-, β-, and γ- exist in various types of cells. Four α-actin isoforms present in various muscle cells and the β- and γ-actin isoforms present in non-muscle cells differ at only four or five positions. Although these differences among isoforms seem minor, the isoforms have different functions: α-actin is associated with contractile structures, and β-actin is at the front of the cell where actin filaments polymerize (Lodish et al., 2000).

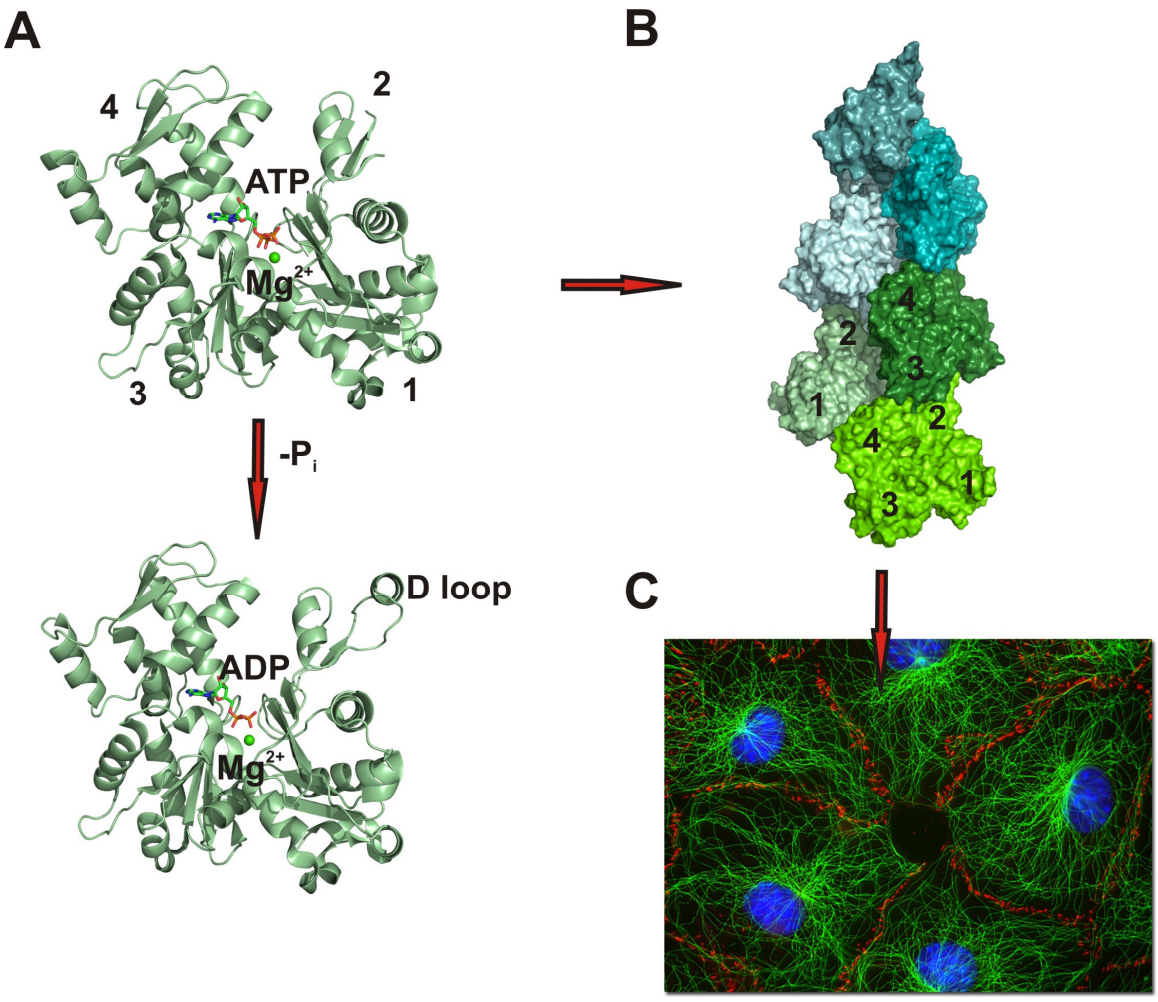

Figure 1.1 Structure of actin. (A) Ribbon representation of monomeric actin in ATP and ADP states. Subdomains of actin are marked with numbers from 1-4, ATP and ADP molecules are in stick representation, magnesium ion is presented as a ball (PDB: ATP actin-1NWK, ADP actin-1J6Z). (B) Filamentous actin (PDB: 2Y83). The subdomain orientation within the filament is shown with numbers. (C) Fluorescently labeled mouse fibroblasts showing actin cytoskeleton (green) (Jan Schmoranzer, Columbia University, New York, USA).

G-actin

Actin exists as a globular monomer called G-actin and as a filamentous polymer called F-actin, which is a linear chain of G-actin subunits. Each actin molecule contains a Mg^{2+} ion complexed with either ATP or ADP. Thus there are four states of actin: ATP-G-actin, ADP-G-actin, ATP-F-actin, and ADP-F-actin. Two of these forms, ATP-G-actin and ADP-F-actin, predominate in a cell. Although G-actin appears globular in the electron microscope, X-ray crystallographic analysis reveals that it is separated into two lobes by a deep cleft (Figure 1.1A). The lobes and the cleft compose the ATPase fold, the site where ATP and Mg^{2+} are bound. In actin, the floor of the cleft acts as a hinge that allows the lobes to flex relative to each other. When ATP or ADP is bound to G-actin, the nucleotide affects the conformation of the molecule. In fact, without a bound nucleotide, G-actin denatures very quickly.

Actin and most members of its structural class, which include the hsp70 molecular chaperones, hexokinase, and the sugar kinases (Kabsch and Holmes, 1995; Hurley, 1996), appear to undergo a conformational change coupled to ATP hydrolysis. The structure and properties of the actin in the cytoskeleton are regulated by ATP hydrolysis within the well-defined nucleotide-binding pocket of individual actin monomers (Reisler and Egelman, 2007). ATP hydrolysis proceeds via a fast reaction step leading to the formation of ADP and bound phosphate (Pi). The ADP-Pi phase of actin is long-lived due to the slow release time of the Pi group (Carlier and Pantaloni, 1986). ATP hydrolysis leads to “softening” of actin filaments and preferential binding of depolymerization factors (Pollard, 1986; Isambert et al., 1995; Chu and Voth, 2005). There is a substantial correlation between the properties of actin and the state of the bound nucleotide. Considerable research has therefore been devoted to quantifying the link between the state of the bound nucleotide and the structure of actin monomers (Otterbein et al., 2001; Chu and Voth, 2005; Rould et al., 2006; Zheng et al., 2007). The hypothesis proposed by Otterbein et al. (2001) concerns the relationship between the actin structure and the state of the bound nucleotide. Actin monomers with bound ADP and labeled with tetramethylrhodamine (TMR)

were found to adopt an α-helical conformation in residues 40-48, i.e., the so-called DNase-I binding loop (DB loop), whereas this region is disordered in the ATP-bound actin (Otterbein et al., 2001). This finding led to the proposal that the DB loop folds on ATP hydrolysis. A more recent study has argued that there are no large conformational changes or domain shifts when ATP and ADP are bound to G-actin based upon the comparison of crystal structures for these two states (Rould et al., 2006). Because solution data from the same work show a very large difference in the subtilisin digestion rates between ADP-G-actin and ATP-G-actin (Rould et al., 2006), it is possible that crystal packing interactions favor a closed state of G-actin even though in solution the state of the cleft may be shifted by the bound nucleotide. This type of conclusion appeared in another recent study of actin crystal structure (Klenchin et al., 2006), which showed that cleavage of the DNase I-binding loop introduces no significant changes in the crystal structure of G-actin, whereas complementary solution studies suggested that the cleavage is associated with an opening of the nucleotide-binding cleft. The origin of nucleotide-dependent properties might lie in a controlled opening of the binding cleft itself. This view is also supported by a study by Belmont et al., (1999) and the proposed γ-phosphate timing mechanism is related to kinesins and G proteins in general (Sablin et al., 1996; Vale, 1996). Analysis of multiple Arp2 (actin-related protein-2), Arp3, and actin crystal structures with different bound nucleotides also demonstrated that there are "inconsistencies" between the structures observed and simple nucleotide-dependent states (Nolen and Pollard, 2007), suggesting that "alternative conformations have similar energies and are readily interconverted." Such a possibility is also advanced by a recent molecular dynamics study of nucleotide-dependent states of G-actin, which favors the helix-coil transition in the DNase I-binding loop (Zheng et al., 2007).

F-actin

Actin continuously cycles through the processes of polymerization and depolymerization in the cytoplasm. In vitro, the addition of ions: Mg^{2+}, K^{+}, or Na^{+} to a solution of G-actin will induce the polymerization of G-actin into F-actin

filaments. The process is also reversible: F-actin depolymerizes into G-actin when the ionic strength of the solution is lowered. The F-actin filaments formed in vitro are indistinguishable from microfilaments isolated from cells. The assembly of G-actin into F-actin is accompanied by the hydrolysis of ATP to ADP and P_i; however, the ATP hydrolysis affects the kinetics of polymerization but is not necessary for polymerization to occur.

Actin filaments contain two ends, termed the “pointed end” and the “barbed end”. Each end has distinct properties. The polarity of the actin filament controls the actin dynamics in the cell where elongation of the filament by polymerization occurs at the barbed end, and shortening by depolymerization occurs at the pointed end. In vitro, the actin filament, without any binding proteins, elongates at the barbed end and shortens at the pointed end in the steady state with ATP and magnesium ions, inducing a so-called “treadmilling” movement (Wegner, 1976; Korn et al., 1987; Bugyi and Carlier, 2010). This suggests that the evolutionary origin of the direction of polymerization and depolymerization in the cell is an intrinsic property of the actin filament.

The most significant difference between the two ends of the actin filament that occurs during these dynamics is that the polymerization rate and the depolymerization rate at the pointed end are much slower than at the barbed end. This largely affects all actin dynamics and likely explains why the barbed end is used for rapid polymerization in the cell. The mechanism underlying this difference is unclear, despite intensive studies of actin dynamics at both ends (Coue and Korn, 1985; Carlier et al., 1986; Pollard, 1986; Fujiwara et al., 2007).

The first model of the F-actin structure, reported in 1963, was a two-stranded helical polymer (Hanson and Lowy, 1963). The crystal structure of G-actin was solved in 1990, and an atomic model for the F-actin structure was also proposed at the same time, based on an X-ray fiber diffraction pattern to 8 Å (Holmes et al., 1990; Kabsch et al., 1990; Holmes, 2010). The model has been widely accepted as an approximate low-resolution structure. However, the conformational changes that occur at the G- to F-actin transition and the accompanying activation of the ATPase have remained elusive. The model was

consistent with many biochemical results, but it provided a limited account of actin's function, because the structures of the monomers were stacked on top of each other without any conformational alterations. Oda et al. (2009) describes a new high-resolution model for the F-actin structure (Figure 1.1B), based on the X-ray fiber diffraction data to 3.3 Å in the radial direction and 5.6 Å along the equator (the initial Holmes´ atomic models were based on fiber diffraction patterns with low resolution up to about 8 Å). The new model reveals that that the essential difference between G-actin and F-actin is the relative rotation of the two major domains by about 20°, which gives the F-actin subunit a flat conformation. A second difference is the conformation of the DNase-I binding loop (D-loop) in subdomain 2 (Figure 1.1A), which adopts an open loop conformation (Oda et al., 2009). There are no other large-scale differences. The flat conformation is also observed in the polymer of MreB, the bacterial actin homologue, and thus it seems to be a common characteristic of polymers among actin homologues (van den Ent et al., 2001). Quite recently, a density map of F-actin at about 7 Å resolution was obtained using electron cryomicroscopy and image analysis, and the model fitted to the density basically confirmed the flattening of the F-actin subunit, although the conformations of some loops in the actin molecule were different (Fujii et al., 2010).

1.1.2 The organization and functions of actin cytoskeleton

The intrinsic difference of the filament pointed and barbed ends significantly affects all actin dynamics in the cell. Actin filaments - compared to microtubules - are much less rigid, but the presence of high concentrations of crosslinking proteins that bind to actin filaments promotes the assembly of highly organized, stiff structures: bundled or branched networks (Fletcher and Mullins, 2010). They constitute major components of a broad variety of higher cellular structures, such as filopodia, lamellipodia or actin stress fibers. Actin filaments elongate steadily in the presence of nucleotide-bound monomers producing the sustained forces that are required to advance the leading edge of a migrating cell (Pollard and Borisy, 2003). The actin cytoskeleton is continually assembled and

disassembled in response to the intra- and extracellular stimuli. Assembly, organization and turn-over of filamentous actin structures are crucial for life, because these processes promote many cellular functions as well as ensure tissue integrity.

Actin filaments are major determinants of cell morphology and adhesion site formation in multicellular organisms. Bundles of aligned filaments support filopodial protrusions, which are involved in chemotaxis and communication between cells. The other type of networks, highly branched filaments, support the leading edge of most motile cells and generate the forces involved in changes of cell shape, for example, during phagocytosis. Protrusive, branched actin-filament networks, such as those in crawling leukocytes, are assembled at the leading edge of the cell in response to signals downstream of cell-surface receptors (Parent, 2004).

The cortical actin cytoskeleton plays important roles in shaping the morphology of cells and of defined membrane areas**.** The assembly of contractile actin-filament bundles known as stress fibers, such as those in adherent fibroblasts, is triggered locally when cell-surface adhesion receptors (integrins) interact with their ligands (Naumanen et al., 2008). Contractile and protrusive forces are generated by the actin cytoskeleton associated with the plasma membrane. Actin filaments assemble at sites of plasma membrane internalization in budding and fission yeast (Kaksonen et al., 2006; Galletta and Cooper, 2009). In these “actin patches,” filaments assemble de novo, provide force to form and internalize an endocytic vesicle from the plasma membrane, and then disassemble in a process that is self-limited in space and time. Actin is associated with endocytosis in many cells besides yeast, with an apparently similar set of molecular players (Doherty McMahon, 2009).

Actin filaments are essential for cell locomotion, a defining feature of animal cells (Ridley et al., 2003). For example, cells of the immune system migrate to search and destroy pathogens or cancer cells. Assembly of actin filaments from their monomeric subunits can suffice to change the shape of the cell and produce a protrusion, which is often the first step in cell locomotion. The

Arp2/3 complex assembles a dense network of short, branched actin filaments. Each filament can produce piconewton forces (Kovar and Pollard, 2004), allowing the front end of cells to move at rates up to about 1 mm per second (Svitkina et al., 1997).

Actin microfilaments provide the “rails” along which myosin “motors” perform work in a variety of cellular functions. All eukaryotic cells use them to transport organelles along actin filaments. Microfilaments cooperate with microtubules via microtubule-associated proteins (MAPs) during the transport of vesicles and organelles (Svitkina et al., 1997). Actin filaments also interact with intermediate filaments, a function that may play an important role in enabling extracellular stimuli to be transmitted to key targets like ribosomes and chromosomes deep within the cell.

Actin cytoskeleton is also involved: in the plasticity of memory (dendritic spine structure) (Hotulainen and Hoogenraad, 2010); in the stereocillia that are crucial in the transduction of sound or motion into the electrical signals (Manor and Kachar, 2008); in cell movement, including infiltration and metastasis of cancer cells (Condeelis et al., 2001; Lai et al., 2008); and in the extension of the pollen tube (Chen et al., 2009).

1.1.3 Actin binding proteins

The dynamics of the actin cytoskeleton is regulated at multiple levels by a variety of proteins. So far, more than 150 proteins have been found to contain binding domains for actin (dos Remedios et al., 2003; Fletcher and Mullins, 2010). These proteins accomplish diverse functions and can be divided into several groups (Figure 1.2) (Pollard and Borisy, 2003; Rafelski and Theriot, 2004; Zigmond, 2004; Winder and Ayscough, 2005; Lee and Dominquez, 2010), as follows:

- monomer binders
- barbed- and pointed-end capping proteins
- severing proteins
- cross linkers and bundlers

- cytoskeletal linkers
- proteins anchoring actin cytoskeleton to membranes and membrane proteins
- myosins
- rulers and stabilizers
- sidebinders and signalers
- branch formation proteins

Many actin binding proteins cannot be simply assigned to one group because of their diversity and multiplicity of cellular functions. From the structural point of view actin binding proteins (which can bind G- F-actin or both) belong to a limited number of folds, including the actin depolymerizing-factor/cofilin (ADF/cofilin) (Lappalainen et al., 1998), Wiskott-Aldrich syndrome protein (WASP)-homology domain 2 (WH2) (Paunola et al., 2002), gelsolin-homology domain (McGough et al., 2003), calponin homology (CH) domain (Gimona et al., 2003), formin homology 2 domain (FH) (Goode and Eck, 2007). Many proteins bind F-actin, and use the actin filaments as a scaffold for their activities. For example, the myosin superfamily, which are molecular motors, use F-actin as a track for motility (Sellers, 2000).

Actin monomer-binding proteins

Despite the large number of actin-monomer-binding proteins, only six evolutionarily and functionally distinct classes of actin-monomer-binding proteins have been identified in organisms from yeast to animals: profilin, actin-depolymerizing factor (ADF)/cofilin, twinfilin, Srv2/cyclase-associated protein (CAP), Wiskott–Aldrich syndrome protein (WASP)/WASP, family verprolin homologous (WAVE) protein and verprolin/WASP-interacting protein (WIP) family proteins. Three of these – ADF/cofilin, profilin and Srv2/CAP – have also been identified in plants (Hussey et al., 2002).

Actin monomer binding proteins are involved in many processes including binding to ADP-actin as it is released from filament ends (e.g. twinfilin, ADF/cofilin), facilitating the nucleotide exchange of ADP for ATP (e.g. profilin and

CAP) and delivering the monomer to barbed ends (to Arp2/3 or formins) to facilitate new rounds of polymerization (e.g. twinfilin, Srv2/CAP, profilin, verprolin/WIP and WASP). As well as promoting polymerization of existing filaments, monomer-binding proteins are involved in nucleating the formation of filaments de novo (formins and Spire) and from the side of existing filaments (Arp2/3) (see Chapter 1.2).

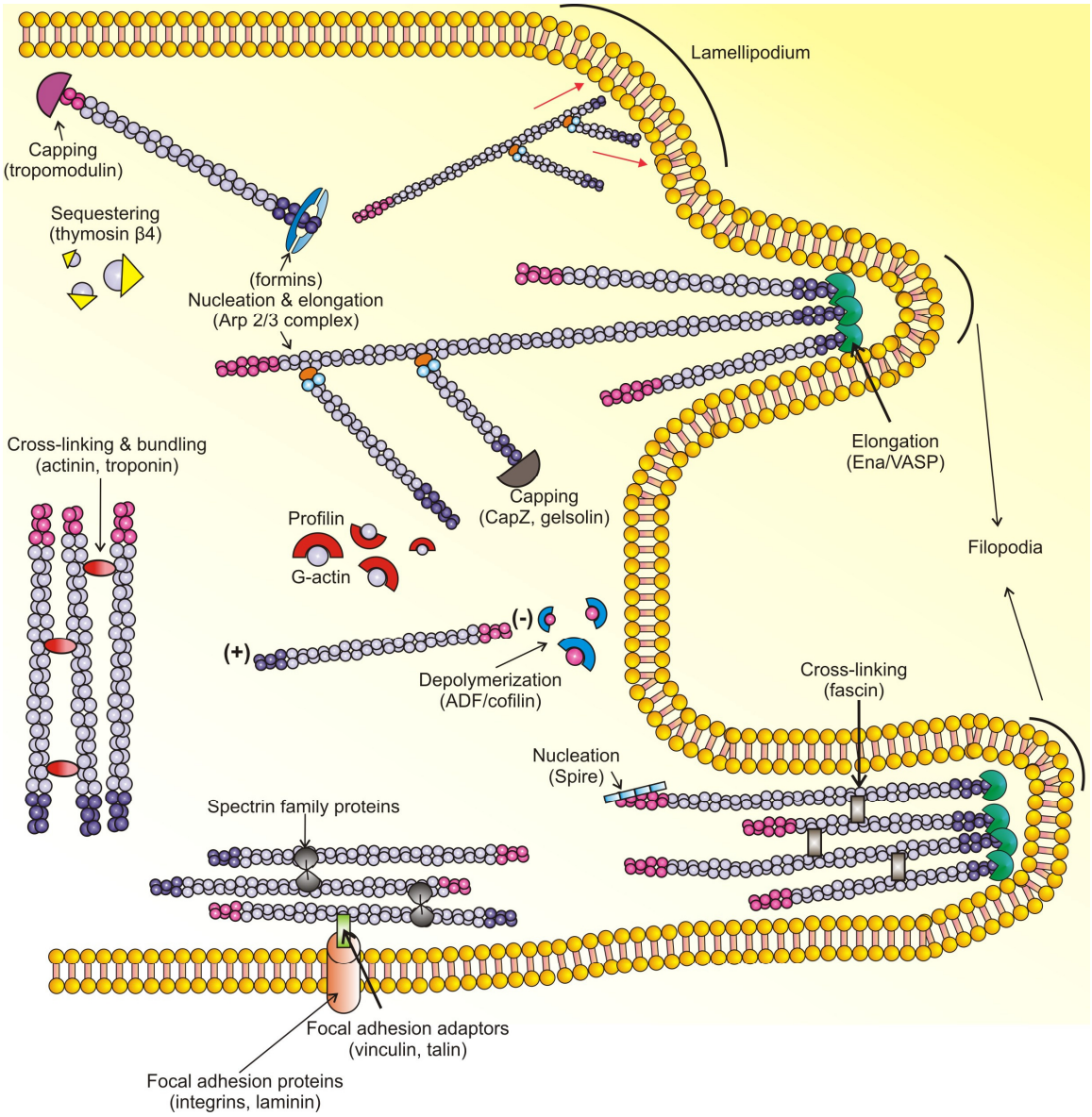

Figure 1.2 Classification of actin-binding proteins.

Proteins that bind the actin monomer play a critical role in controlling the pool of unpolymerized actin in cells, by sequestering actin monomers and thereby modulating the pointed and barbed ends addition/dissociation of actin monomers. The most abundant actin monomer-binding proteins in vertebrate cells are profilin, (ADF)/cofilin and thymosin-β4.

Profilin is a small, highly conserved protein that binds with high affinity to monomeric actin and functions at the center of dynamic actin assembly (Carlsson et al., 1977). Profilin binding to G-actin, prevents spontaneous nucleation of new actin filaments, and suppresses assembly at the pointed end of a filament. When filament ends are capped, then profilin maintains the pool of unpolymerized actin. Profilin plays also a role in adding ATP-actin monomers to the growing end of the filament (Tilney et al., 1983; Pring et al., 1992; Pantaloni and Carlier, 1993).

Actin-depolymerizing factor (ADF)/cofilin family members cooperate with profilin to enhance the flux of subunits through filaments by up to 75-fold (Blanchoin and Pollard, 1998; Didry et al., 1998). ADF/cofilin: increases the dissociation rate of actin subunits from the pointed end of filaments, creates new filament ends by severing, increases the rate of phosphate release following actin polymerization.

Thymosin-β4 forms a 1:1 complex with actin monomers and it binds ATP-actin monomers with a 100-fold higher affinity than ADP-actin monomers. Thymosin-β4 prevents actin polymerization and its high cellular concentration allows it to maintain the large unpolymerized actin monomer pool in the cytoplasm. Although actin bound to thymosin-β4 does not polymerize, proflin can compete with thymosin-β4 for actin-binding and may release the actin monomer from thymosin-β4 onto the barbed end of the actin filament (Krishnan et al., 2009).

Capping proteins

After nucleation actin filaments grow rapidly by addition of monomers at their barbed ends. Filament length is controlled by capping proteins. For example, barbed end capping proteins (gelsolin and tensin) inhibit addition of

new monomers, so acting to decrease the overall length of the filament. Additionaly, gelsolin can sever actin filaments, thereby rapidly increasing actin dynamics (Burtnick et al., 2004). Depending on the environment in the cell this can have various outcomes, but it is usually a mechanism to disassemble F-actin containing structures. Pointed end cappers, by contrast, reduce loss of monomer from the pointed end and thereby can lead to rapid filament extension (Winder and Ayscough, 2005).

Actin filament crosslinking proteins

The arrangement of actin filaments is mediated by proteins containing multiple actin-binding domains, but in general the two domains are separated by longer, more flexible spacer regions, which allow a more perpendicular arrangement of actin filaments (Winder, 2003). Spectrin-family proteins, including α-actinin, tetrameric spectrins, and dystrophin, are the most important group of proteins involved in crosslinking actin filaments, both among them and with cellular organelles and membranes (Broderick and Winder, 2005). Crosslinking is also achieved by small monomeric proteins, such as transgelin, which under certain conditions organizes actin filaments into dense mesh works. These proteins are predominantly localized to the submembrane cytoskeleton, such as the leading edge and focal contacts of migrating cells (Blanchard et al., 1989; Otto, 1994; Pascual et al., 1997; Knight et al., 2000). Actin crosslinking proteins frequently function as molecular scaffolds, connecting actin filament networks to extracellular matrix proteins, such as ankyrin, laminin and dystroglycan (Campbell and Kahl, 1989; Kennedy et al., 1991; Bennett and Baines, 2001; Rando, 2001).

Cytoskeletal linkers and membrane anchors

Several actin binding proteins are involved in connecting actin cytoskeleton to membranes or membrane proteins as well as to different cytoskeletal elements. First group of proteins, such as dystrophin and utrophin or talin and vinculin, connect the actin cytoskeleton to the cell adhesion receptors:

dystroglycans or integrins, respectively. The second group, such as annexins, can bind directly to membranes and also interact with actin. The latter category comprises a small but important group of proteins that can link actin to microtubules, actin to intermediate filaments or, in the case of plectin, actin to both microtubules and intermediate filaments. These proteins are important for the integration of structure and signaling between the cytoskeletal elements and the maintenance of cell integrity.

Myosins

Myosins are molecular motors that produce movement and force through the hydrolysis of ATP. These proteins use actin filaments as a track along which they move, exclusively from the pointed to the barbed end of the filament, with specific cargo such as membranes, vesicles, actin filaments. There are over 17 different classes of myosins identified until now with various functions (Hodge and Cope, 2000).

Ena/VASP and filament elongation

The Ena/VASP proteins are the WH2-based, filament elongation factors, implicated in multiple cellular functions such as axon guidance and the migration of cancer cells (Brindle et al., 1996). These proteins form tetramers through their C-terminal coiled coil (C-C) domains (Bachmann et al., 1999; Kuhnel et al., 2004), and are thought to bind to the barbed ends of actin filament bundles (multiple parallel filaments), catalyzing their synchronized elongation against the plasma membrane (Brindle et al., 1996; Krause et al., 2003, 2004). In this way, the filament bundles grow to form cellular structures such as filopodia, which are actin-rich finger-like projections used by cells to sense the environment (Mattila and Lappalainen, 2008).

1.2 Actin-nucleating proteins

The actin filament is a helical, polarized polymer (with the fast- and slow-growing ends) in which each actin subunit makes two longitudinal and two lateral bonds with its neighbors. The formation of actin filament requires a nucleation step followed by elongation.The first step in the assembly of actin filaments is nucleation – the formation of a stable dimers and trimers of actin monomers (Sept and McCammon, 2001; Chesarone and Goode, 2009). The nucleus is defined as the shortest actin oligomer that exposes an elongating site identical to the filament elongating site (Renault et al., 2008). Instability of the actin multimers is the rate-limiting step in actin filaments assembly. To overcome this kinetic barrier, as well as the activity of sequestering proteins, cells developed diverse mechanisms of nucleation driven by sets of actin nucleating proteins.

Actin nucleators function according to one of three different mechanisms (Chesarone and Goode, 2009):

- structural mimicry of polymerization intermediates,
- stabilization of spontaneously formed intermediates
- recruitment and alignment of actin monomers to form a polymerization “seed”.

Three classes of actin nucleation proteins, utilizing all three mechanisms mentioned above, have been identified until today: the Arp2/3 complex together with newly recognized nucleation-promoting factors such as WASH, WHAMM and JMY (Mullins and Pollard,1999; Campellone et al., 2008; Liu et al. 2009; Zuchero et al., 2009; Campellone and Welch, 2010), formins (Evangelista et al., 2002; Evangelista et al., 2003; Sagot et al., 2002; Xu et al., 2004) and the third group of proteins commonly named tandem-monomer-binding nucleators (Quinlan et al., 2005; Bosch et al., 2007; Qualmann and Kessels, 2009; Firat-Karalar and Welch, 2011) (Figure 1.3).

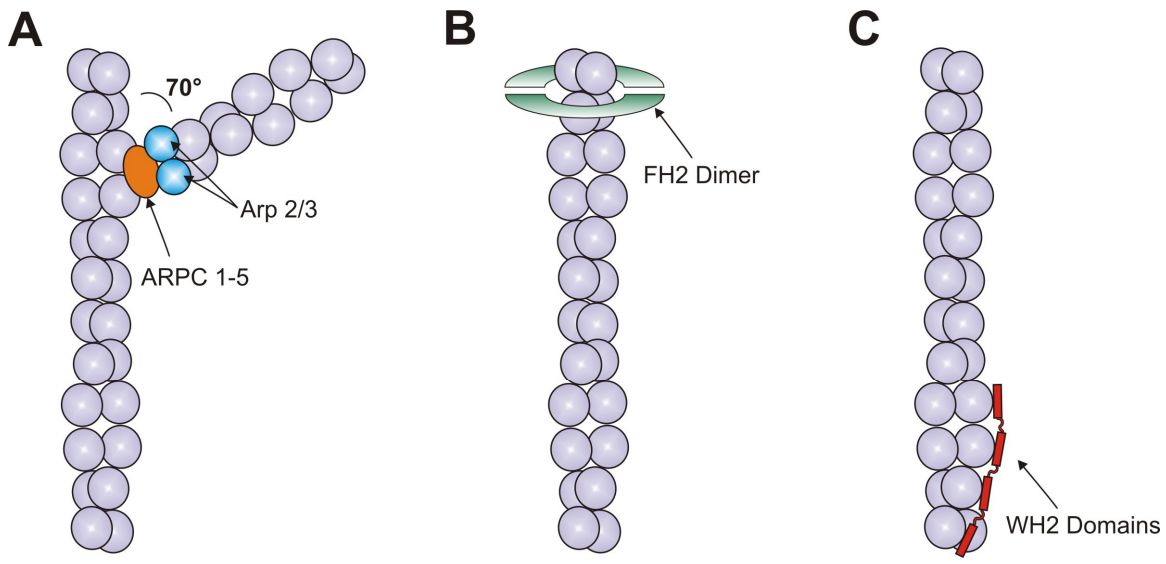

Figure 1.3 Actin nucleating proteins. (A) Arp 2/3 is a complex of seven proteins. (B) Formins. (C) The WH2 domain-based nucleator – Spire.

1.2.1 Arp2/3

The Arp2/3 was the first and for a long time the only known cellular actin nucleator. The macromolecular complex consists of seven subunits: two actin-related proteins, Arp2 and Arp3, which in inactive states are stabilized by five other subunits (Robinson et al., 2001). The accepted nomenclature for these subunits is ARPC1 (for the 40-kDa subunit), ARPC2 (35-kDa subunit), ARPC3 (21-kDa subunit), ARPC4 (20-kDa subunit), and ARPC5 (16-kDa subunit) (Pollard, 2007). All subunits are expressed in metazoans, fungi, amoebae and plants (Beltzner and Pollard, 2004) but they are absent in genomes of algae, microsporidia, or apicomplexa (Muller et al., 2005).

Arp2/3 has a low nucleating activity by itself, this is why it requires nucleation promoting factors (NPFs) (Welch and Mullins, 2002). NPFs are members of the WASP/WAVE family of proteins consisting of WASP, N-WASP, the Scar/WAVE proteins, WASH and WHAMM (Goley and Welch, 2006; Pollard, 2007; Chesarone and Goode, 2009). These proteins recruit one to three actin subunits and promote a conformational change within the Arp2/3 complex. NPFs

are themselves regulated by various factors, in particular the Rho-family GTPases.

This nucleator acts by serving as a template for monomer addition by mimicking the barbed end of a growing filament. Arp2/3 complex initiates branching of actin filaments on the sides of already existing ones (Figure 1.3A). It anchors the pointed end of the daughter filament at an angle of 70° to the mother filament as the free barbed end of the daughter grows away from the complex (Mullins et al., 1998).

Recent model, obtained by docking crystal structure of an inactive Arp 2/3 complex into 3D reconstruction of the branch obtained by electron tomography, revealed that Arp2 and Arp3 interact with the pointed end of the daughter filament, while ARPC2 and ARPC4 stay in contact with the mother filament (Rouiller et al., 2008). In motile cells the Arp2/3 complex generates a network of branched actin filaments. The tips of the branches push the cell membrane forward to protrude a pseudopod (Pollard and Borisy, 2003).

1.2.2 Formins

The second class of actin-nucleating proteins are the formins (Pruyne et al., 2002; Sagot et al., 2002). These large modular proteins are highly conserved in eukaryotes with a great diversity in plants (21 in Arabidopsis thaliana) and vertebrates (15 in the mouse genome). Metazoan formins have been divided into seven subgroups: Dia, FRL, DAAM, Delphilin, INF, FHOD and Fmn. Excluding their common C-terminal FH1 and FH2 domains, they differ substantially in their N-terminal parts (Higgs et al., 2005). Formins mediate assembly of unbranched filaments in a wide range of cellular processes including filopodia, stress fibers, and actin cables formation.

Bni1, yeast homologue formin, was first recognized to effect actin polymerization (Evangelista et al., 1997). At the same time Rho GTPases were identified as activators of the formin function (Watanabe et al., 1997).

Formins are unique among actin nucleators. They use the formin homology domain 2 (FH2) for interaction with actin (Figure 1.3B). The

homodimeric FH2 domain catalyzes nucleation by stabilizing actin dimer. Two rod-shaped domains of FH2 are connected in head-to-tail fashion by highly flexible linkers (Figure 1.3B) (Xu et al., 2004). The flexibility of the linkers and the ring-like overall structure suggest that FH2 subunits might move semi-independently. The “stair-stepping” mechanism mediates incorporation of actin monomers at the barbed end during processive actin filament elongation (Xu et al., 2004). Each of the FH2 domains binds actin monomer in such manner that the ring-shaped dimer of formin stabilizes a short pitch actin dimer, which constitutes a nucleus (Pruyne et al., 2002; Li and Higgs, 2003). After nucleation, the FH2 dimer remains associated with elongating barbed ends of actin filaments, protecting the filament from being capped and allowing it to grow. The crystallographic structure of FH2 of Bni1 formin with actin provided more data to support this proposed mechanism. In the structure, the asymmetric unit of the crystal contains only one FH2 domain with one actin bound. However, a C2 symmetry axis positions an identical FH2-actin complex at 28 Å rotated by 180° with respect to the reference complex and produces a ring-like structure, which provides a model for the formin-actin nucleus (Otomo et al., 2005).

1.2.3 WH2 domain-containing nucleators

The third group of the actin nucleating proteins consists of Spire (Quinlan et al., 2005), Cordon-bleu (Ahuja et al., 2007), Leiomodin from muscle cells (Chereau et al., 2008), JMY which also nucleates actin itself (Zuchero et al., 2009), recently discovered APC (adenomatous polypolis coli) (Okada et al., 2010), and bacterial VopL/VopF (Liverman et al., 2007; Tam et al., 2007). These proteins share the common capability, mediated by WH2 domains, to gather the actin monomers into the nucleation complex, but the arrangement of nuclei might vary significantly between various members of the class. WH2 (Wiskott - Aldrich Syndrome homology domain 2) domains have been found in >60 modular proteins (Qualmann and Kessels, 2009). It is a small (20–50 amino acids), highly abundant intrinsically disordered domain, which folds upon binding to the target protein: actin (Czisch et al., 1993; Paunola et al., 2002; Meszaros et al., 2007).

During actin binding, distinct WH2 domains fold and all bind actin in the same manner. The two main structural elements involved in the actin binding are: a conserved N-terminal amphipathic helix of variable length, and the C-terminal L++V/T motif. Binding of helix to the hydrophobic pocket between subdomains 1 and 3 of actin, accounts for most of the actin binding affinity (Chereau et al., 2005). Actin hydrophobic cleft is a binding site for a variety of actin-binding proteins (including actin itself) as well as actin-binding drugs (Hertzog et al., 2004; Irobi et al., 2004; Chereau et al., 2005; Dominguez, 2004). The leucine of the L++V/T motif is almost invariant and binds in a hydrophobic pocket of actin (Ile341+ Ile345). The basic central residues of the L++V/T motif are probably of high importance in the long-range recognition of an acidic patch on actin (Asp24+ Asp25), whereas the hydrophobic contacts of the leucine dominate interaction at close range (see Relults; Chereau et al., 2005) The fourth amino acid of the motif binds in a small pocket on the actin surface. Amino acids such as threonine, valine, alanine, and serine are the most often found at this fourth position of the motif. The remaining C-terminal part of the WH2 domain (with a variable sequence and length) extends along the nucleotide binding cleft of actin. In the case of β-thymosins, this extension is long, contains a second helix attaching to the pointed end surface of subdomain 2 and is important for the G-actin sequestration activity of β-thymosins (Hertzog et al., 2004). Other WH2 domains lack the C terminal extension completely and/or the extensions seem to follow slightly different paths on actin. It has been proposed that the C-terminal extension of the WH2 domain determines the functions, for example: actin sequestration (e.g. β-thymosins), promotion of actin filament elongation (e.g. Ena/VASP), promotion of actin filament nucleation (WASP family proteins and WH2-domain-containing nucleators) (Qualmann and Kessels, 2009).

1.3 Spire

Spire proteins have been found in all higher eukaryotic cells. Genetic studies identified Spire as an actin-binding factor required for the correct establishment of polarity axes of the oocyte in *Drosophila* (Manseau and Schupbach, 1989). In

Drosophila, three different Spire isoforms have been described to be encoded by the *Spire* locus:

- the full-length Spire protein (Spire long form, also called p150–Spir or *SpireA*) (Wellington et al., 1999; Otto et al., 2000);

- a splice variant that includes the KIND domain and the WH2 domain cluster (Spire short form, also called *SpireD*);

- a splice variant that includes the C-terminal region encoding the Spir-box and the FYVE zinc finger (*SpireC*) (Rosales-Nieves et al., 2006).

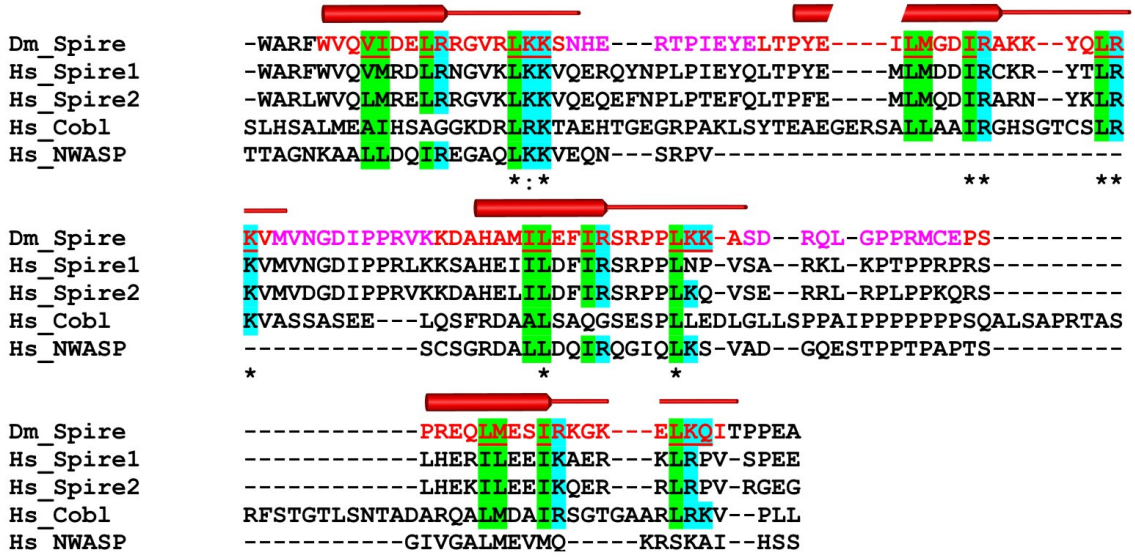

Figure 1.4 The amino acid sequence alignment of the WH2-containing actin nucleators. Dm_Spire (*Drosophila melanogaster*; Q9U1K1); Hs_Spire1 (*Homo sapiens*; Q08AE8); Hs_Spire2 (*Homo sapiens*; Q8WWL2); Hs_Cobl **(***Homo sapiens*; O75128); Hs_NWASP (*Homo sapiens*; O00401). Conserved residues are colored as follows: green – hydrophobic; cyan – basic; residues present in all WH2 domains are marked with asterisks. The residues directly interacting with actin are underlined. Sequence of the Spire protein studied in this thesis is shown in red (the WH2 domain) and magenta (linkers).The secondary structure is depicted above the sequence.

Spire mediates actin-microtubules interactions and has important roles in membrane transport, although the upstream signalling pathways that regulate these functions have not been fully studied (Kerkhoff et al., 2001; Rosales-Nieves et al., 2006; Quinlan et al., 2007). Although much of what is known about Spire comes from characterizations of the fly protein, orthologues have been identified in metazoans. Mammals exhibit two isoforms. Spire-1 is preferentially expressed in the nervous system (Schumacher et al., 2004). Spire-2 mRNA is present in the nervous system, digestive tract, liver and testis (Kerkhoff, 2010).

1.3.1 Domain organization of Spire

Spire is a 1020 amino acid long, multidomain protein. The most important domains, from the point of view of actin organization, are localized in the N-terminal part of the protein. For example, the N-terminal domain of Spire (SpireNT, residues 1-520) was shown to interact with G-actin (see Results and Quinlan et al., 2005; Bosch et al., 2007). The KIND domain shows homology to the C-terminal protein kinase catalytic fold (C-lobe), although it lacks the sequence similarity critical for kinase activity (Ciccarelli et al., 2003). So far, four proteins containing KIND domains have been identified in mammals: Spire (Otto et al., 2000; Kerkhoff, 2006), the nonreceptor-type protein tyrosine phosphatase 13 (PTPN13) (Erdmann, 2003; Wansink et al., 2004), FERM and the PDZ-domain-containing 2 (FRMPD2) family of proteins (Stenzel et al., 2009), the Ras guanine exchange factor (RasGEF), and the very-KIND (v-KIND, or kinase noncatalytic C-lobe domain containing 1) (Mees et al., 2005). The KIND domains in these proteins are localized to the N-terminal region, and their specific functional domains are located in the C-terminal regions. The C-lobe of protein kinases mediates the interaction with activators, substrates and regulatory subunits, implying that the KIND domain, an atypical noncatalytic C-lobe, is involved in the interaction with signaling proteins (Ciccarelli et al., 2003; Kerkhoff, 2006; Quinlan et al., 2007). However, the structural and functional properties of the KIND domains remain unknown. The KIND domain of the *Drosophila* Spire

(residues 90-328) is known to interact with another actin-nucleating factor, Cappuccino (fly formin) (Rosales-Nieves et al., 2006; Quinlan et al., 2007).

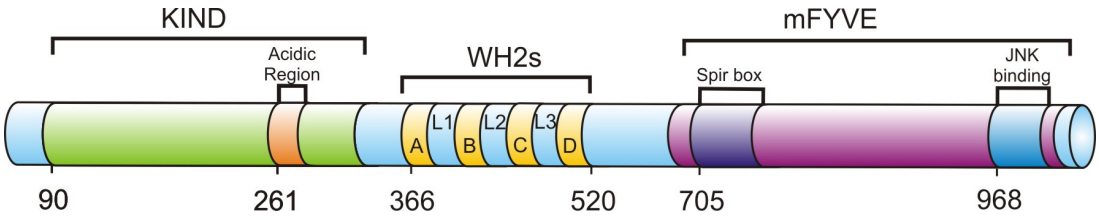

Figure 1.5 Domain organization of the full-length *Drosophila* Spire. The WH2 (Wiskott-Aldrich Syndrome Protein homology domain 2) domains are shown in yellow. KIND, the kinase noncatalytic C-lobe domain; mFYVE, a modified FYVE zinc-finger; JNKB, the JNK-binding domain.

Spire has a cluster of four WH2 domains (Figures 1.4, 1.5). These WH2 repeats, designated A, B, C, and D, contain 20-21 amino acid long actin-binding motifs, separated by three linkers: L1 (10 aa long) between domains A and B, L2 (11 aa long) between domains B and C, and L3 (12 aa long) between domains C and D.

The C-terminal region of Spire proteins encodes the FYVE zinc finger membrane localization domain (Otto et al., 2000; Kerkhoff, 2006). FYVE zinc fingers comprise eight cysteine residues, which bind two zinc ions (Misra and Hurley, 1999). The structure forms a hydrophobic loop, which penetrates the membrane. The Spire FYVE domain is different in that it lacks a basic pocket that specifically binds the phospholipid phosphatidylinositol 3-phosphate (PI(3)P) (Otto et al., 2000).

The Spir-box (Figure 1.5) is a highly conserved region, N-terminally, adjacent to the Spire FYVE domain. It shares sequence homology with an α-helical N-terminal flanking region of the rabphilin-3A FYVE domain, which mediates the interaction between rabphilin-3A and the GTP-loaded Rab3A GTPase (Ostermeier and Brunger, 1999; Kerkhoff et al., 2001). Spire proteins

co-localize with the Rab11 GTPase, which is localized at the trans-Golgi network, post-Golgi vesicles and the recycling endosome (Sonnichsen et al., 2000; Kerkhoff et al., 2001). The Spire-1 protein was localized on early endosomes (Morel et al., 2009). Although the Spir-box is a potential Rab GTPase-binding domain, a direct interaction of Spire with a Rab GTPase has not yet been shown.

1.3.2 Biochemical and structural properties of Spire and its cellular functions

Nucleation activity

Spire proteins have the potential to form a string of four actin monomers. It is believed that the complexes of Spire with actin are formed in efficient and cooperative association reactions, are stable, and adopt the shape of one strand of the long pitch helix of the actin filament, thus making a filament template (Quinlan et al., 2005; Bosch et al., 2007; Rebowski et al., 2008). Mutational studies indicated that, among the four WH2 domains of Spire, the C and D domains have the strongest nucleation potential and the CD fragment is sufficient to initiate the polymerization process (Quinlan et al., 2005). Additionally, the L3 linker was identified as an actin monomer binding element (Zuchero et al., 2009) In an actin assembly assay, the ABCD nucleating region of Spire nucleates actin at low Spire/actin ratios and sequesters actin at high Spire/actin ratios (Quinlan et al., 2005, 2007; Campellone and Welch, 2010). Comparing NMR and crystal structures of different WH2 domains, this conserved α-helix is shown to be the principal structural actin-binding element that binds to actin in its hydrophobic pocket between actin's subdomains 1 and 3 (Hertzog et al., 2004; Irobi et al., 2004; Chereau et al., 2005; Aguda et al., 2006; Lee et al., 2007; Ducka et al., 2010). The rest of the WH2, comprising the LKK motif, extends along the outer surface of the actin subdomain 1 up to subdomains 2 and 4.

Cooperation of Spire with formins and profilins

Spire is a nucleator itself in vitro, but in vivo works closely with Cappuccino (fly formin) (Quinlan et al., 2005, 2007). Quinlan et al. (2007)

suggested that Spire, with the help of Cappuccino, nucleates filaments, which are then “handed over” to the Cappuccino formin for the barbed-end elongation. Mammalian Spire and the Cappuccino ortholog formin-2 have been shown to interact in the same way in mammalian cells (Quinlan et al., 2007). Such a model would be in agreement with analyzes suggesting that Spire stays associated with the pointed end of filaments (Quinlan et al., 2005) whereas formins processively move along with barbed ends (Higgs, 2005; Kovar, 2006; Goode and Eck, 2007). However, very recent publication by Ito and colleagues suggests that Spire binds only to the barbed end of existing filament (Ito et al., 2011). If one formin dimer binds two molecules of Spire, and each Spire binds to four actin molecules, this could bring together eight actin molecules which could form a complete filament seed and thereby create a powerful nucleation complex. “Handing over” actin seeds to the formin-promoted actin filament elongation would require actin-polymerization-dependent dissociation of the Spire-Cappuccino complexes. Dissociation might be caused by binding the profilin–actin complexes to the formin homology 1 domains within the complex. Spire and formin, together with profilins, might form thus an efficient nucleation machinery (Qualmann and Kessels, 2009).

The cytoplasmic actin mesh, which is assembled by Cappuccino and Spire, helps to maintain microtubule organization and to tether the vesicles, the kinesin-driven movement that starts cytoplasmic streaming (Dahlgaard et al., 2007). A similar actin mesh that is vital for the spindle positioning during asymmetric partitioning of the cytoplasm was recently described for vertebrate oocytes (Azoury et al., 2008; Li et al., 2008; Schuh and Ellenberg, 2008) and is important for oogenesis and female fertility (Leader et al., 2002). In vertebrates, Spire proteins are important in the female germline; e.g, Xenopus Spire-2 is a maternal gene detected only in unfertilized eggs, during oogenesis, and very early stages of embryogenesis (Le Goff et al., 2006).

Regulation of Spire functions

Two different Spire regulatory mechanisms were proposed based on the studies of the Spire-protein interactions and protein phosphorylation (Kerkhoff, 2006).

- A binding site for the Rho-family GTPases RhoA, Rac1 and Cdc42 was identified in the N-terminal region of the *Drosophila* Spire protein (Wellington et al., 1999). However, this region is not conserved in all other Spire proteins. Two additional Rho-binding sites were proposed: one located within the WH2 cluster and the other in the C-terminal region containing the Spir-box and the FYVE domain (Figure 1.5) (Rosales-Nieves et al., 2006).

- In the second potential regulatory mechanism, described by Otto et al. (2000), the *Drosophila* Spire proteins are phosphorylated by the mitogen-activated protein (MAP) kinase JNK. The reaction is mediated by the C-terminal region of the *Drosophila* Spire protein, which is not highly conserved within the Spire-family proteins. Transient expression studies in mouse fibroblasts show a co-localization of Spire and JNK proteins, and the expression of Spire with the activated JNK causes extensive phosphorylation of the Spire protein (Otto et al., 2000).

2 Goals of the study

The principal goal of this thesis was to determine molecular bases of Spire-dependent nucleation of actin filaments using several biochemical and biophysical techniques: X-ray crystallography, small angle X-ray scattering, nuclear magnetic resonance spectroscopy and fluorescence assays.

The Spire protein is an important player in actin dynamics in a large number of actin-dependent processes. Three-dimensional structures of the Spire/actin complexes, determined by X-ray and SAXS, together with biochemical and biophysical studies provide the molecular basis for the understanding of structure-function relationships between Spire, actin and actin filaments.

3 Materials and laboratory methods

3.1 Materials

3.1.1 *E. coli* strains and plasmids

Cloning strains	
XL1-Blue	Stratagene (USA)
One Shot TOP10	Invitrogen (USA)
DH5α	Novagen (Germany)
GigaSingles	Novagen (Germany)
Protein expression strains	
BL21 Codon Plus (DE3)	Stratagene (USA)
BL21 Arctic Express (DE3)	Stratagene (USA)
BL21(DE3) Codon+ RIL	Stratagene (USA)
BL21 (DE3) pLysS	Novagen (Germany)
BL21 Rosetta (DE3)	Novagen (Germany)
Plasmids	
pET 16b	Novagen (Germany)
pGEX 6P-1	GE Healthcare (UK)
pGEX 6P-2	GE Healthcare (UK)

3.1.2 Cell growth media and stocks

Media

For 1 liter LB medium:	10 g peptone from casein
	5 g yeast extract
	10 g sodium chloride

25 ml of K-phosphate was added to adjust the pH. For preparation of the agar plates medium was supplemented with 15 g agar (for 1l).

Minimal medium (MM) for uniform enrichment with ^{15}N:

For 1 liter MM:

0.5 g NaCl
1.3 ml trace elements solution
1 g citric acid monohydrate
36 mg ferrous citrate
4.02 g KH_2PO_4
7.82 g K_2HPO_4 x $3H_2O$
1 ml Zn-EDTA solution
1 g NH_4Cl or $^{15}NH_4Cl$

pH was adjusted to 7.0 with NaOH, the mixture was autoclaved, upon cooling separately sterilized solutions were added: 25 ml glucose, 560 µl thiamin, antibiotics, 2 ml $MgSO_4$ stock.

Defined medium for selective ^{15}N labeling of proteins

For 1 liter of medium:

400 mg Ala, Gln, Glu, Arg, Gly
255 mg Asp, Met
125 mg cytosine, guanosine, uracil
100 mg Asn, Leu, His, Lys, Pro, Thr
100 mg Try
400 mg Ile, Val
50 mg Phe, thymine, thymidine
1.6 g Ser
10 mg $CaCl_2$
2 2 g NaAc
10 g K_2HPO_4
1 g citric acid
1.3 ml trace element solution
36 mg ferrous citrate
1 ml Zn-EDTA solution
1g NH_4Cl

pH was adjusted to 7.0 with NaOH, the mixture was autoclaved. To the cooled medium, separately sterilized solutions were added: 25 ml glucose, 560 µl thiamin, antibiotics, 2 ml 1 M $MgSO_4$, sterile filtered:

50 mg Cys, Trp, nicotinic acid
0.1 mg biotin
X mg ^{15}N-amino acid

Another portion of the ^{15}N-amino acid is added at the time of induction as well (same amount as added before, 0.22 µm filtered).

Stock solutions

Ampicillin: 100 mg/ml of ampicillin in deionised H_2O, sterilized by filtration, stored in aliquots at -20°C until usage. Working concentration: 150 µg/ml.

Chloramphenicol: 34mg/mlof chloramphenicol in ethanol, stored at -20°C until usage. Working concentration: 34 µg/ml.

Gentamycin: 50 mg/ml of gentamycin in deionised H_2O, sterile filtered, stored in aliquots at -20°C until usage. Working concentration 7µg/ml.

Kanamycin: 100 mg/ml of kanamycin in deionised H_2O, sterile filtered and stored in aliquots at -20°C until used. Working concentration: 100 µg/ml.

Streptomycin: 60 mg/ml of streptomycin in deionised H_2O, sterile filtered and stored in aliquots at -20°C until usage. Working concentration 60 µg/ml.

Tetracyclin: 10 mg/ml of tetracyclin in ethanol. Working concentration: 10 µg/ml.

Isopropyl-β-thiogalactopyranoside (IPTG): A sterile filtered 1 M stock of IPTG in deionised water was prepared and stored in aliquots at -20°C until used.

Glucose: 20% (w/v) in deionised H_2O, autoclaved.

Thiamin, 1%, in deionised H_2O, sterilized by filtration.

$MgSO_4$, 1 M, in deionised H_2O, sterilized by filtration.

For 1 liter K-phosphate, pH 7.1:	23.1 g KH_2PO_4 125.4 g K_2HPO_4
Zn-EDTA solution:	5 mg/ml EDTA 8.4 mg/ml Zinc acetate
Trace elements solution:	2.5 g/l H_3BO_3 2.0 g/l $CoCl_2 \times H_2O$ 1.13 g/l $CuCl_2 \times H_2O$ 9.8 g/l $MnCl_2 \times 2H_2O$ 2.0 g/l $Na_2MoO_4 \times 2H_2O$ pH adjusted with citric acid or HCl.

3.1.3 Solutions for making chemically competent *E. coli* cells

Solutions used for competent cells preparation

Buffer A	100 mM $MgCl_2$ x 6H2O
Buffer B	100 mM $CaCl_2$ - 15% glycerol

3.1.4 Protein purification – buffers

Size exclusion chromatography buffers

PBS	140 mM NaCl 2.7 mM KCl 10 mM Na_2HPO_4

	1.8 mM KH_2PO_4
	0.05% NaN_3
	pH 7.3
G buffer (general actin buffer)	5mM Tris-HCl
	0.2mM $CaCl_2$
	0.2mM ATP
	0.5mM DTT
	pH 8.0
KMEI buffer	
(actin polymerization buffer)	50mM KCl
	1mM $MgCl_2$
	1mM EGTA
	10mM imidazole
	pH 7.0
Crystallization buffer	5 mM Tris-HCl
	50 mM NaCl
	pH 8.0
Actin crystallization buffer	5mM Tris-HCl
	50mM NaCl
	0.2 mM ATP
	5mM β-mercaptoethanol
	pH 8.0
Affinity chromatography buffers - Sepharose glutathione	
Binding buffer	PBS
Wash buffer	PBS
Elution buffer	50 mM Tris-HCl

	150 mM NaCl
	30 mM glutathione
	pH 8.0

Buffers for immobilized metal-chelate chromatography (IMAC) under native conditions

Binding buffer	50 mM NaH_2PO_4
	300 mM NaCl
	10 mM imidazole
	pH 8.0
Wash buffer	50 mM NaH_2PO_4
	300 mM NaCl
	20 mM imidazole
	pH 8.0
Elution buffer:	50 mM NaH_2PO_4
	300 mM NaCl
	250 mM imidazole
	pH 8.0

Protease buffers:

Buffer PP	50 mM Tris
(PreScission Protease cleavage buffer)	150 mM NaCl
	1 mM EDTA
	1 mM DTT
	pH 7.0

3.1.5 Buffer for DNA agarose gel electrophoresis

50X TAE buffer (for 1 l)

40 mM Tris-acetate	242 g of Tris base

1 mM EDTA	100 ml of 0.5 M EDTA (pH 8.0)
Glacial acetic acid	57.1 ml

3.1.6 Reagents and buffers for the SDS-PAGE

Anode buffer (+):	200 mM Tris pH 8.9
Cathode buffer (-):	100 mM Tris pH 8.25 100 mM tricine 0.1% SDS
Separation buffer:	1 M Tris pH 8.8 0.3% SDS
Stacking buffer:	1 M Tris pH 6.8 0.3% SDS
Acrylamide solution:	Rotiphorese® Gel 30 (37, 5:1) Roth (Germany)

Casting of polyacrylamide gels

Separation gel:	0.35 ml H_2O 5 ml separation buffer 8 ml acrylamide solution 1.6 ml glycerol 50 µl APS 5 µl TEMED
Intermediate gel:	3.825 ml H_2O 3.75 ml separation buffer 3.6 ml acrylamide solution 37.5 µl APS 3.75 µl TEMED

Stacking gel:	5.15 ml H_2O
	0.975 ml stacking buffer
	1.25 ml acrylamide solution
	25 µl 0.5 M EDTA, pH 8.0
	75 µl APS
	4 µl TEMED

Protein visualization

Coomassie-blue solution:	45% ethanol
	10% acetic acid
	1g Coomassie Brilliant Blue R
Destaining solution:	5% ethanol
	10% acetic acid

3.1.7 Reagents and buffers for Western blots

Transfer buffer	25 mM Tris
	192 mM glycine
	pH 8.3

For final working solution 80 ml of the transfer buffer was mixed with 20 ml of methanol.

Alkaline phosphatase buffer	100 mM Tris
	100 mM NaCl
	5 mM $MgCl_2$
	pH 9.5
Wash buffer	10 mM Tris
	150 mM NaCl
	0.05% Tween20
	pH 8.0

Primary antibody solution	1:2000 diluted in the wash buffer
Secondary antibody solution (linked to alkaline phosphatase)	1:5000 diluted in the wash buffer
Substrate for alkaline phosphatase	Sigma*FAST* BCIP/NBT (Sigma); dissolve 1 tablet in 10 ml of water

3.1.8 Enzymes and other proteins

BSA	New England BioLabs (USA)
CIP	New England BioLabs (USA)
BamH I	New England BioLabs (USA)
EcoR I	New England BioLabs (USA)
Hind III	New England BioLabs (USA)
Nhe I	New England BioLabs (USA)
Sal I	New England BioLabs (USA)
Xho I	New England BioLabs (USA)
Phusion HF DNA Polymerase	Finnzymes (Finland)
Taq Polymerase	Fermentas (Lithuania)
T4 DNA Ligase	New England BioLabs (USA)
Dpn I	New England BioLabs (USA)
PreScissionProtease	GE Healthcare (USA)
Anti His antibodies (mouse)	Santa Cruz biotech (USA)
Goat anti mouse antibodies	Santa Cruz biotech (USA)

3.1.9 Kits and reagents

QIAquick Gel Extraction Kit	Qiagen (Germany)
QIAquick PCR Purification Kit	Qiagen (Germany)
QIAprep Spin Miniprep Kit	Qiagen (Germany)

QIAGEN Plasmid Midi Kit	Qiagen (Germany)
Pre-Crystallization Test (PCT)	Hampton Research (USA)
Complete Protease Inhibitor Cocktail	Roche (Germany)
pET LIC cloning Kits	Novagen (Germany)
Gel Filtration LMW Calibration Kit	GE Healthcare (UK)
Gel Filtration HMW Calibration Kit	GE Healthcare (UK)

3.1.10 Protein and nucleic acids markers and sample loading dyes

Markers

Page Ruler ^{TM} Prestained Protein Ladder	Fermentas (Lithuania)
Spectra Multicolor ^{TM}	Fermentas (Lithuania)
Broad Range Protein Ladder	
Precision Plus Protein Kaleidoscope	BioRad (USA)
Gene Ruler ^{TM} DNA Ladder	Fermentas (Lithuania)
100 BP DNA marker	New England BioLabs (USA)
1Kb DNA marker	New England BioLabs (USA)

Sample loading dyes

5x protein loading dye:	0.225 M Tris-HCl, pH 6.8
	50% glycerol
	5% SDS
	0.05% bromophenol blue
	0.25 M DTT
6x DNA Loading Dye	Fermentas (Lithuania)
SYBR® Safe DNA gel stain	Invitrogen (USA)

3.1.11 Chromatography equipment, columns and media

ÄKTA basic	GE Healthcare (Germany)
ÄKTA explorer	GE Healthcare (Germany)
Peristaltic pump P-1	Amersham Pharmacia (Sweden)
Fraction collector RediFrac	Amersham Pharmacia (Sweden)

Recorder REC-1	Amersham Pharmacia (Sweden)
UV flow through detector UV-1	Amersham Pharmacia (Sweden)
BioLogic LP System	Biorad (USA)
HiLoad 26/60 Superdex S75pg	GE Healthcare (UK)
HiLoad 16/60 Superdex S75pg	GE Healthcare (UK)
HiLoad 16/60 Superdex S200pg	GE Healthcare (UK)
HILoad 16/60 Superdex S30pg	GE Healthcare (UK)
HiLoad 10/300 Superdex S75GL	GE Healthcare (UK)
HiLoad 10/300 Superdex S200GL	GE Healthcare (UK)
GSTrap FF Columns	GE Healthcare (UK)
HiTrap IMAC FF	GE Healthcare (UK)
ProBond Resin	Invitrogen (USA)
NTA Superflow	Qiagen (Germany)
Glutathione Sepharose 4 Fast Flow	GE Healthcare (UK)

3.2 Laboratory methods and principles

3.2.1 Construct design and choice of the expressions system

Optimization of protein constructs is essential for X-ray crystallography and NMR studies. Unstructured and flexible fragments of proteins or loop regions usually inhibit crystallization or result in crystals of low quality. The idea behind designing the protein constructs is to have well defined, folded and stable domains and at the same time to have them biologically active. Determination of stable and folded constructs requires employing various techniques like for example: limited proteolysis, protein sequencing, mass spectrometry, and NMR spectroscopy (Rehm et al., 2002). In some cases designing of the constructs may be based on previously published literature and secondary structure prediction with the help of bioinformatics tools.

Successful expression of heterologous proteins requires proper expression system (Makrides, 1996). Large fusion tags, such as glutathione S-transferase, maltose binding protein, Nus protein or thioredoxin often increase solubility and promote proper folding of recombinant fusion partners. Presence of

a 6-histidine fusion peptide (His-Tag) enables rapid purification with use of immobilized metal chromatography (IMAC).

In this work pET and pGEX series of vectors were used for the expression of proteins in *E. coli* (pET system manual, Novagen, 2003; pGEX manual, Amersham Pharmacia, 2003). The first Spire construct (SpireNT(1-520)) has been designed for the expression in pET16b with the N-terminal His-tag as a purification tag. Another constructs (SpireABCD, SpireBCD, SpireCD, SpireL3-D, SpireD) were amplified using SpireNT as a template and cloned into pGEX 6-P-1 vector with glutathione S-transferase as a purification tag. Removal of the fusion tag was achieved with an aid of a PreScission Protease which cleaves after Q in a LEVLFQGP sequence located between GST and a target protein. The following constructs: SpireAB, SpireBC, SpireA, SpireB, SpireC, SpireL3 were produced by site directed mutagenesis introducing stop codons at positions 388 (generates SpireA if SpireABCD is a template), 419 (generates SpireAB if Spire ABCD is a template and SpireB if SpireBCD is a template), 450 (generates SpireC if SpireCD is a template and SpireBC if SpireBCD is a template) and 461 (generates SpireC-L3 if SpireCD is a template and SpireL3 if SpireL3-D is a template) of the Spire sequence. SpireDD and SpireDDD were engineered by duplication and triplication of WH2-D domain, respectively, as it is presented in Figure 3.1. SpireDD was obtained after amplification, restriction cleavage and ligation of two fragments of Spire gene: (BamH)461-D-479(NheI) and (NheI)448-L3D-479(SalI). NheI restriction enzyme was selected because its cleavage site (gct agc) encodes alanine and serine which are present in L3 linker at positions 448 and 449. Original alanine and serine (gcc agc) codons were exchanged to gct agc by PCR using primer containing overhang with a modified codon sequence. SpireDDD was produced after ligation of three fragments of the Spire gene: (BamH)461-D-479(NheI), (NheI)448-L3D-479(blunt end), and (blunt end)448-L3D-479(SalI). Both, the cohesive ends and blunt ends ligation technology was applied to obtain desired construct (Figure 3.1).

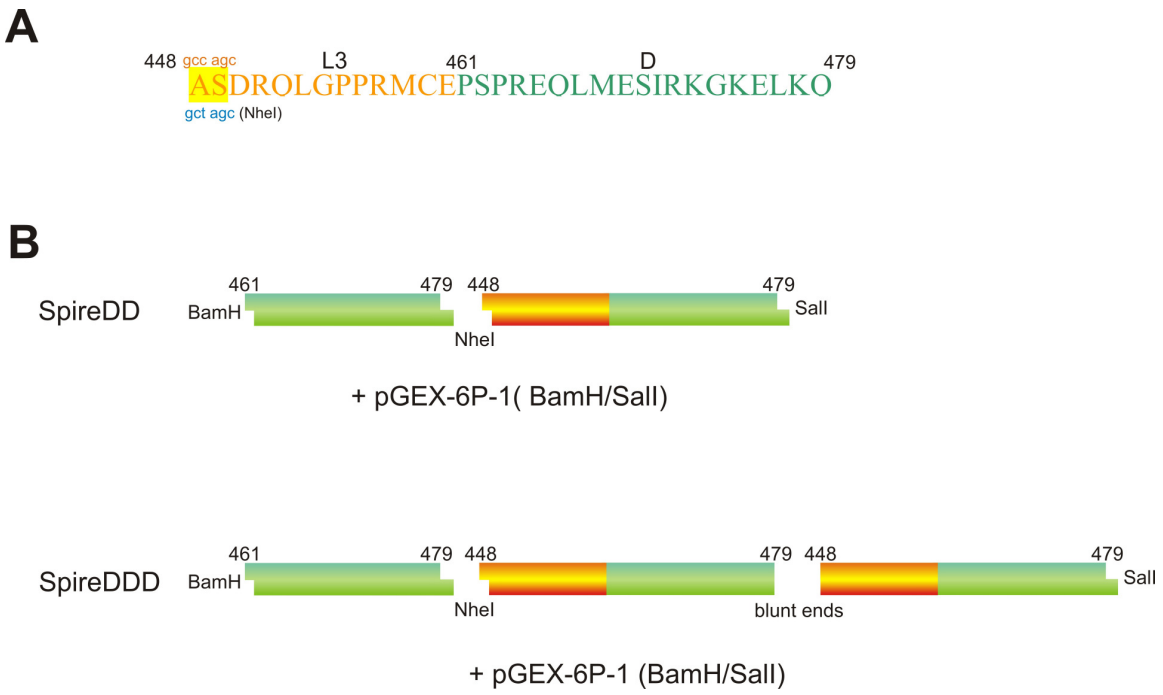

Figure 3.1 Strategy for the generation of SpireDD and SpireDDD constructs. (A) Amino acid sequence of SpireL3-D (orange, green). The GCC codon encoding alanine was mutated to GCT. This did not change the amino acid sequence but allowed to introduce the cleavage site for the NheI enzyme (blue). (B) The cohesive end ligation of SpireD (green) and SpireL3-D (orange/green) resulted in the formation of SpireDD (upper scheme). The cohesive and blunt ends ligation between SpireD (green) and two repeats of SpireL3-D (orange/green) produced the SpireDDD construct (lower scheme).

The following constructs, SpireABCD-Lx-Thelix and SpireBCD-Lx-Thelix were obtained after extension of the C-termini of SpireABCD and SpireBCD by the PCR reaction (Figure 3.2). The extended fragment was based on the sequence of the previously published structure of the thymosin β4 - gelsolin fusion protein complexed with actin (PDB: 1T44; Irobi et al., 2004). The DNA fragment corresponding to the polypeptide chain of thymosin helix (Asn158 – Gln171), was generated in four steps of a PCR reaction using SpireABCD and SpireBCD as starting templates and four primers carrying desired extensions in their overhangs. SpireABCD-Ly-Thelix and SpireBCD-Ly-Thelix were produced

by site directed mutagenesis inserting three alanines between the last amino acid (Ala485) of the WH2-D domain and the first amino acid (Asn158) of the thymosin helix.

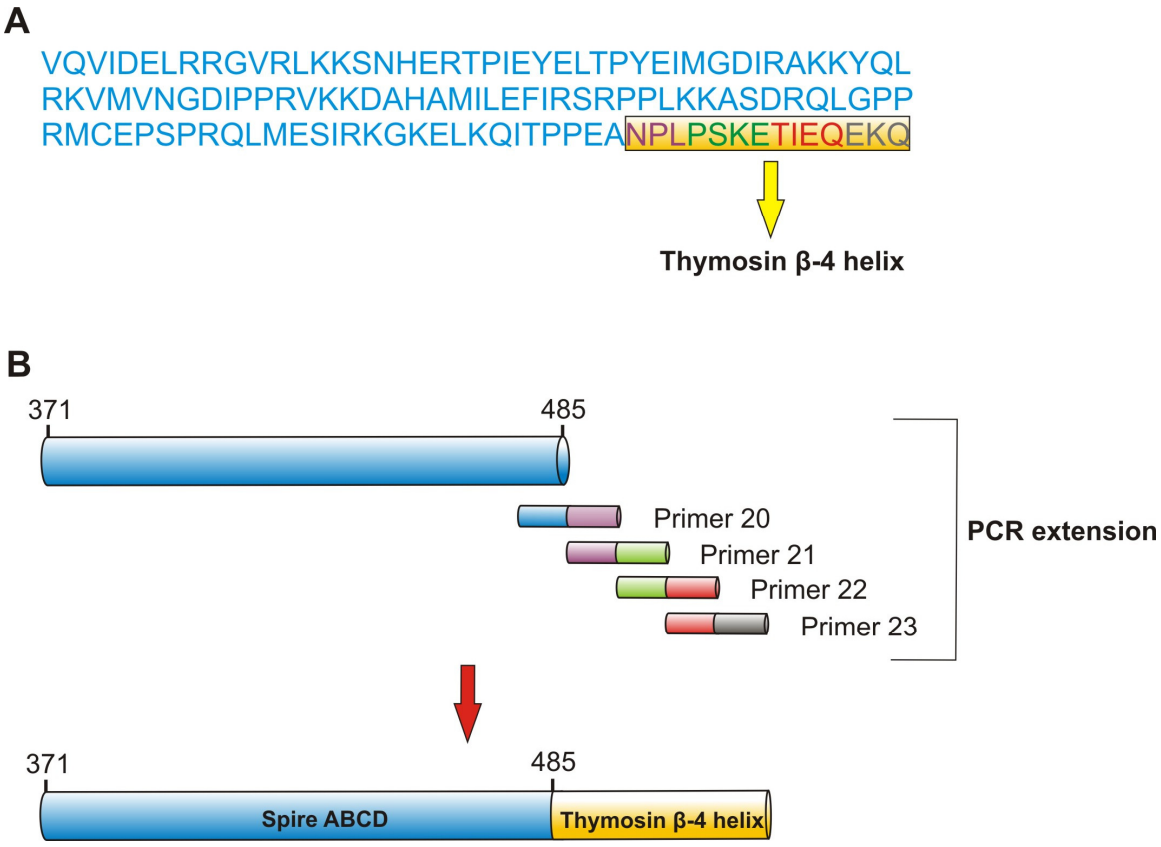

Figure 3.2 Generation of the SpireABCD-Lx-Thelix construct. (A) Amino acid sequence of SpireABCD 371-485 (blue) elongated with the thymosin β4 helix (yellow frame). (B) The multi-step PCR reaction generating the thymosin β4 helix at the C-terminus of SpireABCD. Sequences of the primers used for the extension are shown in Table 3.1.

3.2.2 DNA techniques

3.2.2.1 Preparation of plasmid DNA

The isolation of plasmid DNA from *E. coli* was carried out using dedicated plasmid purification kits from Qiagen. The kits employ a standard alkaline lysis of the precipitated bacteria in the presence of RNAse and a strong ionic detergent,

SDS, followed by neutralization/DNA renaturation with acetate. For purification, a crude cell lysate is loaded onto a silica gel column, washed with an ethanol-containing buffer, and eluted in a small volume, yielding up to 20 µg of the plasmid DNA.

3.2.2.2 PCR

A polymerase chain reaction was employed to amplify desired DNA fragments and genes, introduce restriction sites, STOP codons and sequences encoding restriction protease cleavage sites. The primers were prepared according to standardized principles regarding the length, GC-content, melting temperature and occurrence of secondary structures of the hairpin type. All primers used for preparation of constructs are listed in Table 3.1. Two different kinds of recombinant thermostable DNA polymerases were used, each operating at slightly different conditions:

	Melting temp.	Annealing temp.	Synthesis temp.
Phusion HF	98°C	55-72°C	72°C
Taq Polymerase	95°C	55-72°C	68-72°C

The stock solution of the primer was always 0.1 nM. The working solution was 0.01 nM. Usually 2 µl of the working solution was used per PCR reaction for each primer.

PCR mixture (50 µl) was prepared as follows:

5x polymerase buffer	10 µl
10 mM dNTP mix	2 µl
10 pM primer F	2 µl
(stock solution was always 100 pM)	
10 pM primer R	2 µl
(stock solution was always 100 pM)	
template DNA	1 µl
polymerase	1 µl

PCR grade water	33.5 µl

3.2.2.3 Agarose gel electrophoresis and extraction of PCR products

For verification of the presence and length of PCR or the restriction digestion products, agarose gel electrophoresis was performed. For this purpose 1% agarose in a TAE buffer supplemented with SYBR DNA gel stain (1:10000) was prepared. The DNA samples were mixed with the 6x sample buffer prior to loading. DNA samples were run along with the 100bp and/or 1kb DNA ladder at 100-120 V DC. Results were vizualized using UV illumination.

DNA bands corresponding to the size of designed constructs were extracted and purified using the QIAquick Gel Extraction Kit (Qiagen) according to the manufacturer protocol.

Table 3.1 Primers used in this work.

No.	Primer name	Sequence
1	Spire1FBamH	aaa gga tcc atg acg gag cac cag gcc g
2	Spire365RHind	ata aag ctt cgc cag ttc ttg ttg cgt ggt ggc
3	SpireCBamF	aaa gga tcc aag aaa gat gcc cac gcc
4	SpireCDHindF2	aga aag ctt ggc ttc aac gac aag aaa gat gcc
5	SpireDSalR	aga gtc gac tta tgc ttc tgg cgg ggt gat ctg
6	SpireDBamF	aaa gga tcc gcc agc gat cgc caa ttg g
7	SpireBBamF	aaa gga tcc gag ctg acg ccc tac gaa ata c
8	SpireCmutSF	cgg gag tag ctc atg gag tcc ata cgg aag
9	SpireCmutSR	cat gag cta ctc ccg cgg aga agg ctc
10	Spire90BamF	aaa gga tcc gtc acg ctg cac gac atc
11	Spire90BamF	aaa gga tcc gca cgc ttc tgg gtg cag
12	Spire328SalR	aga gtc gac tta gag ctc tat ggt ctc cgt cac
13	Spire371BamF	aaa gga tcc gtg cag gtg atc gac gaa c
14	Spire461BamF	aaa gga tcc cct tct ccg cgg gag
15	Spire479NheR	aga gct agc ctg ctt gag ctc ctt ccc
16	Spire448NheF	aga gct agc gat cgc caa ttg ggc ccg

17	Spire479SalR	aga gtc gac tta agc ctg ctt gag ctc ctt ccc
18	Spire479PhoR	agc ctg ctt gag ctc ctt ccc
19	Spire448PhoF	agc gat cgc caa ttg ggc ccg
20	Spireh1R	cag cgg gtt tgc ttc tgg cgg ggt gat
21	Spireh2R	ttc ttt gct cgg cag cgg gtt tgc ttc
22	Spireh3R	ctg ttc aat ggt ttc ttt gct cgg cag
23	Spireh4R	ctg ttt ttc ctg ttc aat ggt ttc ttt gct
24	Spireh5SalR	aga gtc gac tta ctg ttt ttc ctg ttc aat
25	Spire520SalR	aga gtc gac tta gag atc gtc gtc ctg
26	SpireA388SF	agc aac tag gag cgc act ccc atc gaa tat
27	SpireA388SR	gcg ctc cta gtt gct ctt ctt cag ccg
28	SpireB419SF	gtg atg tag aac gga gat att ccg ccg cgc
29	SpireB419SR	tcc gtt cta cat cac ctt gcg caa ctg ata ctt
30	SpireC450SF	gcc agc taa cgc caa ttg ggc ccg c
31	SpireC450SR	ttg gcg tta gct ggc ctt ctt cag cgg c
32	SpireD461SF	ctg gga tcc cct tct ccg cgg gag cag
33	SpireD461SR	agg gga tcc cag ggg ccc ctg gaa cag aac
34	Spireh3AF	gca gca gca aac ccg ctg ccg agc aaa gaa acc
35	Spireh3AR	gtt tgc tgc tgc tgc ttc tgg cgg ggt gat ctg

xyz restriction enzyme cleavage site

xyz stop codon

xyz overhang sequence

xyz phosphorylation site

3.2.2.4 Digestion with restriction enzymes

Usually, 1-2 units of each restriction enzyme were used per 1 µg of plasmid DNA to be digested. The digestion was performed in a buffer specified by the manufacturer at the optimal temperature (37°C) for 2-6 h.

To eliminate possibility of plasmid recirculation (possible when double-digestion does not occur with 100% efficiency), 5'-ends of a vector were

dephosphorylated using calf intestine phosphatase (CIP). The CIP treatment was performed with 1 unit of enzyme per 3 μg of the plasmid DNA, at 37 °C for 1 h.

3.2.2.5 Purification of PCR and restriction digestion products

DNAs obtained from restriction digestion, phosphatase treatment, or PCR were purified from primers, nucleotides, enzymes, buffering substances, mineral oil, salts, agarose and other impurities, using a silica-gel column (QIAquick PCR Purification Kit, Qiagen). The QIAquick system uses a simple bind-wash-elute procedure. A binding buffer was added directly to the PCR sample or other enzymatic reaction, and the mixture was applied to the spin column. Nucleic acids adsorbed to the silica-gel membrane in the high-salt conditions provided by the buffer. Impurities and short fragments of single or double-stranded DNAs were washed away and pure DNA was eluted with a small volume of 10 mM Tris pH 8.5 or water.

3.2.2.6 Ligation

The ligation of digested and purified inserts and vectors was performed according to the protocol described in the T4 DNA Ligase instruction (New England BioLabs).

The ligation mixture contained (20 μl):

Insert (0.15 μM)	16 μl
10 x T4 DNA ligase reaction buffer	2 μl
vector	1 μl
T4 DNA Ligase	1 μl

3.2.2.7 Mutagenesis

Site directed mutagenesis of Spire was performed using the Phusion HF DNA Polymerase (Finnzymes), following a standard protocol of the PCR reaction (see below). The mutagenic oligonucleotide primers were designed according to suggestions provided by the manufacturer. The desired point mutation was

surrounded by ~ 9 bases of a correct sequence at the 5' end and ~ 15 bases from the 3' side (Table 3.1, primers). Vectors (pGEX 6P-1) containing copies of a gene encoding different constructs of Spire were used as DNA template. Low number of PCR cycles combined with high accuracy and fidelity of Phusion HF DNA Polymerase minimizes the occurrence of unwanted mutations.

The mutagenic PCR reaction mixture contained:

5 × reaction buffer	10µl
10 mM dNTP mix	1 µl
Plasmid	1 µl
oligonucleotide primer F	2 µl
oligonucleotide primer R	2 µl
Phusion HF DNA Polymerase (2 U/µl)	1 µl
PCR grade water	37 µl

PCR cycling parameters:

denaturation:	98°C, 1'
denaturation:	98°C, 30''
annealing:	65 – 72 °C, 30''
synthesis (1 min per 1000 base pairs):	72°C, 6' (for pGEX 6P-1)

Following the temperature cycling, the product was treated with Dpn I (10 U, 37°C, for 2 h). The Dpn I endonuclease (target sequence: 5´-Gm^{6}ATC-3´) is specific for methylated and hemimethylated DNA and is used to digest the parental DNA template and to select for the mutation-containing synthesized DNA. 2 µl of the mixture were used to transform the XL1-Blue or Top10 chemically competent cells. Plasmid DNA was isolated using the QIAprep Spin Miniprep Kit (Qiagen) and was subjected to the verification by automated sequencing.

3.2.3 Transformation of *E. coli*

3.2.3.1 Making chemically competent cells

A single colony of overnight grown bacteria from a LB agar plate was inoculated into 100 ml of the LB media in a 500 ml flasks. Culture was incubated at 37℃ with vigorous agitation, monitoring the growth of cells. Cells were grown till the OD600 reached ~0.6. The bacterial culture was transferred to sterile, disposable, ice-cold 50 ml polypropylene tubes and cooled down to 4℃ on ice for 10 min. Cells were centrifuged at 3000 g for 10 min at 4℃. Supernatant media was decanted and tubes were kept in an inverted position on a pad of paper towel for 1 min to allow the last traces of media to drain away. Pellets were resuspended by gentle vortexing in 30 ml of the ice-cold MgCl2 solution. Again, cells were centrifuged at 3000 g for 10 min at 4℃. Supernatant solution was decanted and tubes were kept in an inverted position on a pad of a paper towel for 1 min to allow the last traces of solution to drain away. The pellet of the cells was resuspended by gentle vortexing in 2 ml of the ice-cold 0.1 M CaCl2 containing 15% glycerol, for each 50 ml of the original culture. Next, cells were dispensed into aliquots of 50 µl, flash frozen in liquid nitrogen and stored at -70℃.

3.2.3.2 Transformation of chemically competent cells

3 µl of a ligation mix or ca. 50 µg of the plasmid DNA was added to 50 µl of chemically competent cells. The mixture was incubated on ice for 30 min followed by a heat shock of 45 s at 42℃, 2 min cooling on ice, and the addition of a 250 µl of glucose and magnesium containing medium. After 1 h of incubation at 37℃, 20-50 µl of the mixture was spread out on LB agar plates (supplemented with selective antibiotic) and incubated overnight at 37℃.

3.2.4 Protein chemistry methods and techniques

3.2.4.1 Protein expression

Optimization of the conditions is important for expressing proteins. The aim is to secure the maximum amount of a protein in a soluble fraction of the

lysate. A number of parameters were checked to get maximum yields of the protein, which include optimization of a type of culture media, temperature, induction duration, induction OD, concentration of inducer (IPTG), and cell types. All proteins were cloned in and expressed from the pET and pGEX vectors, which are IPTG inducible. The general strategy for protein expression and purification is shown in Figure 3.3.

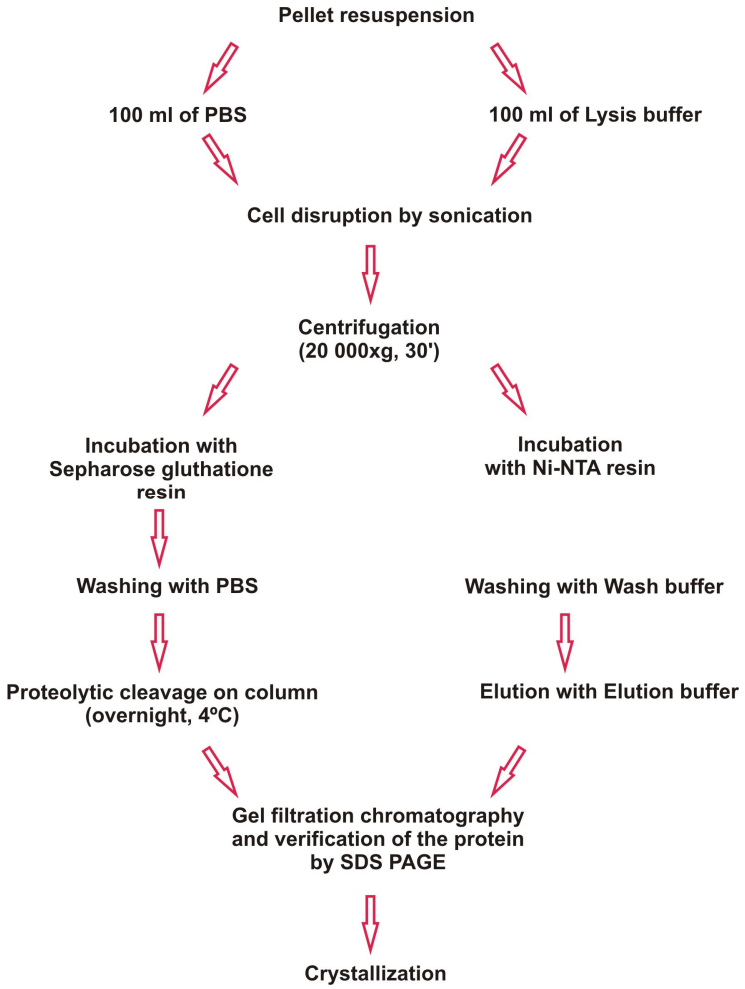

Figure 3.3 General strategy in protein expression, purification and crystallization.

3.2.4.1.1 Expression and purification of the Spire protein

The vectors (pGEX-6P-1 and pET 16b) containing *Drosophila* Spire constructs were transformed into the BL21(DE3) Codon+ RIL or BL21 Arctic Express (DE3) expression cells (Stratagene) and grown for approximately 4 h at 37ºC until the OD at 600 nm reached 0.9. Protein expression was carried out at 18ºC for 14-16 h after induction with 0.5 mM IPTG. The cells were harvested by centrifugation at 5000 rpm for 15 min, and pellets were resuspended in PBS containing 1 mM EDTA, 1 mM DTT, and 0.5 mM PMSF. The lysis was performed by sonication followed by centrifugation at 20000 rpm for 30 min. The supernatant, containing GST-tagged Spire constructs, was applied on Glutathione Sepharose 4 Fast Flow beads (GE Helthcare). Bound protein was washed with 50 mM Tris (pH 7.0), 150 mM NaCl, 1 mM EDTA and 1 mM DTT and cleaved by the PreScisson protease (GE Helthcare) to release the Spire protein. The cleaved Spire proteins were collected, concentrated and further purified on the Superdex 75 (SpireCD, SpireBCD, SpireDDD and SpireABCD) or Superdex 30 (SpireC and SpireD) in the PBS buffer. The His-tagged SpireNT encoded in a pET 16b vector was expressed in BL21(DE3) Codon+ RIL and purified by Ni-NTA agarose beads (Qiagen) followed by gel filtration on Superdex 200 (GE Helthcare). The purity and homogeneity of proteins were confirmed by mass spectrometry and N-terminal Edman sequencing.

3.2.4.2 Sonication

Pulsed mode of operation was applied (output control 8, 60% duty cycle) and sonication was carried out on ice, in 5 repeats of 3 min each, with 5 min intervals in between, to avoid overheating of the sample.

3.2.4.3 SDS polyacrylamide gel electrophoresis (SDS-PAGE)

The SDS polyacrylamide gel electrophoresis was performed at various stages of purification to check the purity and identity of eluted proteins. For all expressed proteins, the tricine gels were applied (Schagger and von Jagow,

1987). Protein samples were prepared by mixing 20 µl of the protein solution with 5 µl of the sample buffer, followed by a 5 min incubation at 100°C.

3.2.4.4 Visualization of separated proteins

For visualization of the protein bands, the gels were stained in a Coomassie-blue solution. Background was cleared by incubation of the gel in a destaining solution. Both processes were greatly accelerated by brief heating with microwaves of the gel submerged in an appropriate solution.

3.2.4.5 Western blot

Western blot is a functional assay to check the identity of proteins or to identify a particular protein out of a number of proteins. The semi-dry Western blot was applied. The Western blot assay starts with running the desired sample on the SDS-PAGE. The nitrocellulose membrane and six Watmann paper of the size of the SDS-PAGE gel were cut and soaked in the transfer buffer. Watmann paper, SDS-PAGE (gel), and nitrocellulose membrane were arranged in the following order over the electroblot: three wet Watmann papers, wet nitrocellulose paper, and SDS-PAGE gel followed by three Watmann wet papers. The apparatus was closed and run (transfer) at constant voltage of 100 V for 1-1:30 h. After the transfer, the nitrocellulose membrane is taken and kept in the blocking solution for 2 h with constant shaking. The SDS-PAGE is stained by the Commassie blue solution to check the success of transfer. After blocking, the membrane is washed three times with the wash buffer and incubated for 1.5 h at room temperature with the first antibody solution (the procedure can be stopped at this point by keeping the blot in the first antibody solution at 4°C for overnight). The membrane was washed with the wash buffer and incubated in the second antibody solution for 1.5 h at room temperature. After this, the membrane was washed three times with the wash buffer and the blot was developed by incubating it in the substrate (BCIP) solution for 10 min.

3.2.4.6 Determination of protein concentration

The concentration of proteins in solution was estimated by means of the Bradford colorimetric assay. 5 µl of the protein sample was added to 1 ml (10 x diluted stock) of the Bradford reagent (BioRad) in a plastic cuvette. After gentle mixing, A_{595} was measured and converted to the protein concentration on the basis of a calibration curve prepared for known concentrations of BSA.

Determination of protein concentration was performed spectrophotometrically. Absorption at 280 nm was measured and converted to a protein concentration on the basis of theoretical extinction coefficients. It has been shown that it is possible to estimate the molar extinction coefficient $E_\lambda(Prot)$ of a protein from knowledge of its amino acid composition (Gill and von Hippel, 1989). From the molar extinction coefficient of tyrosine, tryptophan and cystine (cysteine residues do not absorb appreciably at wavelenghts >260 nm, while cystine does) at a given wavelength λ the extinction coefficient of a protein can be computed using the equation:

$$E_\lambda(Prot) = Numb(Y)xExt_\lambda(Y) + Numb(W)xExt_\lambda(W) + Numb(C)xExt_\lambda(C)$$

Protein concentration (C_p) can be calculated using the following formula:

$$A_\lambda\ (Prot) = E_\lambda(Prot) \times C_p(Prot) \times (\text{cuvette path length in cm})$$

3.2.5 NMR spectroscopy

All NMR experiments were carried out at 300 K on a Bruker DRX 600 spectrometer equipped with a triple resonance, triple gradient 5 mm probehead. The samples contained typically 0.1-0.5 mM protein in the PBS buffer, supplemented with 10% ^2H_2O. All 1D ^1H NMR spectra were recorded with a time domain of 32 K complex points and a sweep-width of 10,000 Hz. The 2D ^1H-^{15}N-HSQC spectra were recorded with a time domain of 1K complex data points with 128 complex increments with a sweep width of 8 kHz in the ^1H dimension and 2 kHz in the ^{15}N dimension.

3.2.6 X-ray crystallography

3.2.6.1 Protein crystallization

Purified SpireABCD, SpireBCD, as well as SpireDDD, and SpireCD were mixed with the AP-actin at a molar ratio of 1:4.1, 1:3.1 and 1:2.1, respectively, and separated by gel filtration on Superdex 200 in 5 mM Tris (pH 8.0), 50 mM NaCl, 0.2 mM ATP, and 5 mM β-mercaptoethanol. Fractions from the peaks corresponding to the expected molecular weight of the complexes were analyzed by SDS-PAGE, pooled, and concentrated to 10-12 mg/ml.

The complexes were crystallized both at 4ºC and 20ºC in several crystallization conditions, using the sitting and hanging drop vapour diffusion methods. The 2-3 µl drops consisted of a 1:1 or 2:1 (vol/vol) mixture of the protein solution and a well solution.

All crystals were soaked in cryo-solutions containing the mother liquor supplemented with 20% MPD or glycerol and were flash frozen in liquid nitrogen.

3.2.6.2 Data collection and structure analysis

X-ray data sets of the SpireD/actin-latrunculin B, SpireBCD/AP-actin, SpireABCD/AP-actin, SpireDDD/AP-actin and SpireCD/AP-actin were collected on the SLS beamline PXII at the Paul Scherrer Institut, Villigen, Switzerland.

The data sets were integrated, scaled and merged with the XDS and XSCALE programs. The structures were determined by molecular replacement using the Molrep program from the CCP4 suite (CCP4, 1994). Model building and refinement were carried out with the programs XtalViev/Xfit (McRee, 1999) and REFMAC5 (CCP4, 1994).

3.2.7 Pyrene actin assays

Pyrenyliodoacetamide-labeled actin monomers (pyrene-actin) provide fluorescent readout of actin filament polymerization because a 30-fold increase in fluorescence occurs on incorporation of a labeled actin subunit into the polymer. Only low levels (5-10%) of the pyrene labeled actin are required for a strong

signal. For the actin assembly, a final concentration of 1.8-2 µM actin was routinely used. The reaction (800 µl) was started by addition of actin.

Fluorescence measurements were carried out on a Perkin Elmer fluorometer with SpirBCD and the rabbit skeletal muscle actin. Fluorescence emission was monitored under polymerizing conditions between 350-500 nm at an excitation of 342 nm and 8 nm slit widths. The actin was added stepwise to a SpirBCD solution in 800 µl F-buffer (10 mM imidazole, pH 7.2, 2 mM $MgCl_2$, 1 mM ATP, 0.2 mM $CaCl_2$); the sample was mixed and incubated for 3 min at room temperature before starting the scan. Under the conditions used (actin concentrations below 1 µM, short time schedule of the measurements), actin alone did not polymerize and the obtained changes in the fluorescence emission required the presence of a Spire construct.

3.2.8 Small angle X-ray scattering

Small-angle X-ray scattering measurements were made at the cSAXS beamline at the Swiss Light Source (Paul Scherrer Institut, Villigen, Switzerland). Solutions of Spire/actin complexes with concentrations varying between 15 mg/ml to 1.0 mg/ml were placed in the 10 µm wall thickness, 1 mm diameter borosilicate glass capillaries (Hilgenberg GmbH, Malsfeld, Germany). The capillaries were held horizontally on a x-y translation stage which has a precision of 1 µm. The volume of solution in each measurement was 50 µl and the temperature of the capillary holder was kept at 10°C. The capillary was centred vertically to the X-ray beam and a total of 200 exposures, 0.5 s each were acquired by horizontally scanning 10 positions in the capillary separated by 0.4 mm and repeating the scan 20 times. The X-ray energy was 12.4 keV and the scattered photons were detected with a Pilatus 2M detector at a distance of 2.15 m from the sample. The time-integrated X-ray flux transmitted through the sample was measured with a PIN-diode attached to the beamstop. Scattering from the buffer solution was measured in the same capillary at the same positions before the measurement of the sample solution, using the same protocol. The 20 image frames from each position in the sample (buffer) capillary

were normalized with the transmitted fluence and radially binned to obtain an I vs q curve.

Basic scattering parameters (radius of gyration R_g, forward scattering intensity I(0) and maximum diameter D_max) and the distance distribution function p(r) were determined from the Guinier plot and by inverse Fourier transform with the program GNOM (Svergun, 1992). Dummy atom modeling was made with the program DAMMIF (Franke and Svergun, 2009).

4 Results and discussion

This section of the thesis contains the description of protein cloning, expression, purification, crystallization, and functional studies of Spire – an actin nucleating protein.

4.1 Cloning, purification, crystallization and structure determination

4.1.1 Construct design and cloning

The principles of constructs designing are presented in Chapter 3.2.1. A detailed list of constructs used in this work is shown in Figure 4.1 and Table 4.1.

Table 4.1 List of Spire constructs used in this work.

No.	Construct name	Primers	Vector	Expression in *E. coli*
1.	SpireNT (1-520)	1, 25	pET 16b	high, soluble
2.	SpireABCD (371-520)	13, 25	pGEX-6P-1	low, aggregates
3.	SpireABCD (367-485)	11, 5	pGEX-6P-1	high, insoluble
4.	SpireABCD (371-485)	13, 5	pGEX-6P-1	high, soluble
5.	SpireBCD (396-520)	7, 25	pGEX-6P-1	low, aggregates
6.	SpireBCD (396-485)	7, 5	pGEX-6P-1	high, soluble
7.	SpireAB (371-419)	28, 29	pGEX-6P-1	high, soluble
8.	SpireBC (396-450)	30, 31	pGEX-6P-1	high, soluble
9.	SpireCD (428-485)	3, 5	pGEX-6P-1	high, soluble
10.	SpireA (371-388)	26, 27	pGEX-6P-1	moderate, soluble
11.	SpireB (396-419)	28, 29	pGEX-6P-1	moderate, soluble
12.	SpireC (428-450)	30, 31	pGEX-6P-1	moderate, soluble
13.	SpireD (461-485)	32, 33	pGEX-6P-1	high, soluble
14.	SpireC-L3 (428-460)	8, 9	pGEX-6P-1	moderate, soluble
15.	SpireL3-D (448-485)	6, 5	pGEX-6P-1	high, soluble
16.	SpireL3	36, 37	pGEX-6P-1	-
17.	SpireDD	14, 15, 16, 17	pGEX-6P-1	high, soluble
18.	SpireDDD	14, 15, 16, 17, 18, 19	pGEX-6P-1	very high, soluble

19.	SpireABCD-Lx-Thelix*	13, 20, 21, 22, 23, 24	pGEX-6P-1	moderate, soluble
20.	SpireBCD-Lx-Thelix*	7, 20, 21, 22, 23, 24	pGEX-6P-1	moderate, soluble
21.	SpireABCD-Ly-Thelix*	34, 35**	pGEX-6P-1	high, soluble
22.	SpireBCD-Ly-Thelix*	34, 35**	pGEX-6P-1	high, soluble
23.	KIND(90-328)	10, 12	pGEX-6P-1	very low, soluble
24.	KIND(1-365)-CD	1, 2, 4, 5	pGEX-6P-1	moderate, soluble

Lx - ITPPEA; Ly – ITPPEAAAA

- constructs produced by site directed mutagenesis, see Chapter 3.2.1.

Physicochemical properties of constructs, such as their theoretical isoelectric points (pI), molecular masses (MW) and extinction coefficients (E_{280}) are shown in Table 4.2. The physicochemical parameters were calculated on the basis of the amino acid composition with the aid of the program ProtParam on www.expasy.org.

Table 4.2 Physicochemical properties of Spire constructs.

No.	Construct name	MW (Da)	E_{280} (M^{-1} cm^{-1})	pI
1.	SpireNT (1-520)	58976.9	34420	4.47
2.	SpireABCD (371-520)	17482.4	4470	10.04
3.	SpireABCD (367-485)	13971.4	9970	10.05
4.	SpireABCD (371-485)	13410.7	4470	9.94
5.	SpireBCD (396-520)	14463.9	2980	10.00
6.	SpireBCD (396-485)	10392.3	2980	9.86
7.	SpireAB (371-419)	5913.9	4470	9.77
8.	SpireBC (396-450)	6378.6	2980	9.90
9.	SpireCD (428-485)	6665.8	0	9.89
10.	SpireA (371-388)	2147.5	0	10.90
11.	SpireB (396-419)	2895.5	2980	9.41
12.	SpireC (428-450)	2652.1	0	9.99
13.	SpireD (461-485)	2863.3	0	8.90
14.	SpireC-L3 (428-460)	3820.5	0	10.02
15.	SpireL3-D (448-485)	4304.9	0	8.22
16.	SpireL3	1459.6	0	6.28

17.	SpireDD	6159.2	0	9.75
18.	SpireDDD	9611.1	125	9.76
19.	SpireABCD-Lx-Thelix	15033.5	4470	9.75
20.	SpireBCD-Lx-Thelix	12015.1	2980	9.63
21.	SpireABCD-Ly-Thelix	15246.8	4470	9.75
22.	SpireBCD-Ly-Thelix	12228.3	2980	9.63
23.	KIND(90-328)	27310.7	18700	4.71
24.	KIND(1-365)-CD	47413.5	18950	5.10

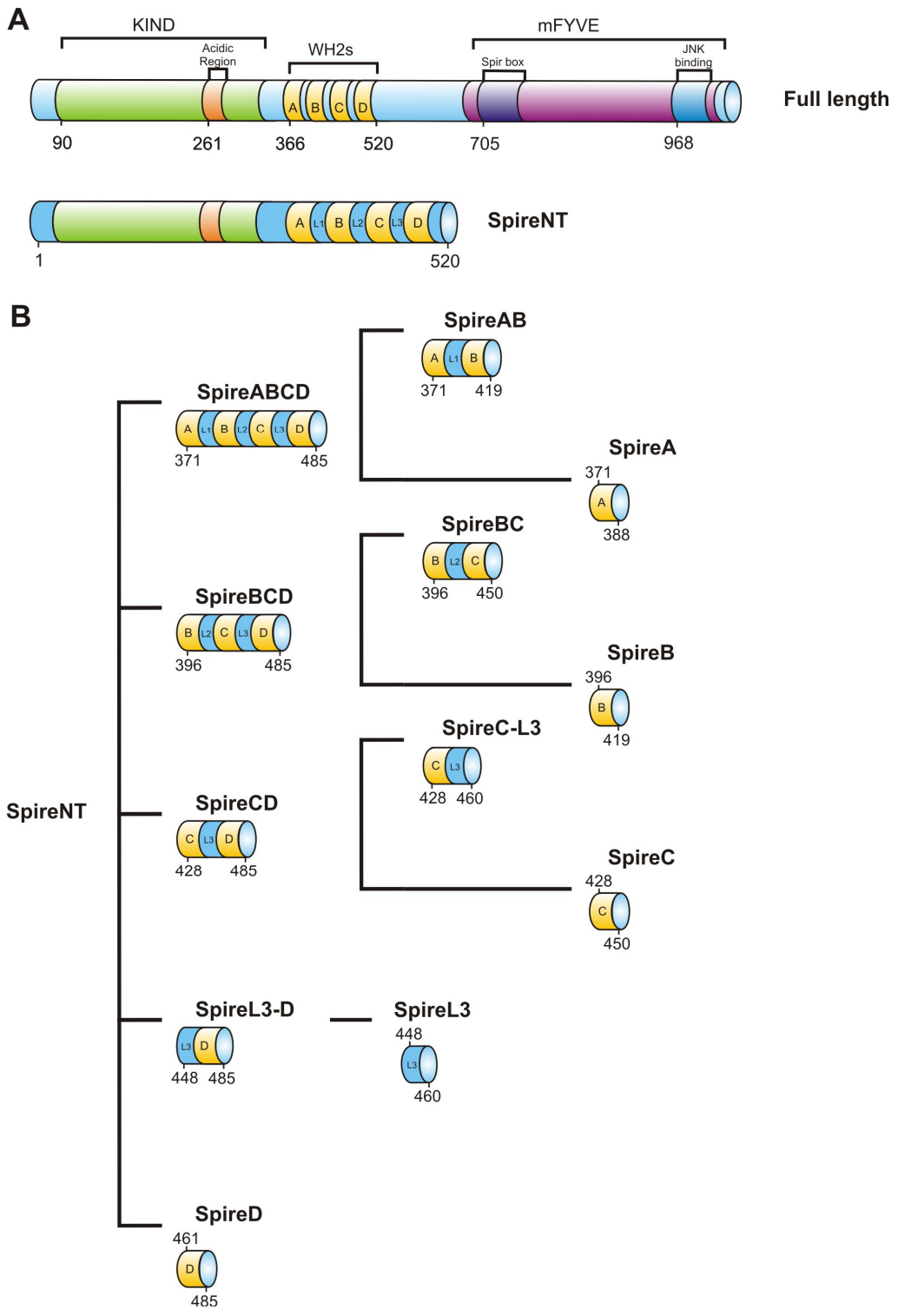

Figure 4.1 Constructs of Spire. (A) Domain organization of Spire from *Drosophila melanogaster* (upper scheme); the first construct used in this work was named SpireNT (lower scheme). (B) Workflow of Spire constructs generation.

4.1.2 Expression and purification

Purification of all Spire constructs followed a similar protocol, involving two different liquid chromatography steps: affinity chromatography on sepharose-glutathione or Ni-NTA resin, followed by the size exclusion chromatography on Superdex 200, Superdex 75, or Superdex 30 depending on the molecular weight of the protein.

4.1.2.1 Expression and purification of Spire constructs

Twenty four constructs of Spire that differed in length were expressed in *E. coli*. All of them were produced as a GST-Spire fusion protein except the SpireNT, which contained the N-terminal His-tag. The yields of expression, solubility, and stability depended on the used construct (Table 4.1). The pure Spire proteins were obtained in flow-through after cleavage of the GST-Spire fusion protein bound to the sepharose-glutathione resin. The final gel filtration resulted in pure and homogenous proteins. Mass spectrometry and the N-terminal Edman sequencing were applied to confirm quality of produced proteins. Majority of Spire constructs were soluble and could be expressed in amounts sufficient for further studies. Only one construct (SpireABCD (371-485)) was insoluble, and two constructs of SpireABCD and SpireBCD with C-terminus extended up to position 520, were produced in low yields and tended to aggregate. The elution profiles from gel filtration and SDS-PAGE analysis of selected constructs are shown in Figures 4.2 – 4.4.

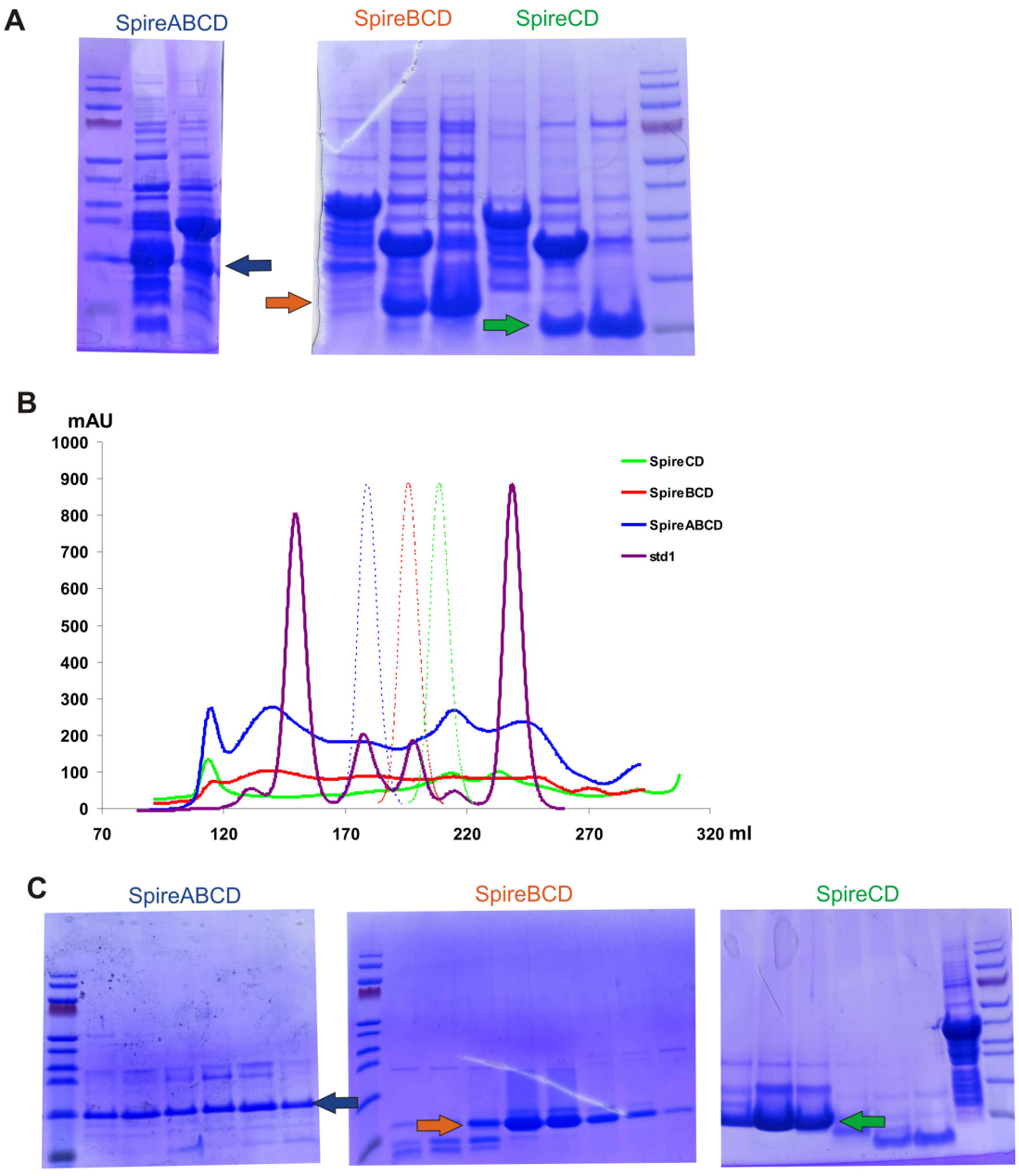

Figure 4.2 Expression and purification of SpireABCD, SpireBCD, and SpireCD. (A) SDS-PAGE analysis of the GST-Spire fusion protein cleavage by the PreScission protease. (B) Elution profiles of SpireABCD, SpireBCD and SpireCD from Superdex 75. (C) SDS-PAGE analysis of peaks' fractions eluted from the column.

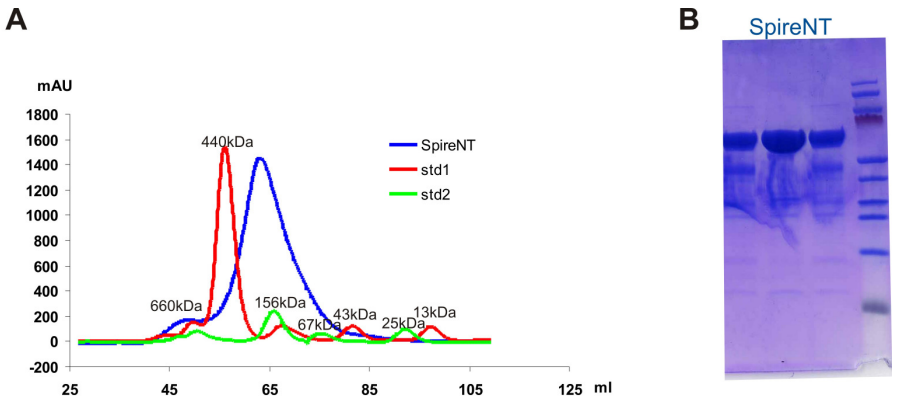

Figure 4.3 Purification of SpireNT. (A) Elution profiles of SpireNT from Superdex 200. (B) SDS-PAGE analysis of peaks' fractions eluted from the column.

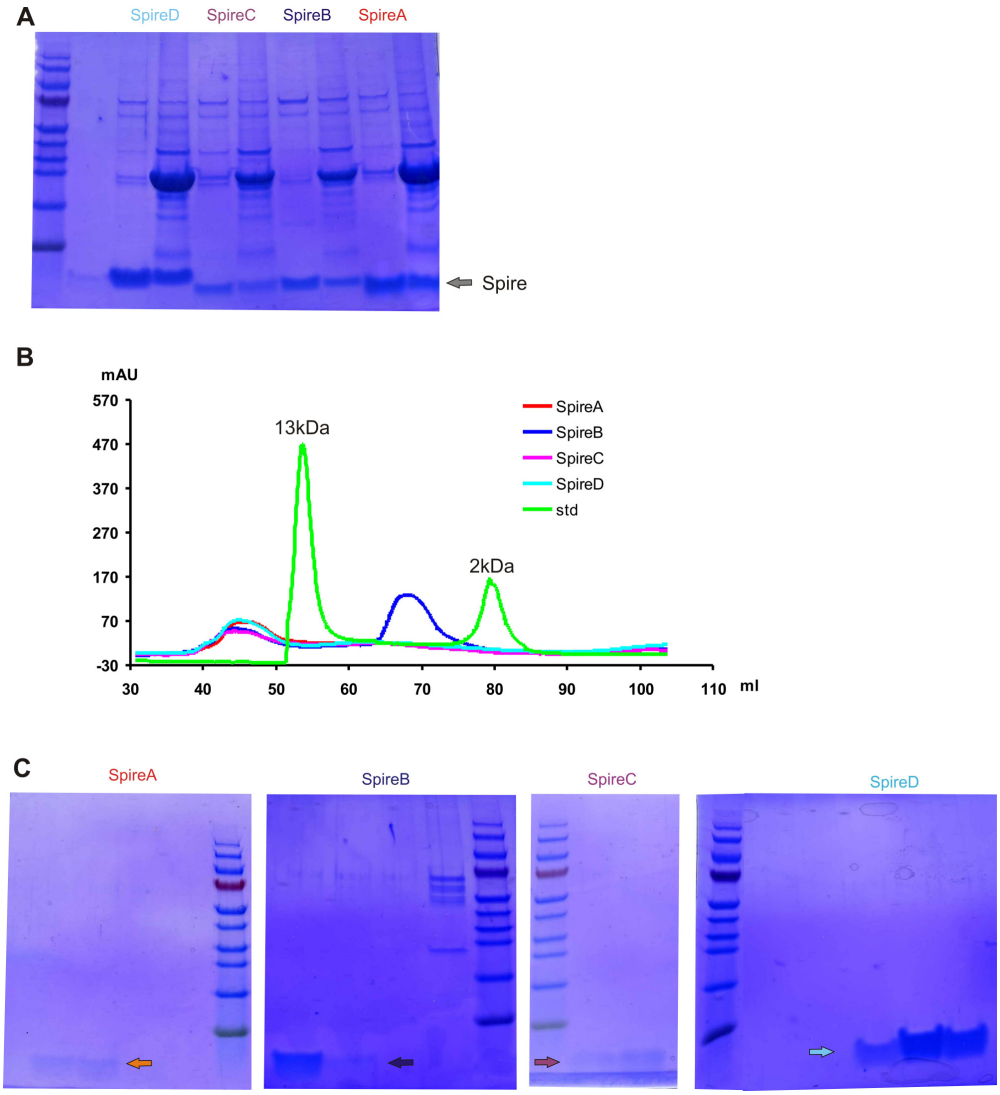

Figure 4.4 Expression and purification of SpireA, SpireB, SpireC and SpireD. (A) SDS-PAGE analysis of the GST-Spire fusion protein cleavage by PreScission protease. (B) Elution profiles of SpireA, SpireB, SpireC and SpireD from Superdex 30. (C) SDS-PAGE analysis of peaks' fractions eluted from the column.

4.1.3 Structural and functional studies

In order to physicochemically characterize the binding properties of Spire, NMR analyses and gel filtration mobility shift assays were performed for several constructs of Spire. Both NMR and gel filtration data showed that SpireABCD, SpireBCD, SpireDDD, SpireCD, and single WH2 of SpireC and SpireD bind four, three, three, two, and one actin molecules, respectively, and create tight and stable complexes with actin.

4.1.3.1 Gel filtration mobility shift assay

In gel filtration, peaks of the complexes from Superdex 200 were sharp and clearly separated from the unbound actin and the sizes of the complexes were determined by the number of WH2 domains in the constructs, which correlated with the number of bound actins. The elution profiles of the unbound monomeric AP-actin, the mutant that was used for crystallization of Spire/actin complexes (Rould et al., 2006), as well as wild type rabbit muscle actin complexed with latrunculin B, were similar to the elution profile of ovalbumin (43 kDa, Stokes radius – 30.5 Å). Because of the expected elongated shape of the complexes, the Stokes radii of complexes of SpireCD, SpireBCD, and SpireABCD were larger than for globular proteins of molecular weight 92, 136, 182 kDa, respectively (Figure 4.5). This, however, did not complicate the analysis because the binding of an additional actin per one WH2 domain more, caused a significant shift in the peak position, well resolved from the species with one actin/WH2 unit less.

Filtration data are, as expected, in agreement with the stoichiometry of Spire-actin binding determined by Bosch et al. (2007), Rebowski et al. (2008), and Quinlan et al. (2005), who found that, for example, the NT-SpireABCD “binds four actin monomers in a tight nonpolymerizable complex” (Bosch et al., 2007). The minimal functional core of the protein that still can assemble actin filaments contains the C-terminal half of the Spire WH2 cluster (SpireCD), which precisely is composed of WH2-C, L-3 and WH2-D (residues 428-485) (Quinlan et al., 2005).

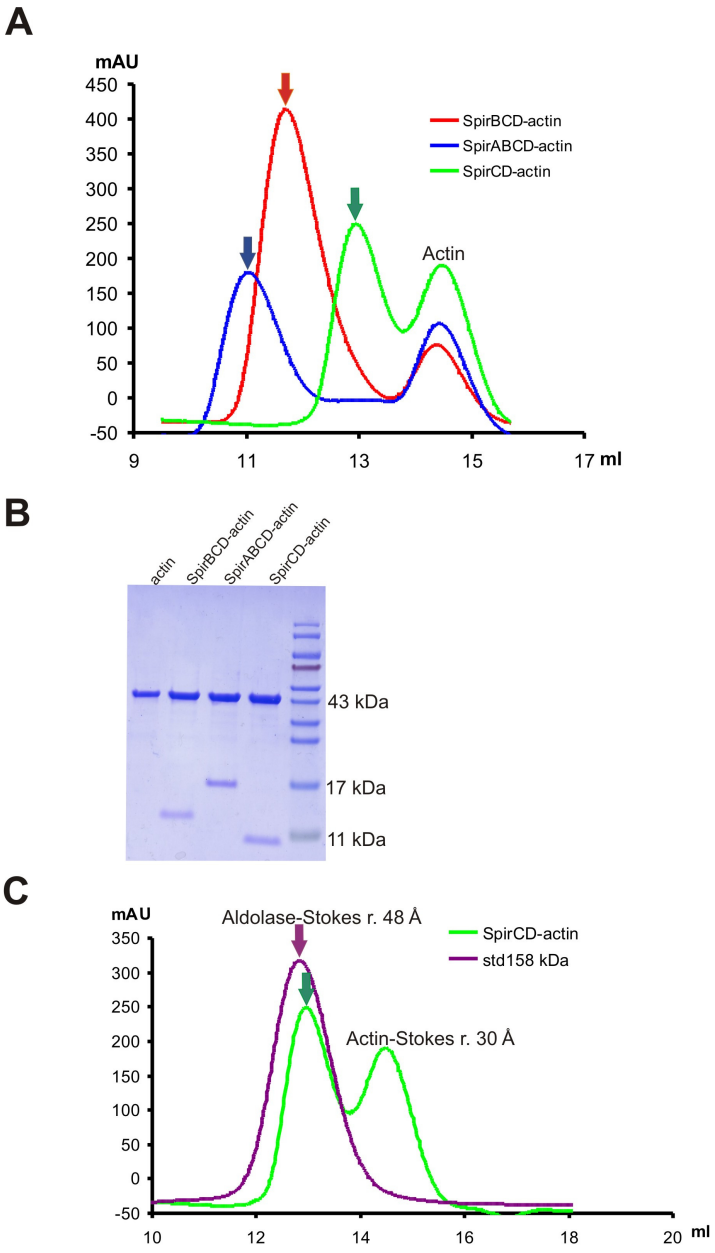

Figure 4.5 Purification of Spire-actin complexes. (A) A Superdex 200 elution profile of SpireCD/AP-actin (green), SpireBCD/AP-actin (red), SpireABCD/AP-actin (blue). Spire and actin form tight and stable complexes clearly separated from monomeric actin. (B) SDS-PAGE analysis of peaks' fractions eluted from the column. (C) Comparison of the SpireCD-actin complex (green) with the molecular weight standard – aldolase (158 kDa; Stokes radius - 48 Å) (violet).

4.1.3.2 NMR studies

NMR indicates that free SpireCD, as well as SpireNT and all other tested constructs are not structured in solution giving a typical NMR spectrum of the polypeptide chain in a random conformation (Figures 4.6 and 4.7) (D'Silva et al., 2005; Wüthrich, 1986). On forming the complex with actin, most of the NMR signals (blue) of SpireCD disappear (Figure 4.7). This is because upon binding the SpireCD residues participate in a well-defined structure of a large SpirCD/actin complex (D'Silva et al., 2005; Wüthrich, 1986). The observed $1/T_2$ transverse relaxation rate of the bound Spire in the complexes increases thus significantly and broadening of NMR resonances results in the disappearance of its signals in the spectra. No strong, sharp NMR signals are visible in the blue spectrum of the complex indicating that there are no highly flexible residues present in the actin bound SpireCD.

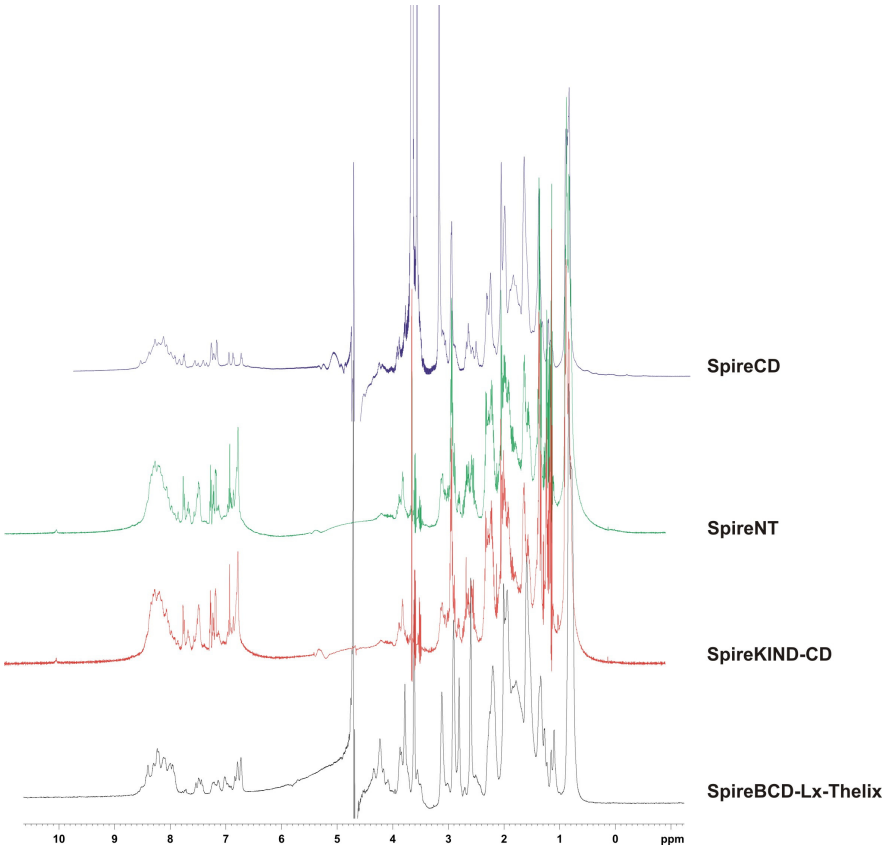

Figure 4.6 Characterization of SpireCD, SpireNT, SpireKIND-CD and SpireBCD-Lx-Thelix structures by one-dimensional proton NMR spectra.

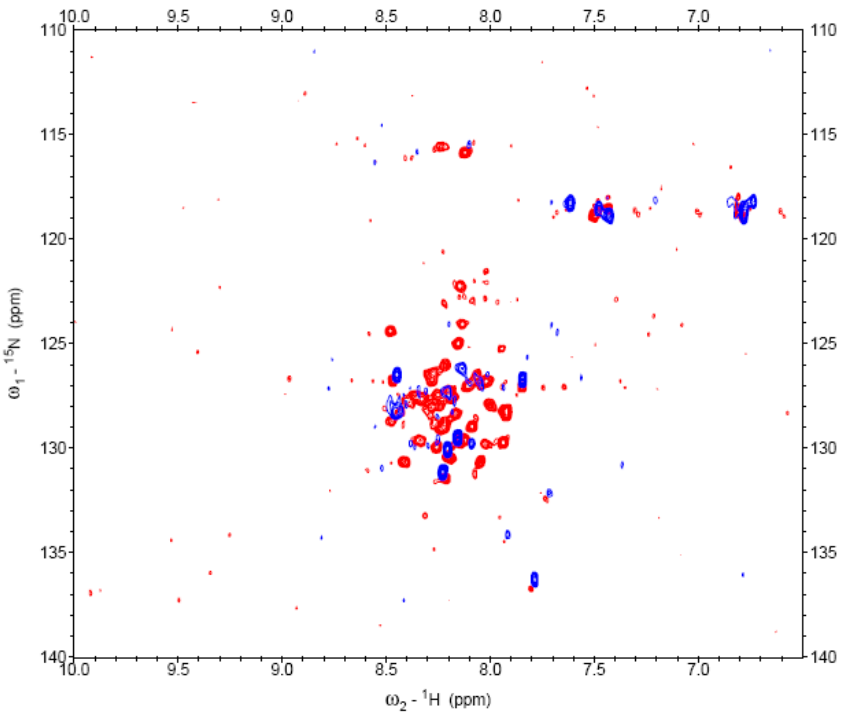

Figure 4.7 Titration of the ^{15}N-labeled SpireCD with unlabeled (^{14}N) AP-actin. The ^{15}N-HSQC spectra of SpireCD before (red), and after addition of actin (blue). Only ^{1}H-^{15}N NMR signals of SpireCD are visible.

4.1.3.3 Pyrene-actin assays

The interaction of SpireBCD with G-actin was studied by fluorescence spectroscopy (Figure 4.8). The monomeric pyrene-actin shows only a very low signal. Therefore, the Spire construct which contains 3 WH2 domains was primed with pyrene-actin at a molar ratio of 2:3 actin: WH2 domains. Under these conditions the actin remains in its G-configuration. The stepwise titration of G-actin into a SpireBCD solution aims at the appearance of the first F-actin signal mediated by pyrenylated G-actin. We find the first F-actin signal only after all three WH2 domains of BCD have been filled with one actin monomer each. The addition of a fourth, even unlabeled G-actin caused a previously non-fluorescent pyrenylated G-actin in the BCD/3xactin complex to change into a fluorescent pyrenylated F-actin (this spectrum is shown in grey in Figure 4.8). It is essential for this assay that the addition of unlabeled actin after the

appearance of the first F-actin signal mediated by pyrenylated G-actin can lead to an increased fluorescence signal only if the preloaded pyrenylated G-actin is transformed into its F-actin conformation. This was the case when unlabeled actin was added beyond the 1:1 ratio of actin: WH2 domains (Figure 4.8). The data thus suggest a stepwise integration of the WH2-bound G-actins into an emerging F-actin nucleus.

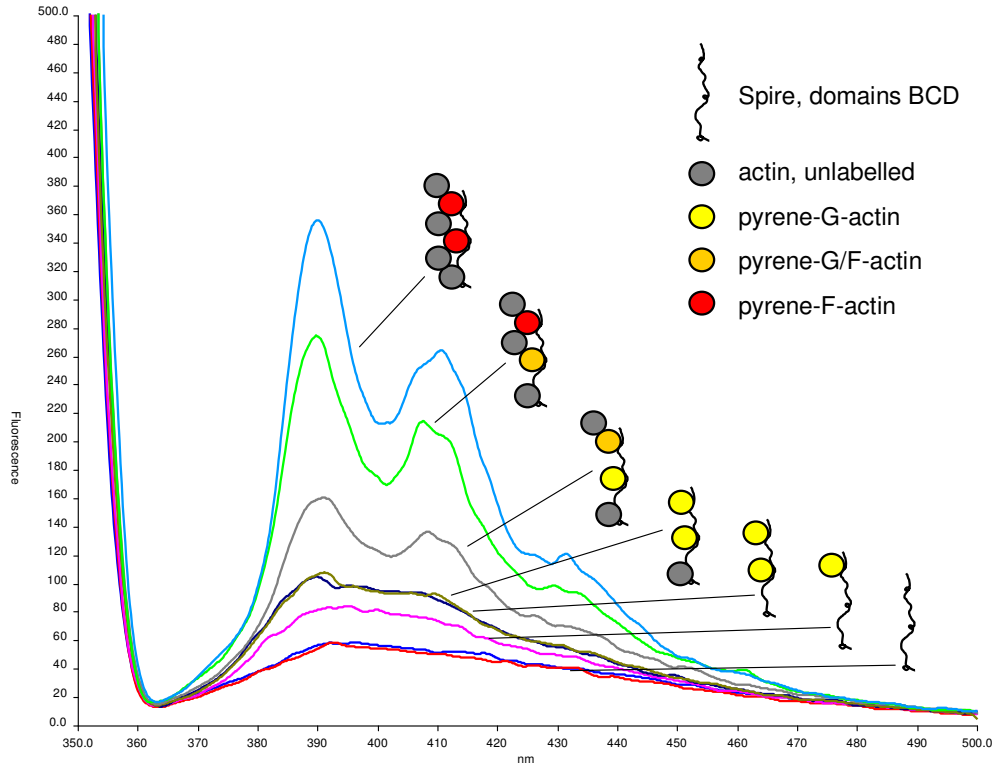

Figure 4.8 Fluorescence emission spectra of SpireBCD titrated stepwise with a two molar excess of pyrene-actin followed by the addition of unlabeled G-actin. 0.2 µM SpireBCD (red, buffer only: blue) was incubated with 2 x 0.2 µM pyrene-actin (purple, olive) which lead to the expected small fluorescence increase of pyrenylated G-actin. Addition of 0.2 µM of unlabeled G-actin (dark blue) did not change this basic level of fluorescence. Only further addition of unlabeled actin in 0.2 µM aliquots (grey, green, light blue) raised the pyrene signal as it is typical for pyrenylated F-actin which is completely integrated in a filament. The cartoons show the putative mechanism of the stepwise formation of an F-actin nucleus along Spire WH2 domains. The cartoons at

the right do not imply a specific binding order of actins, they just highlight the first and most-likely formation of an F-actin in the complex.

4.1.4 Structures of Spire-actin complexes

4.1.4.1 Crystallization

Purified SpireABCD, SpireBCD as well as SpireDDD, and SpireCD were mixed with AP-actin at a molar ratio of 1:4.1, 1:3.1 and 1:2:1, respectively, and separated by gel filtration on Superdex 200 (GE Healthcare) in 5 mM Tris (pH 7.0), 50 mM NaCl, 0.2 mM ATP, and 5 mM β-mercaptoethanol. Fractions from the peaks shown in Figure 4.5 were analysed by SDS-PAGE, pooled, and concentrated to 10-12 mg/ml. The complexes were crystallized both at 4ºC and 20ºC in a several crystallization conditions, using the sitting and hanging drop vapour diffusion method. The 2-3 µl drops consisted of a 1:1 or 2:1 (vol/vol) mixture of protein solution and a well solution. Crystals appeared after 2 days and grew to the final size after 2-4 weeks of incubation.

The best diffracting crystals of the SpireABCD/AP-actin, SpireBCD/AP-actin, SpireDDD/AP-actin complexes grew in 0.2 M ammonium formate pH 6.6, 20% PEG 3350 and the crystals of SpireCD/AP-actin appeared in 0.2 M ammonium sulphate, 0.1 M MES pH 6.5, 20% PEG 8000. All crystals were soaked in cryo-solutions containing mother liquor supplemented with 20% MPD or glycerol and were flash frozen in liquid nitrogen. Crystals of the SpireD/actin-latrunculin B complex appeared after one week at 4ºC in the solution containing 0.2 M magnesium formate, pH 5.9 and 20% PEG 3350. Crystals were treated as described above. To exclude the possibility of proteolytic cleavage of Spire during crystallization, several crystals of the complexes were dissolved and analyzed by SDS-PAGE and mass spectrometry, proving that both SpirCD and SpirBCD remain intact during crystallization.

The list of conditions in which crystals appeared is presented in Appendix Table 6.1.

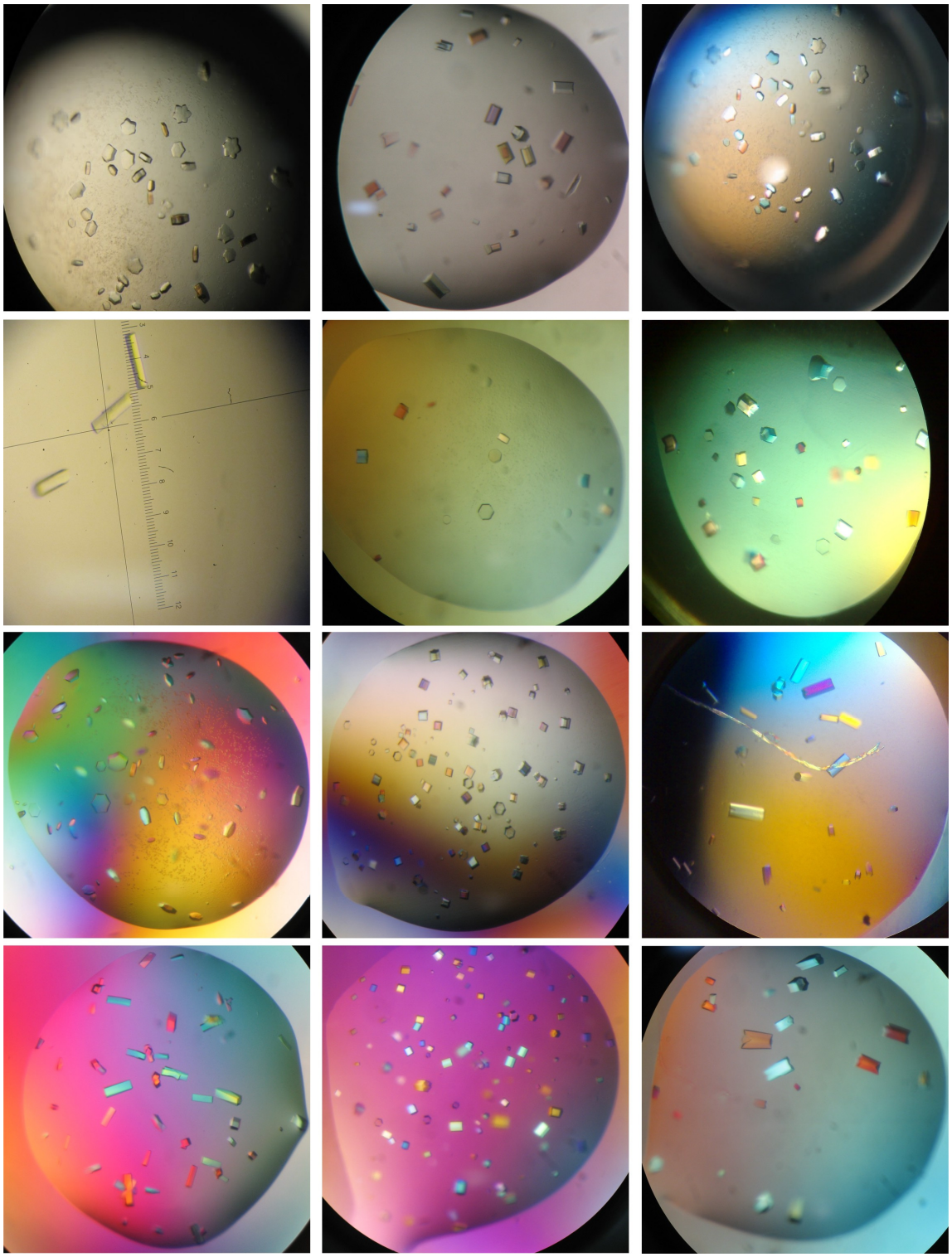

Figure 4.9 Selected crystals of different Spire/actin complexes, obtained from different crystallization conditions. Most crystals appeared after few days at 4ºC.

4.1.4.2 Structure determination

X-ray data of the SpireD/actin-latrunculin B (1.6 Å), SpireBCD/AP-actin (2.0 Å), SpireABCD/AP-actin (2.2 Å), SpireDDD/AP-actin (2.1 Å) and SpireCD/AP-actin (2.6 Å) were collected on the SLS beamline PXII at the Paul Scherrer Institut, Villigen, Switzerland. The data sets were integrated, scaled and merged with the XDS and XSCALE programs (Kabsch, 1993) in space group $P2_12_12_1$ for SpireD-actin-latrunculin B, $P6_5$ for SpireCD/AP-actin, SpireABCD/AP-actin, SpireDDD/AP-actin and $P2_1$ for SpireBCD/AP-actin (Table 4.3). The structures were determined by molecular replacement using the Molrep program from the CCP4 suite (CCP4, 1994) and the structures of the AP-actin and rabbit skeletal muscle actin complexed with latrunculin A as a search model. Model building and refinement were carried out with the program XtalViev/Xfit (McRee, 1999) and REFMAC5 (CCP4, 1994). Data collection, refinement and statistics are shown in Table 4.3.

Table 4.3 Data collection and refinement statistics.

	SpirD	SpirCD	SpirBCD	SpirABCD	SpirDDD
Data collection					
Space group	$P2_12_12_1$	$P6_5$*	$P2_1$*	$P6_5$	$P6_5$
Cell constant:					
A	52.96	125.51	125.30	126.08	125.82
b	71.81	125.51	55.95	126.08	125.82
c	100.72	56.1	125.37/ β=120.036	56.37	56.02
Resolution range (Å)	50-1.5	50-2.6	50-2.0	50-2.2	50-2.1
Observed reflections	380081	84313	339766	228321	266481
Unique reflections	49209	11584	82718	22506	26371
Whole resolution range:					
Completeness (%)	79.0	73.6	80.8	76.2	86.4
Rmerge	4.9	8.6	5.6	6.7	3.0
I/σ (I)	21.4	12.6	19.0	15.54	32.6
Last resolution shell:					
Resolution range (Å)	1.5-1.6	2.6-2.8	2.0-2.1	2.2-2.3	2.1-2.2
Completeness (%)	38.1	40.5	47.6	38.5	36.9
R_{merge}	20.3	29.7	19.5	26.9	23.6
I/σ (I)	4.4	4.4	5.0	3.9	4.0
Refinement					
No. of reflections	46688	9783	85442	20832	23718
Resolution (Å)	39-1.5	25-2.8	20-1.6	50-2.0	50-2.0
R-factor (%)	17.2	25.1	16.3	18.4	25.6
R_{free} (%)	21.6	33.0	22.9	25.1	27.5
Average B (Å2)	19.8	48.9	31.3	42.8	57.8
R.m.s bond length (Å)	0.027	0.012	0.03	0.018	0.006
R.m.s angles (°)	2.4	1.5	2.5	1.5	0.9
Content of asymmetric unit					
No. of complexes	1	1	3	1	1
No. of protein residues/atoms	367/3418	381/2949	1132/9468	377/2912	378/2967
No. of solvent atoms	489	-	915	142	63
PDB Data Bank ID code	3MN5	3MMV	3MN6	3MN9	3MN7

*Space groups $P6_5$ and $P2_1$ are equivalent (See the section: Crystal structures of the SpirCD/AP-actin, SpirBCD/AP-actin, SpirDDD/AP-actin and SpirABCD/AP-actin complexes.)

4.1.4.3 Overall structures

Crystal structure of a single WH2 domain of Spire and actin

A high-resolution structure of the SpireD/actin-latrunculin B complex was determined at up to 1.6 Å in space group $P2_12_12_1$ and a unit cell a = 52.96 Å, b = 71.81, Å c = 100.72 Å by the Patterson search molecular replacement using the model of rabbit actin (PDB: 1NWK) (Graceffa and Dominguez, 2003). The overall structure of the single WH2 domain is similar to those previously solved structures of WASP, WAVE, WIP (PDB: 2A32, 2A40, 2A41), (Chereau et al., 2005), N-WASP (PDB: 2VCP), and Ciboulot (PDB: 1SQK), (Hertzog et al., 2004) (Figure 4.10A). SpireD comprises residues Ser449-Glu484; Pro461 is the first residue defined by the electron density, which, at the C-terminal part, is truncated after Ile480. The structure of the SpireD WH2 consists of a three-turn amphipatic α-helix, whose hydrophobic side includes the highly conserved residues Leu467, Met468, and Ile471 (Figure 4.10). These residues are bound in the hydrophobic cleft formed between subdomains 1 and 3 at the barbed end of the actin monomer followed by the approximately ten amino acids long C-terminal tail covering the surface of actin between subdomains 2 and 4.

The conserved Leu477, belonging to the LKQI motif, directly interacts with the hydrophobic pocket of actin residues Ile341 and Ile345 (Figure 4.10A right panel). This interaction appears to be essential for the binding of the C-terminal end of the SpireD WH2 domain to actin; however, the long-range electrostatic interaction between Spire's Lys478 and Lys475 with a negatively charged surface formed by actin the Asp24, Asp25, should also contribute to the binding. Additionally, the entire C-terminal tail of Spire, between Arg462 and Ile480, is stabilized by hydrogen bonds created by the guanidinium group of the Spire Arg472, which is the last amino acid of the α-helix, with both the hydroxyl group of the actin Thr148, and the carboxyl group of the actin Glu167, and the ε-amino group of the Spire Lys475 is hydrogen-bonded to the hydroxyl group of the actin Ser348 (at the C-terminus). The side chain of the Spire Arg472 forms in addition a salt bridge with the actin Glu167 and Spire's Glu465, which may further stabilize Spire's α-helix. The N-terminal part of the α-helix directly interacts with

actin through hydrogen bonds formed between the side chain of Spire Arg464 and the carbonyl group of actin Glu167.

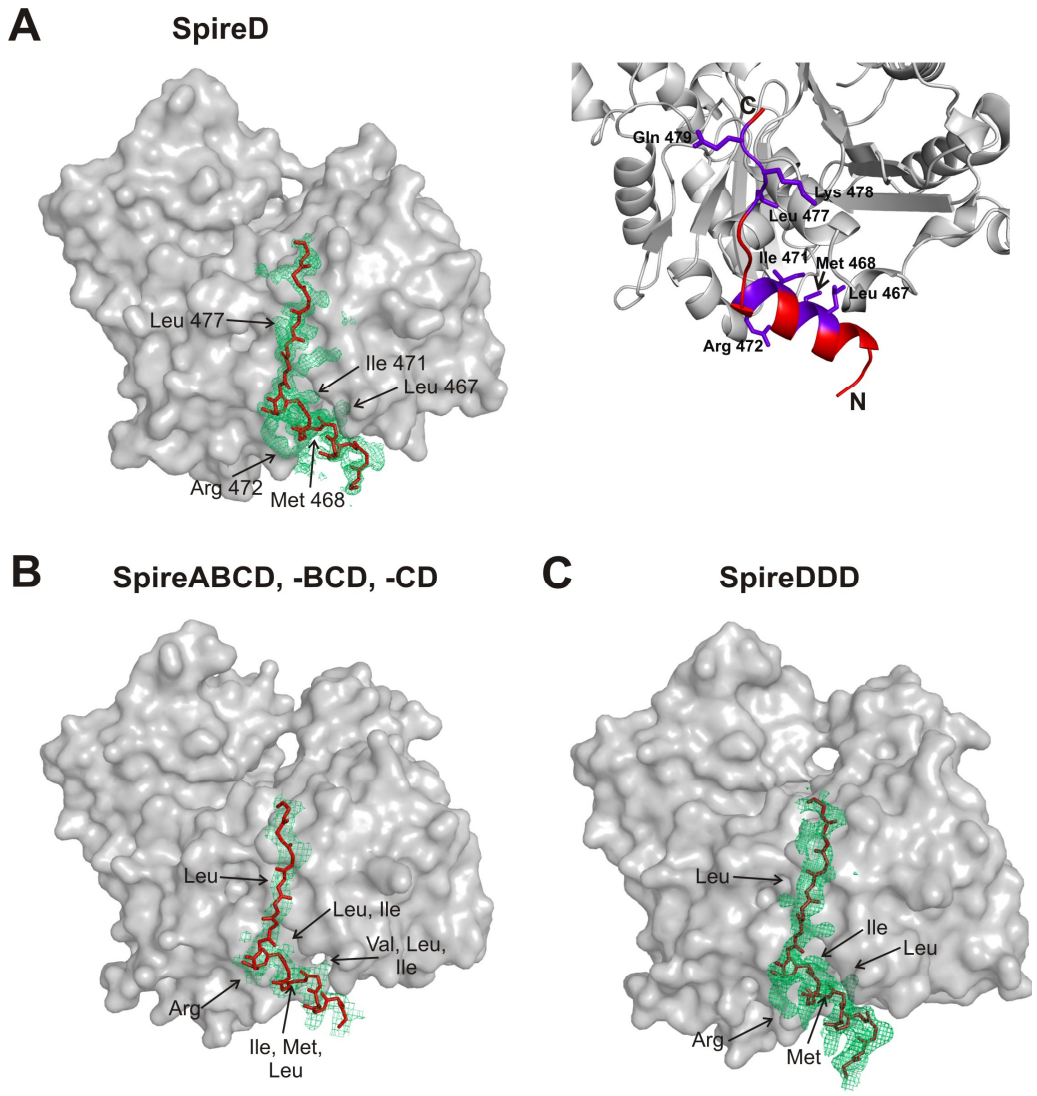

Figure 4.10 Structures of the WH2 domain of Spire (red and purple in right panel) and actin (grey). (A) Surface plot of the SpireD/actin-latrunculin B complex. (B) Surface plot of a single WH2-D domain of Spire bound to actin in the SpireDDD/AP-actin complex. (C) Conserved residues of the WH2 domain (purple).

Crystal structures of the SpireCD/AP-actin, SpireBCD/AP-actin, SpireDDD/AP-actin and SpireABCD/AP-actin complexes.

Complexes of SpireCD/AP-actin, SpireBCD/AP-actin, SpireDDD/AP-actin, and SpireABCD/AP-actin, which diffracted to 2.6 Å, 2.0 Å, 2.1 Å, and 2.2 Å, respectively, crystallize in the space group $P6_5$, with one molecule in the asymmetric unit (Table 4.3). Processing the SpireBCD/AP-actin data in the sub-group of lower symmetry, $P2_1$, and three actin molecules in the asymmetric unit, gave insignificantly better integration statistics (R_{meas} were 5.7% for $P2_1$ and 6.8% for $P6_5$). The analysis of the SpireBCD data were carried out in the lower symmetry to check for any differences in the electron densities among the three WH2 repeats and possibly to see electron density for the linker segments. This, however, was not materialized.

In all complexes entire actin molecules are well-defined in the electron density maps, except for the first three amino acids and the region between residues 39-49, which corresponds to the DNase I-binding loop in domain 2.

As expected from crystal symmetry and packing, the electron densities for the WH2 domains in all complexes correspond to one structure that resulted from averaging between the three B, C and D domains in the SpireBCD/AP-actin complex, two C and D domains in the SpireCD/AP-actin complex and four A, B, C and D domains in the SpireABCD/AP-actin, and three D domains in SpireDDD (Figure 4.10). Except for SpireDDD, we thus could not fit specific amino acids of WH2-A, WH2-B, WH2-C and WH2-D to the electron density (except for the conserved residues) and therefore a poly-alanine model of SpireABCD, SpireBCD and SpireCD was built in. The conserved residues of the three WH2 repeats marked in Figure 4.10 can be recognized, but have not well-defined electron densities (Figure 4.10B). The fact that there is no difference in the structures of the SpireBCD, SpireABCD and SpireCD obtained from the $P6_5$ and lower symmetry groups argues for the equivalent averaging of all WH2 domains.

It is important to realize that the “averaging” could result from two scenarios. The first possibility is the crystallization of a mixture of complexes where one actin binds one WH2 domain of SpireCD, SpireBCD, or SpirABCD,

with the rest of the WH2 domains having a random conformation. In this case the stoichiometry of the complex would be, for example for SpireCD: one actin molecule per one SpireCD. This scenario is not in agreement with the experimental data because we have always the binding of 2 actin molecules per one SpireCD and so on. In the second mechanism, the “averaging” in the crystals of SpireCD/AP-actin, SpireBCD/AP-actin, and SpireABCD/AP-actin results from the “shifted” binding of different WH2 domains to equivalent actins along the longitudinal arrangement of actins “columns” in the crystal. To unequivocally characterize the averaging seen in the crystals, an artificial Spire WH2 construct comprising three identical D repeats (SpireDDD) was prepared. The structure of the SpireDDD/AP-actin complex (Table 4.3, Figure 4.10C) has been solved and this structure unequivocally points towards the second mechanism, as now the side chains of the Spire helix are well determined by the electron density (Figure 4.10C). The fact that the electron density for the linkers between D-D modules is not seen in the maps suggests that these fragments may be flexible.

The structures show that the “averaged” WH2 domain of SpireABCD, SpireBCD, SpireCD and the D domain of SpireDDD binds between subdomains 1 and 3 of actin, and starting at the N-terminal part, forms a short 11-residue helix which further extends to the top of actin between subdomains 2 and 4 (Figures 4.10B and 4.13). The C-terminal tail of each of the WH2 domain is terminated around Asp25 of the actin molecule. In total, it gives 19 amino acids (glycines or alanines) that could be fitted into the electron density. Linkers L-2 and L-3, consisting of 11 and 12 amino acids, respectively, and L1 from SpireABCD containing 10 amino acids, have no electron density and are not visible in the structure (Figure 4.10).

The arrangements of the complexes in the unit cell of SpireCD, SpireBCD, SpireDDD and that of SpireABCD, are identical, but different from the organization of actin molecules in the crystals of the AP-actin alone (Rould et al., 2006) and that of our SpireD/actin-latrunculin B complex (Figure 4.11). In the Spire/actin complexes the actin-actin interfaces are through the sides of the actin

molecules on which the binding of Spire takes place (designated as the outer side of actin, Figures. 4.12A and 4.12B), whereas in actin alone and in the SpireD/actin-latrunculin B, the actin-actin interfaces are mostly through their inner sides – the parts of actins that participate normally in the central core of a filament (Figures 4.12B and 4.12C). This suggests that the specific arrangement of Spire/actin complexes is determined by the cluster of WH2 domains (although the crystal packing for short-range interactions between subdomains 1-3 of one actin molecule and subdomains 2-4 of the neighboring actins are solely determined by contacts between the large actin molecules) (Figure 4.11).

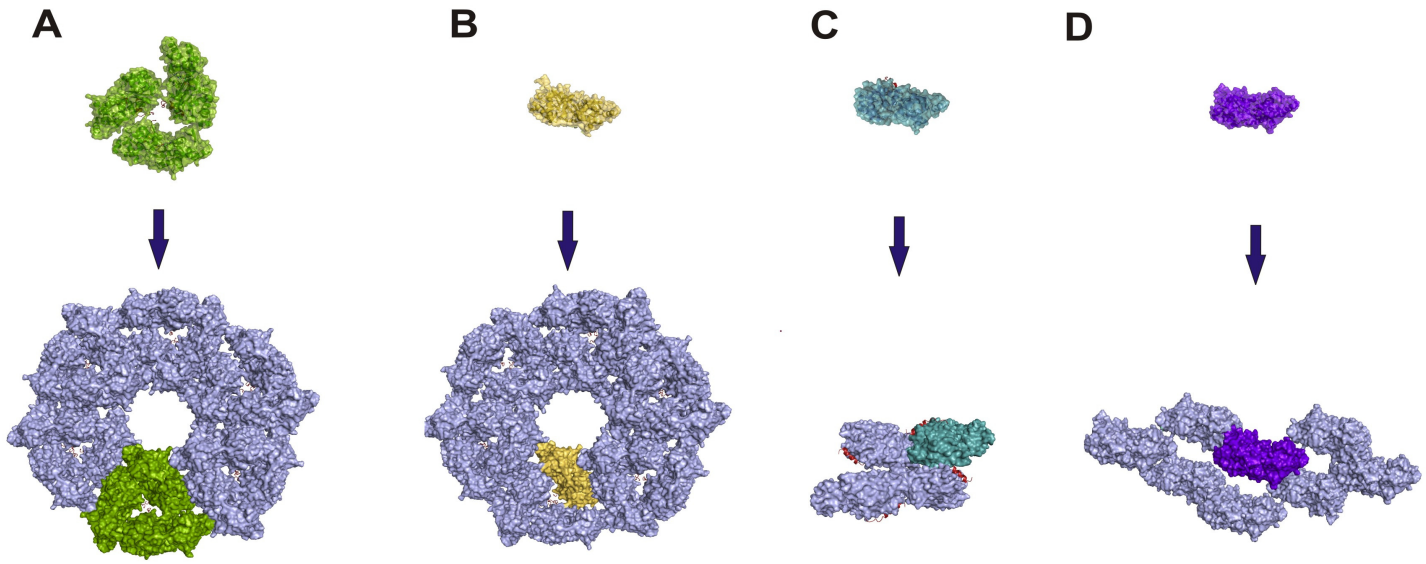

Figure 4.11 Crystal packing of different Spire/actin complexes and AP-actin alone. (A) SpireBCD/AP-actin, space group $P2_1$. (B) SpireCD/AP-actin, SpireABCD/AP-actin and SpireDDD/AP-actin, space group $P6_5$. (C) SpireD/actin-latrunculin B, space group $P2_12_12_1$. (D) AP-actin, space group C121 (PDB: 2HF4; Rould et al., 2006). Crystal packing of SpireBCD/AP-actin and SpireCD/AP-actin, SpireABCD/AP-actin and SpireDDD/AP-actin reveals that, despite different space groups, the arrangement of molecules in both crystals is similar. This suggests the influence of double and triple WH2 domains (in red) on the organization of actin in forming filaments. For comparison, the SpireD/actin-latrunculin B and AP-actin alone do not reveal similarities to the SpireBCD/AP-actin, SpireABCD/AP-actin, SpireCD/AP-actin and SpireDDD/AP-actin architectures.

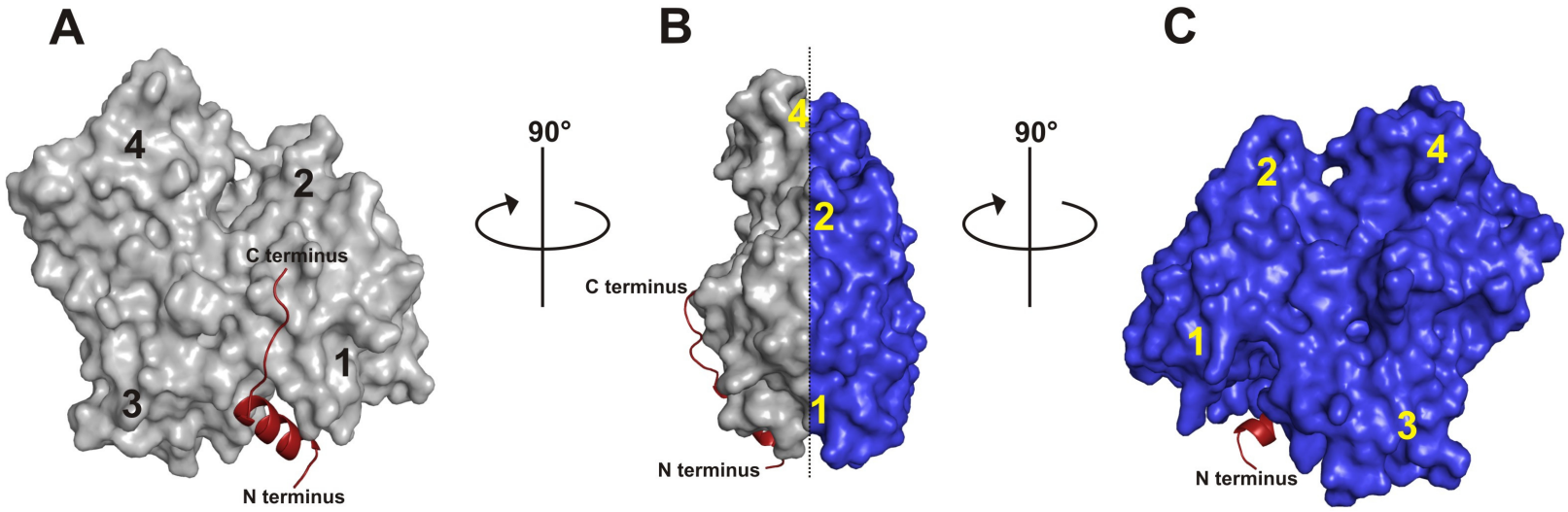

Figure 4.12 The sides of the actin molecule. (A) The front view of the outer side of the actin molecule (grey). (B) The side view, the outer side is in grey and the inner one in blue. (C) The front view of the inner side of actin (blue). The subdomains of actin are marked with numbers. Spire is depicted as ribbon plot and coloured red. This designation should not be confused with that of Holmes (1990).

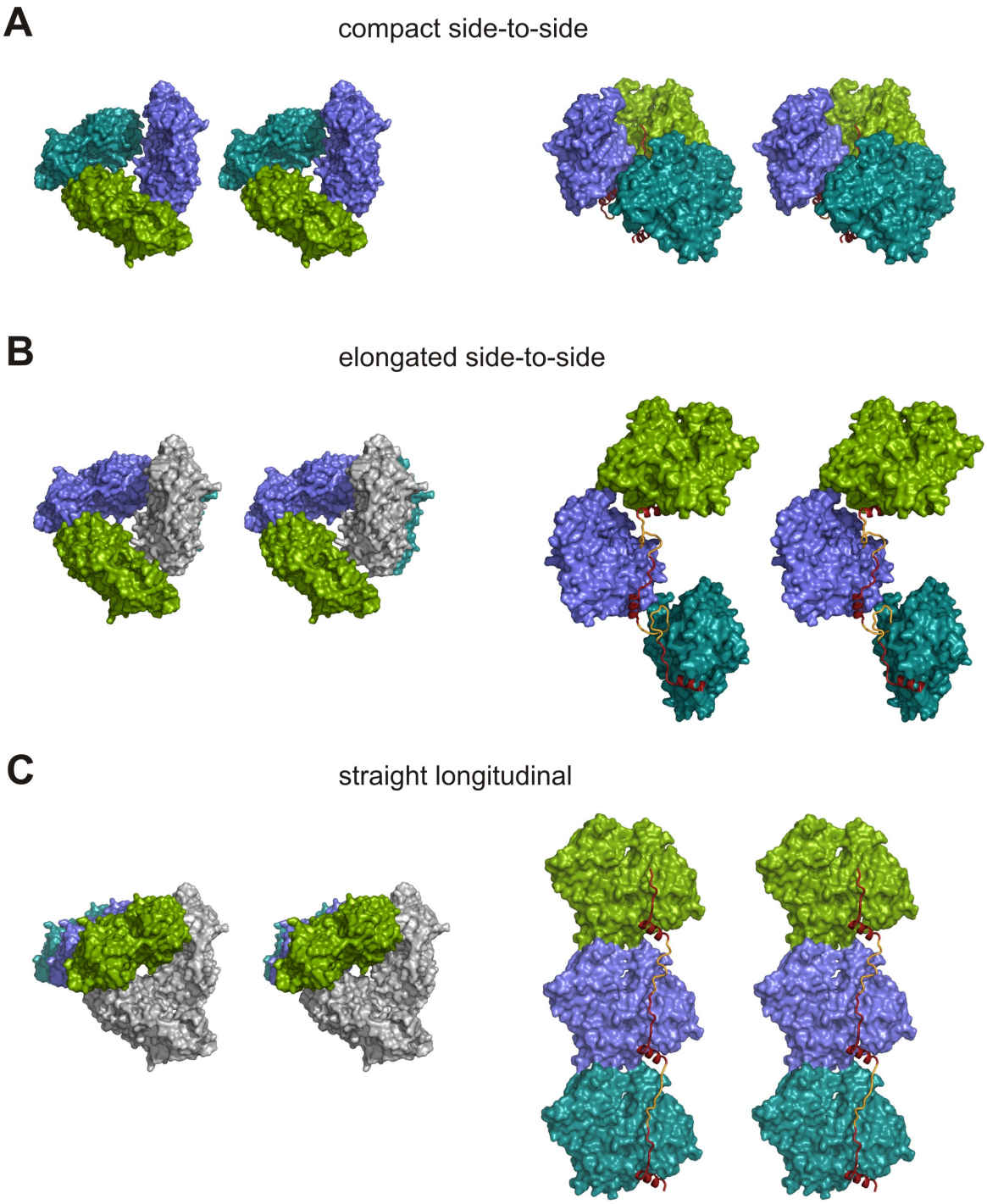

Figure 4.13 The two main architectures of packing in the SpireBCD/AP-actin crystal. Actin molecules are shown as surface plots; WH2 domains as ribbon plots in red/yellow. “Missing” linkers are depicted as ribbons and colored in yellow. Left panels represent a view along the axis of actin nucleation seed. Right panels are a side view ca. perpendicular to the long axis of the actin nucleation

seed. (A-B) show the “side-to-side” architectures. (A) The primary nucleus (colored green, blue and cyan) is built by the Spire/AP-actin complex inside one asymmetric unit (“compact side-to-side”). (B) The primary nucleus is built by the Spire/AP-actin complex, which belongs to two neighboring asymmetric units. Actin in grey belongs to the asymmetric unit that contains the two other actins in green and blue. (C) shows the “straight-longitudinal” architecture of packing in the SpireBCD/AP-actin crystal. In this model one molecule of actin (i.e. the molecule colored in green) and its two symmetry related ones (actins in blue and cyan) constitute an actin nucleation seed. Actins in grey belong to the asymmetric unit that contains the actin is shown in green.

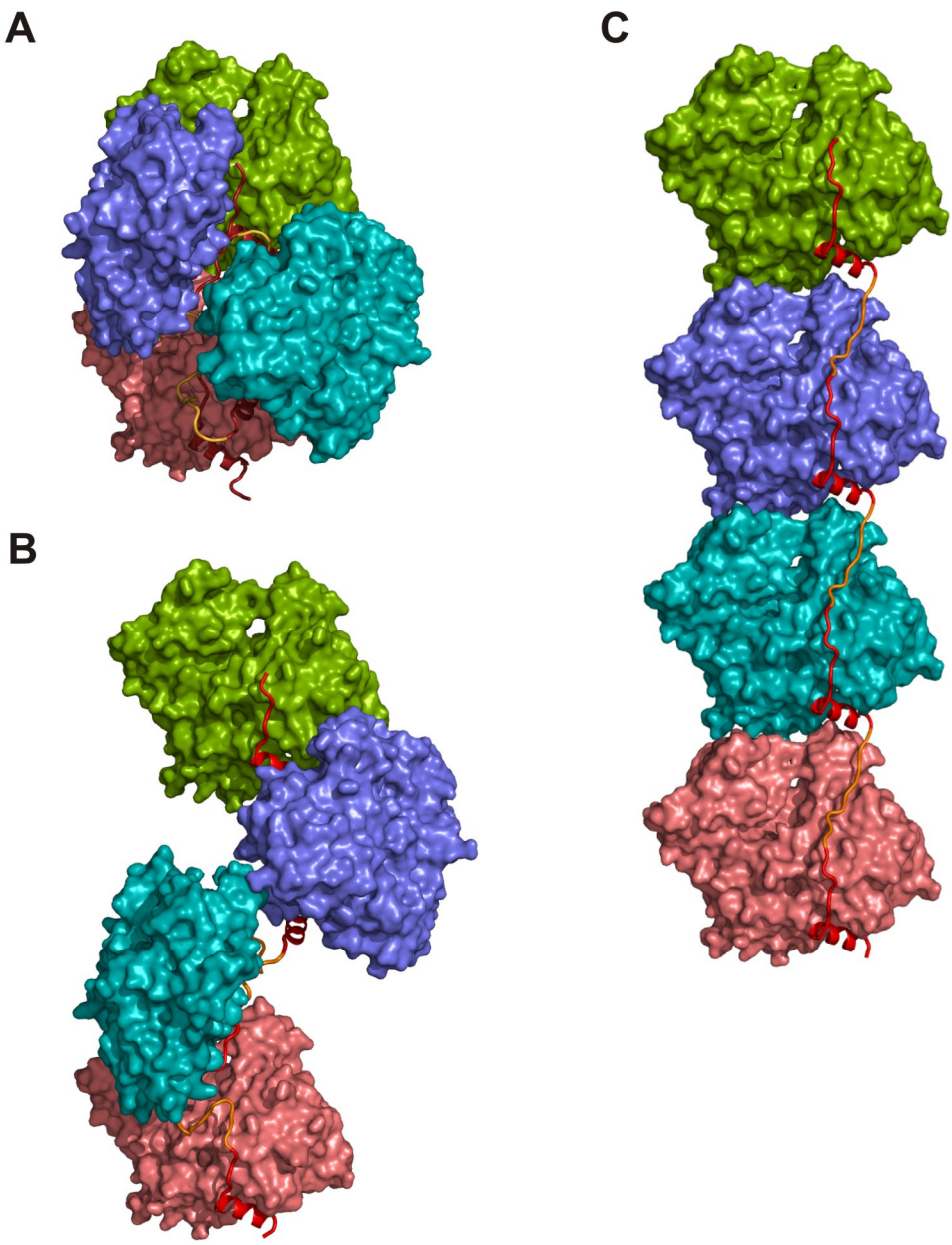

Figure 4.14 Representation of the SpireABCD/AP-actin complex in all possible configurations. (A) “compacted side-to-side”, actin molecules, colored green, blue and cyan belong to one asymmetric unit (in the $P2_1$ space group) for “compacted side-to-side” arrangement. The fourth actin of the complex (colored in brown) belongs to the neighboring asymmetric unit. (B) “elongated side-to-side”, actin molecules colored green and blue belong to one asymmetric unit for “elongated side-to-side” arrangement. The third and fourth actin molecules of the complex

(colored in cyan and brown) belong to the neighboring asymmetric unit. (C) “straight-longitudinal”, actin molecules colored green, blue, cyan and brown belong to four neighboring asymmetric units.The WH2 domains are shown in red, “missing” linkers are depicted as ribbons and colored in yellow.

4.1.4.4 Models for the nucleating arrangement between actin and Spire

The structures of the SpireCD/AP-actin, SpireBCD/AP-actin, SpireDDD/AP-actin and SpireABCD/AP-actin complexes suggest the molecular architecture of an actin/Spire nucleation seed. Because of the “averaging” of the structures of the WH2 domains, model building was based on the analysis of the distances between the C- and N-terminal parts of each single Spire repeat in the crystal arrangement. For this purpose, we searched for distances containing a proper number of amino acids of the linkers (not seen in the structures) that would be compatible with filling the gaps between the WH2 domains’ N- and C-termini. There are actually only two ways for connecting the “averaged” WH2 domains of Spire. The nucleating arrangement can be either “side-to-side” (Figures 4.13A-B; 4.14A-B) or “straight-longitudinal” (Figures 4.13C; 4.14C). The first one can be „compacted” when formed inside the one asymmetric unit (Figures 4.13A; 4.14A) or more “elongated” when connecting the neighboring asymmetric unit (Figures 4.13B; 4.14B). Here I present the models derived from the structure of the SpireBCD/AP-actin complex; identical to those of the SpireCD/AP-actin, SpireABCD/AP-actin and SpireDDD/AP-actin complexes.

The arrangement of actin molecules in the SpireBCD/AP-actin complex is such that one asymmetric unit contains three WH2 domains (Figures 4.13 and 4.11A*).* In the “elongated side-to-side” model in Figure 4.13B, two WH2 domains bound to the two actins coloured in green and blue are linked to one WH2 domain bound to the actin located below this asymmetric unit. In Figure 4.13B, the distance between the C-terminus of the Spire molecule bound to one actin and the N-terminus of Spire bound to neighbouring actin is approximately 16 Å, which is sufficient for both linkers L-2 and L-3 to connect the corresponding WH2 domains.

For the “compacted side-to-side” architecture, the distances between the N- and C-termini of WH2 domains bound to actins inside one asymmetric unit are approximately 23 Å. The calculated area of the interface between two actin molecules for this configuration (“compacted side-to-side” arrangement) is ca. 250 $Å^2$ and it is twice as large as the one calculated for the “elongated side-to-side” arrangement. Because there are three actins in the asymmetric unit, the total area of actin-actin interactions for SpireBCD/AP-actin is equal to 750 $Å^2$, which in solution should produce a tight Spire/actin complex. It should be noted here that the “compacted side-to side” conformation for SpireABCD would have to include a fourth actin molecule (Figure 4.14A), which is located in the neighbouring asymmetric unit; however, the actin-actin interface between the 3rd and 4th actins is still 250 $Å^2$.

In the “straight-longitudinal” model, Spire connects one actin with its two symmetry closest molecules (Figures 4.13C; 4.14C). The distances between the N- terminus of one WH2 domain and the C-terminus of the next molecule are approximately 30 Å. This configuration of Spire/actin shows some intersubunit actin contacts that occur in one strand of the filament helix: i.e. the interface between subdomains 4 and 2 of one actin molecule (the bottom actin in Figure 4.13C) and subdomains 3 and 1 of the next actin molecule (the middle actin molecule in Figure 4.13C). The area of the actin-actin interface in the “straight-longitudinal” model is approximately 350 $Å^2$.

4.1.5 Small angle X-ray scattering of actin-Spire complexes

4.1.5.1 Solution structures of SpireABCD/actin, SpireBCD/actin

To further investigate the organisation of Spire/actin complexes inferred from crystal structures, Spire/actin complexes have been examined with small-angle X-ray scattering (SAXS). SAXS, combined with crystal structures restraints, can accurately define flexible conformations and ensembles in solution, and can also identify structures that most closely match the measured experimental scattering. Arrangements of several constructs of Spire bound to both the skeletal rabbit actin and the cytoplasmatic non-polymerizable drosophlila 5C actin (AP-actin) were studied. SAXS data was collected for solution samples of SpireABCD/actin/latrunculin B, SpireBCD/actin/latrunculin B, SpireBCD/actin, SpireBCD/APactin, SpireBCDhelix/AP-actin.

Out of the three models derived from crystal structures of Spire/actin complexes, the “straight-longitudinal” model fits best to the solution arrangements of the SpireABCD/actin and SpireBCD/actin. The SAXS results do not depend on the type of the actin used (Figures 4.15; 4.16).

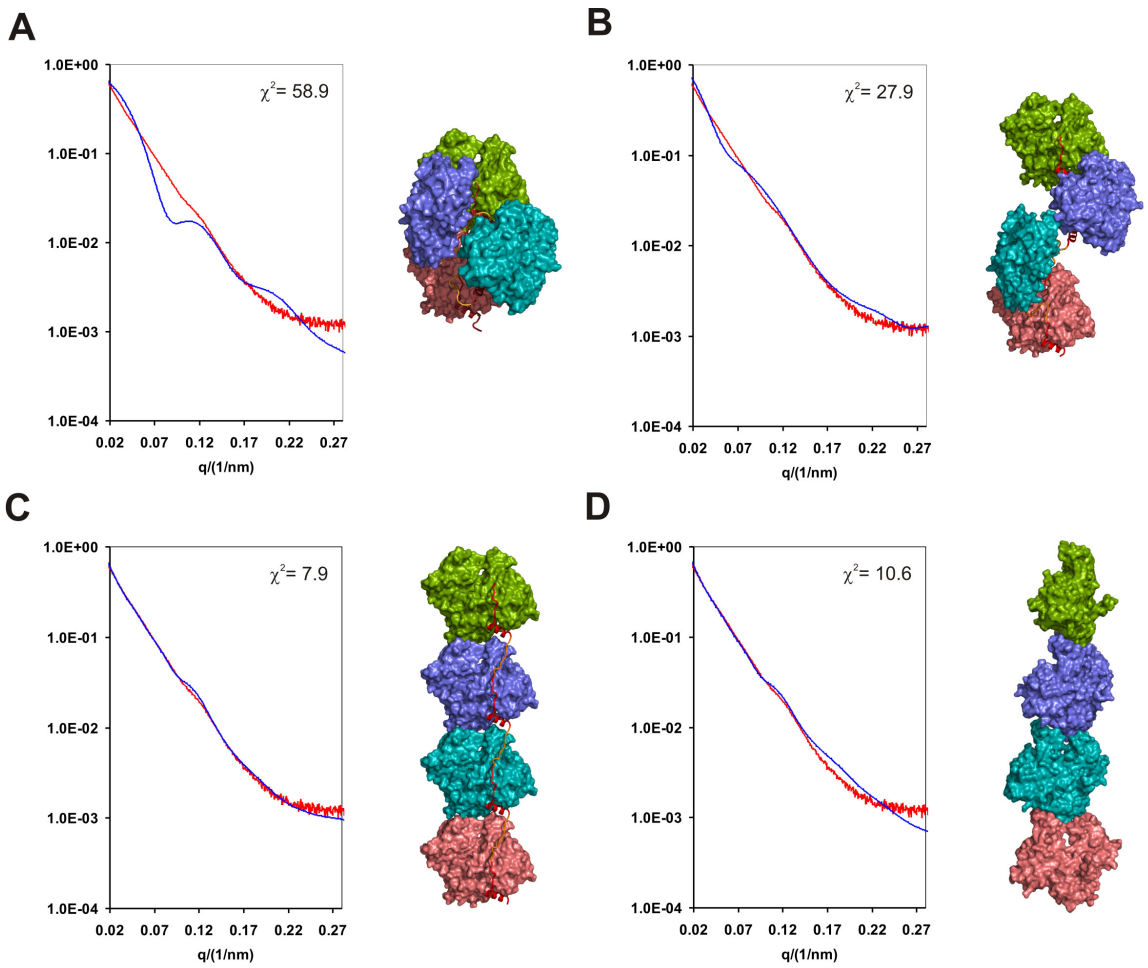

Figure 4.15 SAXS data for the SpireABCD/actin complex. Fitting statistics of (A) the “compacted side-to-side” model, (B) the “elongated side-to-side” model, (C) the “straight-longitudinal” model, (D) one strand of F-actin.

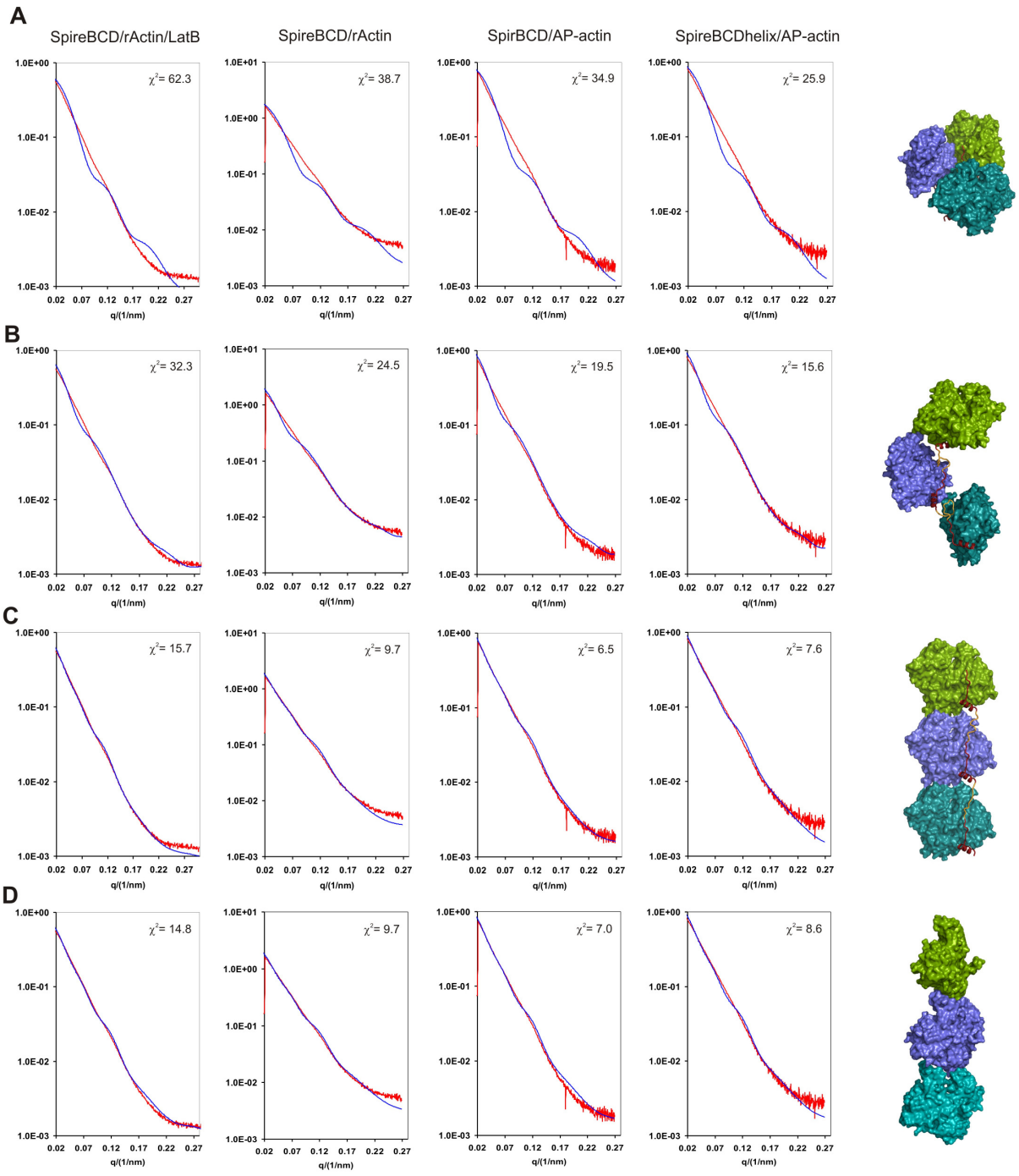

Figure 4.16 SAXS data for the SpireBCD/actin complexes; from the left: SpireBCD/actin-latrunculinB; SpireBCD/actin; SpireBCD/AP-actin; SpireBCDhelix/AP-actin. Fitting statistics of (A) the “compacted side-to-side”

model, (B) the “elongated side-to-side” model, (C) the “straight-longitudinal” model, (D) one strand of F-actin.

4.1.5.2 Solution structures of SpireCD/actin, SpireBC/actin

In the case of WH2-domain/actin complexes with two WH2 domains the “elongated side-to-side” model fits almost as well as the “straight-longitudinal”, and the elongated model cannot be ruled out by the data alone. The two WH2/actin complexes of SpireBC and SpireCD do show some differences, the models from SpireBC/actin are more longitudinal-like than for SpireCD/actin, which could also be interpreted as elongated and filamentous. The difference between these two in the scattering data is, however, small (Figure 4.17).

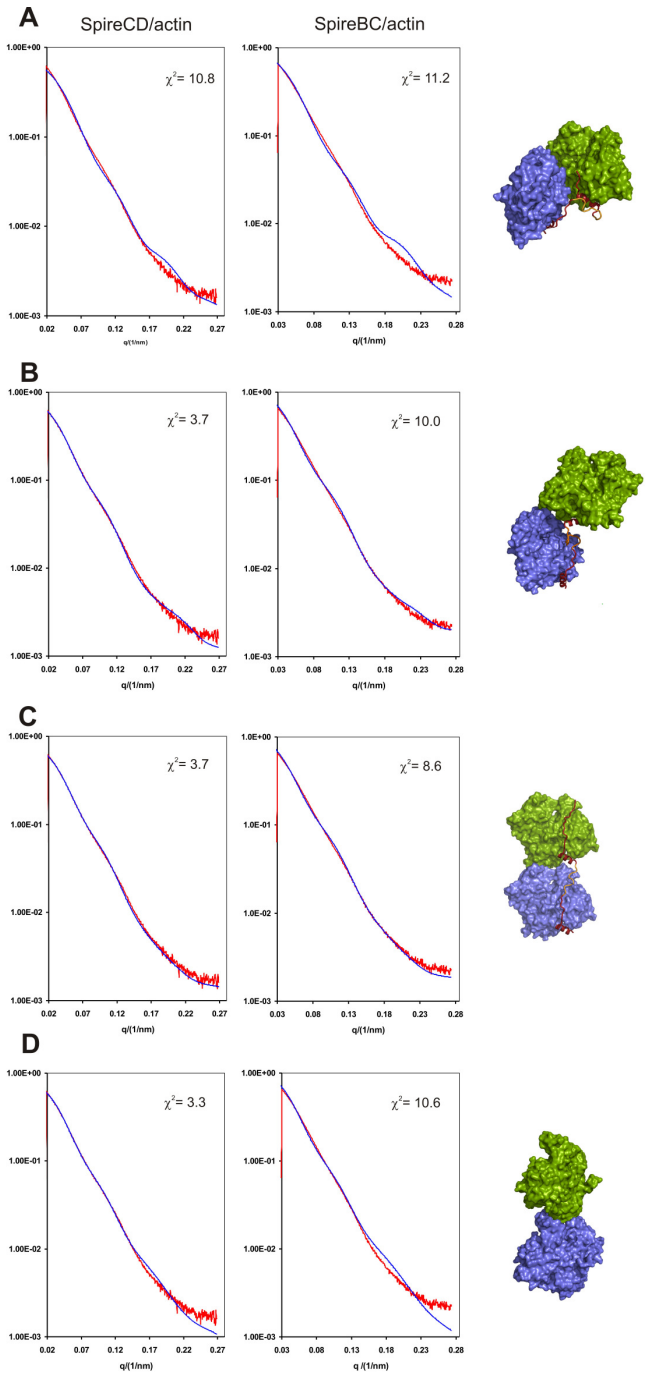

Figure 4.17 SAXS data for the SpireCD/actin (left panel) and SpireBC/actin (right panel) complexes. Fitting statistics of (A) the “compacted side-to-side” model, (B) “elongated side-to-side” model, (C) “straight-longitudinal” model, (D) one strand of F-actin.

4.2 Discussion

The spatial arrangement of actin molecules in the four SpireABCD, SpireBCD, SpireCD, and SpireDDD structures seen in crystal and solution conditions are of significance because they directly show the organization of a seed for actin nucleation, which represents a primary species that can evolve into a filament (Figures 4.13; 4.14; 4.18). A stretch of WH2 domains is assumed to promote filament nucleation by positioning actin subunits for an emerging filament. Spire assembles the nucleus by tethering WH2-bound actin monomers into the “straight-longitudinal” arrangement.

The X-ray data suggest that the “elongated side-to-side” model is also possible. In this structure, each actin molecule is at 60^{o} to each other. The “elongated side-to-side” conformation is much looser than that seen in F-actin; there are short pitch actin-actin contacts between one actin molecule and its neighbouring actins, but these are not the F-actin type interfaces (Holmes et al., 1990; Oda et al., 2009). This Spire-actin structure is different from the long-pitch twist seen in the filament assemblies (Holmes et al., 1990; Oda et al., 2009). The principal difference between this structure and the filament-like arrangement is that in the SpireCD/AP-actin complexes the actin sides which participate in the inner interface of a filament are flipped inside-out, with Spire in the core of the “side-to-side” nucleus (c.f. Figure 4.12). This last feature of the “elongated side-to-side” conformation is also present in the “compacted side-to-side” arrangement – which can be ruled out by SAXS solution structure. To “decorate” a full-fledged filament, the Spire has to be on the outside of the filament, and thus it must assume a less energetically favourable conformation, in which all loops (L-1, L-2, L-3) are stretched into extended secondary structures (Figure 4.18).

In the “straight-longitudinal” model, the twist characteristics of the F-actin filament are not observed. There are some intersubunit actin contacts between adjacent actins. It is clear that “straight-longitudinal” and “elongated side-to-side“ architectures constitute “open” conformations that are solvent permeable with the exposed ATP binding sites, the “elongated side-to-side” conformation being looser than the “straight-longitudinal” one.

In polymerization assays presented here, models would predict that Spir/pyrene-actin complexes show comparable fluorescence emission spectra to pyrenyl-G-actin alone. This is indeed observed. Further, and crucially important, the binding of the unlabeled G-actin to the preformed purified complex of SpireBCD/pyrenyl-actin should be associated with a significant increase of fluorescence after each step of the titration until complete saturation of all lateral binding sites and the formation of longitudinal bonds between actin subunits in one strand of the filament has taken place, as seen in Figure 4.8.

Studies of Bosch and co-workers (Bosch et al., 2007) show that at concentrations of SpireNT/actin 0–0.1 µM/2.5 µM, respectively, Spire effectively nucleates actin (SpireNT, residues 1-520). However, at these concentration ratios more than 99% of SpireNT is in the SpireNT/actin complex. At the concentration ratio of SpireNT/actin of 10 nM/2.5 µM, the polymerization is two orders of magnitude slower than expected if a total fraction of the SpireNT/actin complex was an actual nucleus. This suggests that only part of the Spire/actin complex forms a highly active nucleus that leads to rapid polymerization of actin.

This work proposes that for SpireABCD and SpireBCD, the “straight-longitudinal” configuration represents an initial step of binding of Spire to actin before the rotation to form the filamentously twisted structure. This suggests a simple, yet internally consistent, mechanism for Spire mediated filament nucleation. The transition from the “straight-longitudinal” arrangement to the “filamentous” conformation of Figure 4.18A is followed by recruitment of free actin monomers (Figure 4.18B). In the “straight-longitudinal” arrangement all “inner” sides of actins (as defined in Figure 4.12) are gathered at one site of the complex. Binding of two free actins to these domains of the actins in the SpireD and SpireC positions (Figure 4.18B) induces rotation of the SpireC/actin by ca. 30º with respect to the SpireD/actin (Figure 4.18C) and so on (Figure 4.18D). This zipper-like nucleation leads to the mature filament. A stable filamentous assembly is thus formed, which is sufficient for rapid filament elongation. In this interpretation, Spire would arrange for filament-like actin conformations that are “tightening” into the “packed” full filaments after being processed by the ring-like

structures of formins (Quinlan et al., 2007; Bosch et al., 2007; Qualmann and Kessels., 2009).

It was initially proposed that actin subunits in the Spire/actin complex interact via the longitudinal bonds that form one strand of the long pitch helix in the filament, thus making a filament template or nucleus (Quinlan et al., 2005). There was, however, little experimental evidence to support such a model (which has different packing of actin molecules from that of our “straight-longitudinal” configuration). Recent X-ray scattering analysis of the complex of actin with an artificial tandem of WH2 domains could be interpreted as if a Spire-like protein promotes polymerization by aligning actin subunits in a single strand along the long pitch helix of the actin filament (Rebowski et al., 2008). It can be suggested that the model described by Rebowski et al. (2008), which is also compatible with the data presented in this work, shows a final stage of the nucleation rather than the initial step of the actin seed formation.

Proposed here model of nucleation by Spire is also supported by the nucleotide exchange studies of Bosch et al. (2007), which show that the nucleotide exchange is only slightly slowed down in the SpireNT-actin complex, indicating an actin arrangement different to filamentous assembly. In SpireNT/actin, ATP dissociates from all four actins in the complex in a single exponential process, indicating that the nucleotide exchange rate is similar for all actin subunits within the complex (Bosch et al., 2007). Thus, the ATP binding sites in all actin molecules have to be freely accessible for the ATP exchange. This is true for the loose “straight-longitudinal” and “elongated side-to-side” structures. In F-actin, the ATP exchange is totally inhibited, as the ATP binding sites are blocked by adjacent actin molecules (Bosch et al., 2007).

Spire nucleation model is also in agreement with the mutational data of Quinlan et al. (Quinlan et al., 2005). Spire promotes filament formation even when all three linker sequences are mutated to the flexible Gly-Ser residues, as long as the lengths of the linkers are preserved. In Spire/actin crystal structures the linkers are flexible but their lengths may influence the specific arrangements of actin molecules. On the other hand recent studies show that the L3 linker is

important for actin assembly, and when it is introduced between the two rat N-WASP WH2 domains, L3 can convert rat N-WASP into the Arp2/3-independent nucleator (Zuchero et al., 2009). Although the linkers are not visible in our structure, their presence might be vital for free actin recruitment and further nucleation. It is worth mentioning here that that the L3 linker is the longest amino acid sequence among all the linkers in Spire (12 residues long vs. 10 and 11 for the two other linkers and longer than the linkers in N-WASP (8 residues, rat and human).

Spire-mediated actin nucleation can also involve direct interaction of the KIND domain of Spire with the FH2 domain of the Cappuccino formin (Quinlan et al., 2007). This interaction influences the actin-nucleation properties of both binding partners. Quinlan et al. (2007) suggest that Spire initiates the nucleation of filaments, which are then elongated at the barbed end by FH2 domains of the Cappuccino formin. This mode of Spire action would be in agreement with the results presented here, which suggest that Spire stays associated with the pointed end of actin filaments whereas formins processively move along with the actin barbed ends of the actin structures similar to those shown in Figure 4.15.

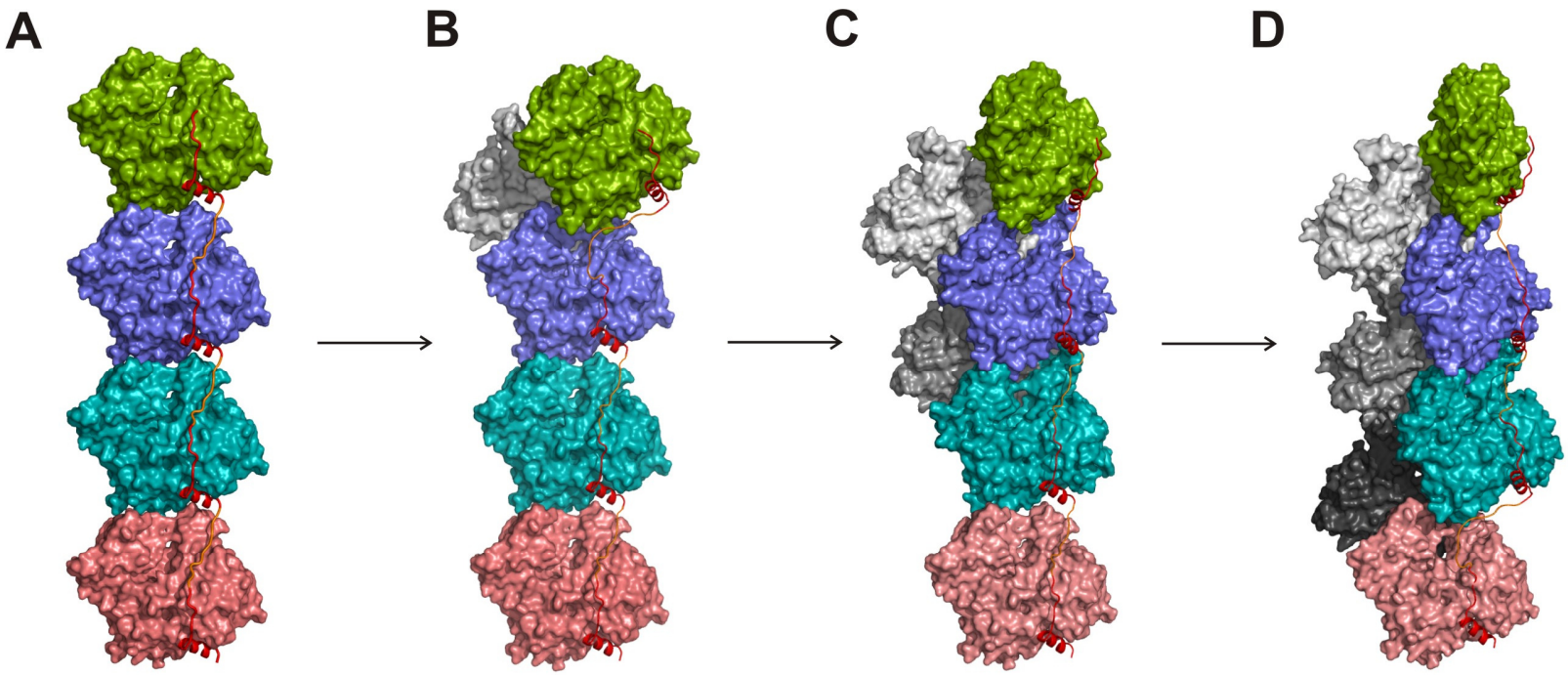

Figure 4.18 Model of actin nucleation by Spire. (A) The crystal structure of a SpirABCD/AP-actin primary nucleus ("straight-longitudinal" configuration) (side view perpendicular to the long axis). (B), (C) Model of G-actin recruitment and nucleus rearrangement. Filament formation and elongation by addition of actin monomers to the barbed end of growing filament. (D) The filament has been formed.

5 Summary

5.1 Summary

The focus of this thesis is the biophysical and biochemical characterization of Spire, an actin-binding protein that nucleates actin filaments. Three classes of proteins are known to nucleate actin filaments: the Arp2/3 complex, formins and the third group of proteins that contains actin-binding motifs called the WH2 repeats. The Spire protein belongs to the third class of these actin nucleators. The most important region, from the point of view of the actin nucleation, is localized in the central part of Spire. It contains 20-21 amino acid long WH2 repeats, designated A, B, C, and D. These are separated by three linkers: L1 (10 amino acid long between domains A and B), L2 (11 amino acid long between domains B and C), and L3 (12 amino acid long between domains C and D).

For this thesis, crystal structures of the complexes between the actin-binding WH2 repeats of Spire and actin were determined for the Spire single WH2 domain D (SpireD), the double (SpireCD), triple (SpireBCD), quadruple (SpireABCD) domains, and an artificial Spire WH2 construct comprising three identical D repeats (SpireDDD). The SpireD-actin complex was obtained for the rabbit actin, and the rest of the complexes were with the mutant actin called the AP-actin. In the structures, the electron densities for the multiple WH2 domains in complexes corresponded to one structure that resulted from averaging between the two C and D domains in the SpireCD-actin complex, three B, C and D domains in the SpireBCD-actin complex, four A, B, C and D domains in the SpireABCD-actin, and three D domains in SpireDDD. Except for SpireDDD, it was not possible to fit specific amino acids of WH2-A, WH2-B, WH2-C and WH2-D to the electron densities and therefore a poly-alanine model was built in.

The arrangements of the complexes in the unit cell of SpireCD, SpireBCD, SpireDDD and that of SpireABCD, are identical, but different from the organization of actin molecules in the crystals of the AP-actin alone and that of SpireD/actin-latrunculin B complex. This suggests that the specific arrangement of Spire/actin complexes is determined by the cluster of WH2 domains.

Analysis of crystal packing of the actin complexes with SpireCD, SpireBCD, SpireABCD, and SpireDDD shows the presence of two types of assemblies that can serve as the actin filament nuclei. The two types of the architectures are: the “side-to-side” (compacted and elongated) and “straight-longitudinal” arrangements. The principal feature of these structures is their loose, open conformations, in which the sides of actins that normally constitute the inner interface core of a filament are flipped inside-out. These Spire structures are distant from those seen in the filamentous nuclei of Arp2/3, formins and in the F-actin filament.

To distinguish between the two possible arrangements seen in the crystals, small angle X-ray scattering (SAXS) for several Spire-actin complexes in solution was carried out. The analysis of the data was carried out by fitting two models based on the crystal structures and, additionally, on a model comprising one strand of the actin filament. For the SpireABCD-actin complex the best fit was obtained for the “longitudinal” model, which gave clearly better results than two “side-to-side” models and slightly better than one strand of the actin filament. The results for the SpireBCD-actin were similar to SpireABCD, however the difference between the “longitudinal” model and the model of a one-strand of actin filament was not significant. For the SpireCD-actin data both the “elongated side-to-side” and “straight-longitudinal” models were possible and could not be differentiated. These results may suggest that increasing number of WH2 domains stabilizes the nucleus and favours one, “straight-longitudinal” conformation.

The spatial arrangement of actin molecules in the Spire-actin structures and the SAXS data indicate the organization of an actin nucleation seed, which represents the primary species that can evolve into a filament. Based on the obtained results, a model of actin nucleation was proposed. This novel model shows the molecular architecture of Spire-actin nucleus which is different from those proposed in the literature.

5.2 Zusammenfassung

Diese Arbeit konzentriert sich auf die biophysikalische und biochemische Charakterisierung von Spire, ein Aktin bindendes Protein, welches Aktinfilamente nukleiert. Es sind drei Arten von Aktin nukleierenden Proteinen bekannt: der Arp2/3 Komplex, Formine und Proteine, die das Aktinbindende Motiv, die WH2-Wiederholungen, enthält. Das Spire Protein gehört zu letzerer Klasse. Die wichtigste Region für die Aktin Nukleierung befindet sich in der Zentralregion von Spire. Es enthält eine 20-21 Aminosäuren lange WH2-Wiederholungssequenz, bezeichnet als A, B, C und D. Diese sind durch drei Linker: L1 (10 Aminosäuren lang, zwischen Domänen A und B), L2 (11 Aminosäuren lang, zwischen Domänen B und C) und L3 (12 Aminosäuren lang, zwischen Domänen C und D) voneinander getrennt.

Für diese Arbeit wurden Kristallsturkturen der folgenden Komplexe zwischen Aktin und der aktinbindenden WH2-Wiederholung von Spire ermittelt: der eizelnen WH2 Domäne D (SpireD), der doppelten (SpireCD), der dreifachen (Spire BCD), der vierfachen (SpireA, B, C, D) Domäne und dem artifiziellen Spire WH2 Konstrukt, welches aus drei identischen Wiederholungen der D Domäne aufgebaut ist (Spire DDD). Der SpireD-Aktin Komplex wurde mit dem Kaninchen Aktin, alle anderen Komplexe mit dem mutierten, so genannten AP-Aktin erhalten. Die Elektronendichte der multiplen WH2-Domänen im Komplex, entsprechen einer Struktur, die sich aus der Durchschnittsberechnung der drei Domänen B, C und D des SpireBCD-Aktin Komplexes, der beiden C und D Domänen des SpireCD-Aktin Komplexes, der vier A, B, C und D Domänen des SpireABCD-Aktin Komplexes und den drei D Domänen des Spire DDD-Aktin Komplexes ergibt. Mit Außnahme von DDD war es nicht möglich bestimmte Aminosäuresequenzen von WH2-A, WH2-B, WH2-C und WH2-D den Elektronendichten zuzuordnen, weswegen ein poly-alanin Modell eingebaut wurde.

Die Anordung der Komplexe in der Einheitszelle von SpireCD, SpireBCD, SpireDDD und dem von SpireABCD, sind identisch, jedoch unterscheidet sich die Anordung der Aktin Moleküle im AP-Aktin Kristall und dem von SpireD/Aktin-

Latrunkulin B Komplex. Dies deutet darauf hin, dass die spezifische Anordnung von Spire-Aktin Komplexen von den WH2-Domäneclustern bestimmt wird.

Die Analyse der Kristalldichte des Aktinkomplexes mit SpireCD, SpireBCD, SpireABCD and SpireDDD zeigt die Präsenz von zwei Aufbauarten, „Seite an Seite“ (kompakt und verlängert) und „aufrecht-longitudinal“, welcher als Nukleus des Aktinfilaments dienen kann. Die wichtigste Besonderheit dieser Strukturen ist deren lose, offene Konformation, in welchen die Seiten von Aktin, die normalerweise die innere Kernschnittstelle des Filaments bilden, nach außen geflipped sind. Diese Spire Strukturen unterscheiden sich von denen die man in den Filamentösen Nuklei von Arp2/3, Forminen und dem F-Aktin Filament findet.

Um zwischen den zwei Möglichen Anordnungen, die man in den Kristallen sieht zu unterscheiden, wurde „small angle X-ray Scattering“ (SAXS) für mehrere Spire-Aktin Komplexe in Lösung durchgeführt. Die Daten wurden durch die Anpassung von zwei kristallstrukturbasierten Modellen und einem Modell welches nur ein Strand Aktin Filament beinhaltet analysiert. Für den SpireABCD-Aktin Komplex wurde die beste Passform für das „longitudinal“ Modell erreicht. Das Ergebnis für SpireBCD-Aktin ist ähnlich zu SpireABCD, jedoch ist der Unterschied zwischen dem „Longitudinal“ und dem Modell von einem Einzelstrand Aktinfilament nicht maßgeblich. Für die SpireCD-Aktin Daten sind sowohl das „Seite an Seite“ verlängerte und das „Longitudinal“ Modell möglich und konnten nicht unterschieden werden. Diese Ergebnisse weisen darauf hin, dass eine vermehrte Anzahl an WH2 Domänen den Nukleus stabilisieren und die „aufrecht-longitudinal“ Konformation begünstigen.

Die räumliche Anordnung der Aktin Moleküle in der Spire-Aktin Struktur und der SAXS Daten deuten auf einen Aufbau durch ein Aktin Nukleationskeim, welcher der Grundbaustein des Aktinfilaments darstellt.

Basierend auf den gewonnenen Ergebnissen wurde ein Modell der Aktinnukleierung erstellt. Dieses neue Modell zeigt die molekulare Architektur des Spire-Aktin Nukleus, welcher sich von den bisherigen Veröffentlichungen unterscheidet.

6 Appendix

6.1 Abbreviations and symbols

1D	one-dimensional
2D	two-dimensional
Å	Ångstrøm (10^{-10} m)
aa	amino acid
ADF	actin depolymerizing factor
ADP	adenosine diphosphate
APC	adenomatous polypolis coli
APS	ammonium peroxodisulfate
Arp2/3	actin related protein 2/3
ATP	adenosine triphosphate
bp	base pair
BSA	bovine serum albumin
BCIP	5-bromo-4-chloro-3-indolyl phosphate
CAP	adenylate cyclase associated protein
C-C	C-terminal coiled coil
Cdc42	cell division control protein 42 homolog
cDNA	complimentary DNA
CIP	calf intestinal phosphatase
Cobl	Cordon-bleu
Da	Dalton (g mol-1)
Dia	Diaphanous-related formin
DMSO	dimethylsulfoxide
DNA	deoxyribonucleic acid
EDTA	ethylenediamine tetraacetic acid
Ena/VASP	enabled/vasodilator stimulated proteins
FH2	formin homology 2 domain
g	gravity (9.81 m s^{-2})
GST	glutathione S-transferase

GTPase	guanine triphosphatase
HSQC	heteronuclear single quantum coherence
Hz	Hertz
IMAC	immobilized metal affinity chromatography
IPTG	isopropyl-β-thiogalactopyranoside
JMY	junction mediating and regulatory protein
JNK	c-Jun N-terminal kinases
JNKB	JNK binding domain
KIND	kinase noncatalytic C-lobe domain
LB	Luria-Broth medium
MAP	mitogen activated protein kinase
MAPs	microtubule associated proteins
mFYVE	modified FYVE (Fab1, YOTB, Vac1, EEA1)
MM	minimal medium
M_W	molecular weight
Ni-NTA	nickel-nitrilotriacetic acid
NMR	nuclear magnetic resonance
NPFs	nucleation promoting factors
OD	optical density
PAGE	polyacrylamide gel electrophoresis
PBS	phosphate-buffered saline
PDB	protein data bank
PDZ	post synaptic density protein (**P**SD90), *Drosophila* disc large tumor suppressor (**D**lgA), zonula occludens-1 protein (**z**o-1)
PI(3)P	phospholipid phosphatidylinositol 3-phosphate
ppm	parts per million
Rac1	Ras-related C3 botulinum toxin substrate 1
RasGEF	Ras guanine exchange factor
RhoA	Ras homolog gene family member A
SAXS	small angle X-ray scattering
SDS	sodium dodecyl sulfate

TAE	tris-acetate EDTA buffer
TEMED	N,N,N',N'-tetramethylethylendiamine
WASH	WASP and SCAR homologue
WASP	Wiskott - Aldrich Syndrome protein
WAVE	WASP family Verprolin-homologous protein
WH2	Wiskott - Aldrich Syndrome homology domain 2
WHAMM	WASP homologue associated with actin, golgi membranes and microtubules
WIP	WASP-interacting protein

6.2 Sequences of proteins

6.2.1 Spire

```
        10         20         30         40         50         60
MTEHQAEEQA DTPPTKVKAT PTPTPSGKFK DAKEDAFLST SPDSANGDAQ HKLPADQLAM

        70         80         90        100        110        120
SSSAHPQQAG QARPLILQAF HRCSSPEQCV TLHDILDSFK APLSEDQAWA LIHQFAGLYH

       130        140        150        160        170        180
QVAVQAHTCA ADYEAALPTG FELHFHRDGS VHFSGPDQLT PKEQLQQEQI PLPPQHDVIV

       190        200        210        220        230        240
DQPDHSASSS GDSSVINRAF DNSNHHHHHQ HHHPPLVVSH RKIISELAEI VYTALDYNLP

       250        260        270        280        290        300
EDEECQVSQE LENLFNFMTA DETDDDCIDE GIDEGDKRWD DESEEERNDT KELEHIIETC

       310        320        330        340        350        360
RNHIKTTLPE NHYRAVCRAL VTETIELRVF LQQVLNNEAG AEKLIKASES SATTQQELAK

       370        380        390        400        410        420
LGFNDWARFW VQVIDELRRG VRLKKSNHER TPIEYELTPY EILMGDIRAK KYQLRKVMVN

       430        440        450        460        470        480
GDIPPRVKKD AHAMILEFIR SRPPLKKASD RQLGPPRMCE PSPREQLMES IRKGKELKQI

       490        500        510        520        530        540
TPPEAPTLRE RVLPSANSTL SRSRQRLIKV DFSKFQDDDL FYDENSISSS HSTAATHQHH

       550        560        570        580        590        600
PHFAEMHRCS QPKMPPYPFG GYMVPSQARQ DCRETASLMR PRRTMEPAKQ VPPPEEPSFT

       610        620        630        640        650        660
KDEYHKFYDT ALESYDLATQ CESRRASLRR HTIVGCQSNL DETHSMPPTR PESRQSDDVS

       670        680        690        700        710        720
KETPKRSPAE QTHPSDEGSS TSSLGPWNKS FMDKQTWMER GDDRLSVTLA EIVHIRSVMT

       730        740        750        760        770        780
KAELEGLPMD VRVKEDVEKR RVCFLCLRTR FSFFGPWGIQ CKLCQRTVCA KCYTKMRIPS

       790        800        810        820        830        840
EHFRNVPLVL ISPSLLSSPA SSSTPSPSHH AQQAHSSSTG NIMDDQFPKS LIERLLRSES

       850        860        870        880        890        900
DRKTRSTVGS APSSPKHQRS NMSTPGISVG PGASSSSAAA TGQAVEALHD QATMSSSYSA

       910        920        930        940        950        960
AMRPSGVHQQ QKQHYNNAMS RSMEGPRSLP VHSPAYRPLS NNSTLERKSR FSRGFNLFSS

       970        980        990       1000       1010       1020
GSHLAQTQEQ KENLRGEQVT VCNDCQGLVN EITSSVKQKR SSARNRTIQN LTLDLTPVWK
```

6.2.2 Rabbit actin (rabbit skeletal muscle actin)

```
        10         20         30         40         50         60
CDEDETTALV CDNGSGLVKA GFAGDDAPRA VFPSIVGRPR HQGVMVGMGQ KDSYVGDEAQ

        70         80         90        100        110        120
SKRGILTLKY PIEHGIITNW DDMEKIWHHT FYNELRVAPE EHPTLLTEAP LNPKANREKM

       130        140        150        160        170        180
TQIMFETFNV PAMYVAIQAV LSLYASGRTT GIVLDSGDGV THNVPIYEGY ALPHAIMRLD

       190        200        210        220        230        240
LAGRDLTDYL MKILTERGYS FVTTAEREIV RDIKEKLCYV ALDFENEMAT AASSSSLEKS

       250        260        270        280        290        300
YELPDGQVIT IGNERFRCPE TLFQPSFIGM ESAGIHETTY NSIMKCDIDI RKDLYANNVM

       310        320        330        340        350        360
SGGTTMYPGI ADRMQKEITA LAPSTMKIKI IAPPERKYSV WIGGSILASL STFQQMWITK

       370
QEYDEAGPSI VHRKCF
```

6.2.3 AP-actin (cytoplasmatic non-polymerizable drosophlila 5C actin)

```
        10         20         30         40         50         60
CDEEVAALVV DNGSGMCKAG FAGDDAPRAV FPSIVGRPRH QGVMVGMGQK DSYVGDEAQS

        70         80         90        100        110        120
KRGILTLKYP IEHGIVTNWD DMEKIWHHTF YNELRVAPEE HPVLLTEAPL NPKANREKMT

       130        140        150        160        170        180
QIMFETFNTP AMYVAIQAVL SLYASGRTTG IVLDSGDGVS HTVPIYEGYA LPHAILRLDE

       190        200        210        220        230        240
LAGRDLTDYL MKILTERGYS FTTTAEREIV RDIKEKLCYV ALDFEQEMAT AASSSSLEKS

       250        260        270        280        290        300
KYELPDGQVI TIGNERFRCP EALFQPSFLG MEACGIHETT YNSIMKCDVD IRKDLYANTV

       310        320        330        340        350        360
LSGGTTMYPG IADRMQKEIT ALAPSTMKIK IIAPPERKYS VWIGGSILAS LSTFQQMWIS

       370
KQEYDESGPS IVHRKCF
```

Mutated amino acids are marked in green.

6.3 Crystallization conditions

Table 6.1 Crystallization conditions in which crystals appeared.

Construct name	Screen name	No.	Formulation
SpireL3-D (448-485) rabbit actin, Lat B	Nextal PEGs	**F8**	0.2M Magnesium formate pH 5.9 20%w/v PEG 3350
SpireL3-D (448-485)	Hampton Index	**E10**	0.1M Bis-tris pH 6.5 45%v/v PPG 400
		H12	0.15M Potassium bromide 30%w/v PEG 2000 MME
	Magic 1	**H1**	0.05M Tris pH 8.0 40%w/v PEG 3350
	Nextal PEGs	**F3**	0.2M Lithium nitrate 20%w/v PEG 3350
		F4	0.2M Magnesium nitrate 20%w/v PEG 3350
	Nextal PACT	**F4**	0.2 M Potassium thiocyanate 0.1M Bis-tris propane pH 6.5 20%w/v PEG 3350
SpireCD (428-485)	Complex suite	**A9**	0.2M Sodium chloride 0.1M MES pH 6.0 20%w/v PEG 2000 MME
		C6	0.15M Ammonium sulfate 0.1M HEPES pH 7.0 20%w/v PEG 4000
		C11	0.1M Sodium cacodylate pH 6.5 25%w/v PEG 4000
		C12	0.2M Potassium iodide 0.1M MES pH 6.5 25%w/v PEG 4000
		D9	0.1M MES pH 6.5 15%w/v PEG 6000 5%v/v MPD
		E12	0.2M Ammonium sulfate 0.1M MES pH 6.5 20%w/v PEG 8000
	Hampton Index	**G8**	0.20M ammonium acetate 0.1M HEPES pH 7.5 25%w/v PEG 3350
	Magic 1	**B2**	0.05M MES pH 6.0 0.2M Sodium malonate 18%w/v PEG 8000

		C2	0.05M MES pH 6.0 0.2M Sodium malonate 26%w/v PEG 8000
	Magic 2	**D9**	0.05M MES pH 6.0 0.2M Lithium sulfate 40%w/v PEG 3350
	Nextal Classics	**H8**	0.2M Ammonium sulfate 0.1M MES pH 6.5 30%w/v PEG 5000 MME 0.01M Magnesium chloride
	Nextal PEGs	**A12**	0.1M MES pH 6.5 25%w/v PEG 2000 MME
		C8	0.1M MES pH 6.5 25%w/v PEG 4000
		C9	0.1M MES pH 6.5 25%w/v PEG 6000
		C11	0.1M MES pH 6.5 20%w/v PEG 10000
		G6	0.2M Ammonium acetate 20%w/v PEG 3350
		H2	0.2M di-Ammonium tartrate 20%w/v PEG 3350
SpireBC rabbit actin, Lat B	Easy Xtal JSCG+	**A7**	0.1M CHES pH 9.5 20%w/v PEG 8000
	Magic 1	**F2**	0.05M Tris pH 8.0 0.2M Sodium malonate 18% PEG 8000
	Magic 2	**F3**	0.05M Tris pH 8.0 25% PEG 400
		F4	0.05M Tris pH 8.0 0.2M Sodium chloride 18% PEG 8000
		G2	0.05M Tris pH 8.0 0.2M Ammonium sulfate 26% PEG 8000
	Nextal MbClass 1	**G5**	30%w/v PEG 4000
	Nextal PACT	**D7**	0.2 M Sodium chloride 0.1M Tris pH 8.0 20%w/v PEG 6000
SpireBC AP actin	Easy Xtal JSCG+	**B5**	0.1M Sodium cacodylate pH 6.5 40%v/v MPD 5 %w/v PEG 8000
	Magic 2	**D12**	50mM MES pH 6.0 70% MPD

		H12	50mM Tris pH 8.0 70% MPD
	Nextal Classics	**B10**	0.1M HEPES pH 7.5 70%v/v MPD
	Nextal pH clear	**H10**	0.1M HEPES 65%v/v MPD Final pH = 7.0
		H11	0.1M TRIS 65%v/v MPD Final pH = 8.0
	Nextal PEGs	**D8**	0.1M TRIS.HCl pH 8.5 25%w/v PEG 4000
	Nextal MbClass 1	**H5**	0.1M TRIS.HCl pH 8.5 0.1M Sodium acetate
SpireBCD (396-485)	Complex suite	**A9**	0.2M Sodium chloride 0.1M MES pH 6.0 20%w/v PEG 2000 MME
		C7	0.1M Sodium citrate pH 5.6 20%w/v PEG 4000 20% (v/v) Isopropanol
		D2	0.1M MES pH 6.5 10%w/v PEG 5000 MME 12% (v/v) 1-propanol
		D9	0.1M MES pH 6.5 15%w/v PEG 6000 5%v/v MPD
		H9	0.1M Imidazole pH 7.0 50%v/v MPD
		H10	0.05M Magnesium chloride 0.1M MES pH 6.5 10%v/v Isopropanol 5%w/v PEG 4000
	Hampton Index	**D6**	0.1M Bis-tris pH 5.5 25%w/v PEG 3350
		F5	0.1M Ammonium acetate 0.1M Bis-tris pH 5.5 17%w/v PEG 10,000
		F10	0.2M Sodium chloride 0.1M Bis-tris pH 5.5 25%w/v PEG 3350
		G6	0.2M Ammonium acetate 0.1M Bis-tris pH 5.5 25%w/v polyethylene glycol 3350
		G7	0.2M Ammonium acetate 0.1M Bis-tris pH 6.5 25%w/v PEG 3350

	Easy Xtal JSCG+	**A8**	0.2M Ammonium formate pH 6.6 20%w/v PEG 3350
		B5	0.1M Sodium cacodylate pH 6.5 40%v/v MPD 5 %w/v PEG 8000
		D5	0.2M Magnesium chloride 0.1M HEPES pH 7.5 70%v/v MPD
		H8	0.2M Sodium chloride 0.1M Bis-tris pH 5.5 25%w/v PEG 3350
		H10	0.2M Ammonium acetate 0.1M Bis-tris pH 5.5 25%w/v PEG 3350
	Magic 1	**A9**	0.05M MES pH 6.0 4%v/v MPD 0.2M Ammonium acetate 10%w/v PEG 3350
		B4	0.05M MES pH 6.0 4% MPD 0.08M Ammonium sulfate 18%w/v PEG 8000
		B9	0.05M MES pH 6.0 4%v/v MPD 0.2M Ammonium acetate 20%w/v PEG 3350
		C2	0.05M MES pH 6.0 0.2M Sodium malonate 26%w/v PEG 8000
		C4	0.05M MES pH 6.0 4% MPD 0.08M Ammonium sulfate 26%w/v PEG 8000
	Magic 2	**D2**	0.05M MES pH 6.0 0.2M Ammonium sulfate 34%w/v PEG 8000
		D9	50mM MES pH 6.0 0.2M Lithium sulfate 40%w/v PEG 3350
	Nextal Clasics	**A3**	0.2M Magnesium chloride 0.1M TRIS pH 8.5 3.4M 1,6-Hexanediol
		A5	0.1M HEPES sodium salt pH 7.5 10%v/v Isopropanol 20 %w/v PEG 4000

		A7	0.1M tri-Sodium citrate pH 5.6 20%v/v Isopropanol 20 %w/v PEG 4000
		B10	0.1M HEPES pH 7.5 70%v/v MPD
		F11	0.2M Sodium acetate 0.1M Sodium cacodylate pH 6.5 30%w/v PEG 8000 0.01M Magnesium chloride
	Nextal pH clear	**H4**	0.1M HEPES 40%v/v MPD Final pH = 7.0
		H10	0.1M HEPES 65%v/v MPD Final pH = 7.0
	Nextal PEGs	**A7**	0.1M MES pH 6.5 40%v/v PEG 200
		A10	0.1M MES pH 6.5 25%v/v PEG 550 MME
		A12	0.1M MES pH 6.5 25%w/v PEG 2000 MME
		C8	0.1M MES pH 6.5 25%w/v PEG 4000
		C9	0.1M MES pH 6.5 25%w/v PEG 6000
		E1	0.2M Sodium fluoride 20%w/v PEG 3350
		E2	0.2M Potassium fluoride 20%w/v PEG 3350
		E10	0.2M Sodium iodide 20%w/v PEG 3350
		G5	0.2M Potassium acetate 20%w/v PEG 3350
		G6	0.2M Ammonium acetate 20%w/v PEG 3350
SpireBCD-Lx-Thelix	Complex suite	**D2**	0.1M MES pH 6.5 10%w/v PEG 5000 MME 12%v/v 1-propanol
	Easy Xtal JSCG+	**A8**	0.2 M Ammonium formate pH 6.6 20%w/v PEG 3350
	Nextal pH clear	**H4**	0.1M HEPES 40%v/v MPD Final pH = 7.0
SpireBCD-Ly -Thelix	Complex suite	**D2**	0.1M MES pH 6.5 10%w/v PEG 5000 MME 12%v/v 1-propanol

	Easy Xtal JSCG+	**A8**	0.2 M Ammonium formate pH 6.6 20%w/v PEG 3350
	Nextal pH clear	**H4**	0.1M HEPES 40%v/v MPD Final pH = 7.0
SpireABCD (371-485)	Complex suite	**D2**	0.1M MES pH 6.5 10%w/v PEG 5000 MME 12%v/v 1-propanol
	Easy Xtal JSCG+	**A8**	0.2 M Ammonium formate pH 6.6 20%w/v PEG 3350
	Nextal pH clear	**H4**	0.1M HEPES 40%v/v MPD Final pH = 7.0
KIND(1-365)-CD	Complex suite	**D9**	0.1M MES pH 6.5 15%w/v PEG 6000 5%v/v MPD
	Magic 1	**B9**	0.05M MES pH 6.0 4%v/v MPD 0.2M Ammonium acetate 20%w/v PEG 3350
SpireDDD	Complex suite	**A9**	0.2M Sodium chloride 0.1M MES pH 6.0 20%w/v PEG 2000 MME
		B9	0.1M Sodium cacodylate pH 6.0 15%w/v PEG 4000
		C4	0.2M Lithium sulfate 0.1M MES pH 6.0 20%w/v PEG 4000
		C10	0.15M Ammonium sulfate 0.1M MES pH 5.5 25%w/v PEG 4000
		D2	0.1M MES pH 6.5 10%w/v PEG 5000 MME 12%v/v 1-propanol
		D7	0.1M Sodium citrate pH 5.5 15%w/v PEG 6000
		H8	0.05M Calcium acetate 0.1M Sodium cacodylate pH 6.0 25%v/v MPD
	Easy Xtal JSCG+	**A8**	0.2 M Ammonium formate pH 6.6 20%w/v PEG 3350
	Magic 1	**A9**	0.05M MES pH 6.0 4% MPD 0.2M Ammonium acetate 10%w/v PEG 3350

		B1	0.05M MES pH 6.0 20%w/v PEG 3350
	Magic 2	**C4**	0.05M MES pH 6.0 0.2M Sodium chloride 26%w/v PEG 8000
	Nextal pH clear	**H4**	0.1M HEPES 40%v/v MPD Final pH = 7.0
	Nextal PEGs	**A7**	0.1M MES pH 6.5 40%v/v PEG 200
		C7	0.1M MES pH 6.5 25%w/v PEG 3000
		C9	0.1M MES pH 6.5 25%w/v PEG 6000
		F11	0.2M Ammonium formate 20%w/v PEG 3350

7 References

Aguda AH, Xue B, Irobi E, Preat T, and Robinson RC (2006) The structural basis of actin interaction with multiple WH2/betathymosin motif-containing proteins. *Structure* 14:469-476.

Ahuja R, Pinyol R, Reichenbach N, Custer L, Klingensmith J, Kessels MM, and Qualmann B (2007) Cordon-Bleu is an actin nucleation factor and controls neuronal morphology. *Cell* 131:337-350.

Azoury J, Lee KW, Georget V, Rassinier P, Leader B, and Verlhac MH (2008) Spindle positioning in mouse oocytes relies on a dynamic meshwork of actin filaments. *Curr. Biol.* 18:1514-1519.

Bachmann C, Fischer L, Walter U, and Reinhard M (1999) The EVH2 domain of the vasodilator-stimulated phosphoprotein mediates tetramerization, F-actin binding, and actin bundle formation. *J. Biol. Chem.* 274:23549–23557.

Belmont LD, Orlova A, Drubin DG, and Egelman EH (1999) A change in actin conformation associated with filament instability after Pi release. *Proc. Natl. Acad. Sci. USA* 96:29-34.

Beltzner CC, and Pollard TD (2004) Identification of functionally important residues of Arp2/3 complex by analysis of homology models from diverse species. *J. Mol. Biol*. 336:551-565.

Bennett V, and Baines AJ (2001) Spectrin and ankyrin-based pathways: Metazoan inventions for integrating cells into tissues. *Physiol. Rev.* 81:1353-1392.

Blanchard A, Ohanian V, and Critchley D (1989) The structure and function of α-actinin. *J. Muscle Res. Cell Motil.* 10:280-289.

Blanchoin L, and Pollard TD (1998) Interaction of actin monomers with Acanthamoeba actophorin (ADF/cofilin) and profilin. *J. Biol. Chem.* 273:25106-25111.

Bosch M, Le KH, Bugyi B, Correia JJ, Renault L, and Carlier MF (2007) Analysis of the function of Spire in actin assembly and its synergy with formin and profilin. *Molecular Cell* 28:555-568.

Brindle NP, Holt MR, Davies JE, Price CJ, and Critchley DR (1996) The focal-adhesion vasodilator-stimulated phosphoprotein (VASP) binds to the proline-rich domain in vinculin. *Biochem. J.* 318:753-757.

Broderick MJ, and Winder SJ (2005) Spectrin, α-actinin, and dystrophin. *Adv. Protein Chem.* 70:203-246.

Bugyi B, and Carlier MF (2010) Control of actin filament treadmilling in cell motility. *Annu. Rev. Biophys.* 39:449-470.

Burtnick LD, Urosev D, Irobi E, Narayan K, and Robinson RC (2004) Structure of the N-terminal half of gelsolin bound to actin: roles in severing, apoptosis and FAF. *EMBO J.* 23:2713-2722.

Campbell KP, and Kahl SD (1989) Association of dystrophin and an integral membrane glycoprotein. *Nature* 338:259-262.

Campellone KG, Webb NJ, Znameroski EA, and Welch MD (2008) WHAMM is an Arp2/3 complex activator that binds microtubules and functions in ER to Golgi transport. *Cell* 134:148-161.

Campellone KG, and Welch MD (2010) A nucleator arms race: cellular control of actin assembly. *Nat. Rev. Mol. Cell Biol*. 11:237-251.

Carlier MF, Criquet P, Pantaloni D, and Korn ED (1986) Interaction of cytochalasin D with actin filaments in the presence of ADP and ATP. *J. Biol. Chem.* 261:2041-2050.

Carlier MF, and Pantaloni D (1986) Direct evidence for ADP-Pi-F-actin as the major intermediate in ATP-actin polymerization. Rate of dissociation of Pi from actin filaments. *Biochemistry* 25:7789-7792.

Carlsson L, Nyström LE, Sundkvist I, Markey F, and Lindberg U (1977) Actin polymerizability is influenced by profilin, a low molecular weight protein in non-muscle cells. *J. Mol. Biol.* 115:465-483.

CCP4 (Collaborative Computational Project, Number 4) (1994) The CCP4 suite: Programs for protein crystallography. *Acta Crystallogr. D. Biol. Crystallogr.* 50:760-763.

Chen N, Qu X, Wu Y, and Huang S (2009) Regulation of actin dynamics in pollen tubes: control of actin polymer level. *J. Integr. Plant Biol.* 51:740-750.

Chereau D, Boczkowska M, Skwarek-Maruszewska A, Fujiwara I, Rebowski G, Hayes DB, Lappalainen P, Pollard TD, and Dominguez R (2008) Leiomodin is an actin filament nucleator in muscle cells. *Science* 320:239-243.

Chereau D, Kerff F, Graceffa P, Grabarek Z, Langsetmo K, and Dominguez R. (2005) Actin-bound structures of Wiskott-Aldrich syndrome protein (WASP) homology domain 2 and the implications for filament assembly. *Proc. Natl. Acad. Sci. USA* 102:16644-16649.

Chesarone MA, and Goode BL (2009) Actin nucleation and elongation factors: mechanisms and interplay. *Curr. Opin. Cell Biol*. 21:28-37.

Chu JW, and Voth GA (2005) Allostery of actin filaments: Molecular dynamics simulations and coarse-grained analysis. *Proc. Natl. Acad. Sci. USA* 102:13111-13116.

Ciccarelli FD, Bork P, and Kerkhoff E (2003) The KIND module: a putative signalling domain evolved from the C lobe of the protein kinase fold. *Trends Biochem. Sci.* 28:349-352.

Condeelis JS, Wyckoff JB, Bailly M, Pestell R, Lawrence D, Backer J, and Segall JE (2001) Lamellipodia in invasion. *Semin. Cancer Biol.* 11:119-128.

Coue M, and Korn ED (1985) Interaction of plasma gelsolin with G-actin and F-actin in the presence and absence of calcium ions. *J. Biol. Chem.* 260:15033-15041.

Czisch M, Schleicher M, Horger S, Voelter W, and Holak TA (1993) Conformation of thymosin beta 4 in water determined by NMR spectroscopy. *Eur. J. Biochem*. 218:335-344.

Dahlgaard K, Raposo AA, Nicolli T, and St Johnston D (2007) Capu and Spire assemble a cytoplasmic actin mesh that maintains microtubule organization in the *Drosophila* oocyte. *Dev. Cell* 14:539-553

Didry D, Carlier MF, and Pantaloni D (1998) Synergy between actin depolymerizing factor/cofilin and profilin in increasing actin filament turnover. *J. Biol. Chem.* 273:25602-25611.

Doherty GJ, and McMahon HT (2009) Mechanisms of Endocytosis. *Annual Review in Biochemistry* 78:857-902.

Dominguez R (2004) Actin-binding proteins - a unifying hypothesis. *Trends Biochem. Sci.* 29:572-578.

dos Remedios CG, Chhabra D, Kekic M, Dedova IV, Tsubakihara M, Berry DA, and Nosworthy NJ (2003) Actin binding proteins: regulation of cytoskeletal microfilaments. *Physiol Rev.* 83:433-473.

D'Silva L, Ozdowy P, Krajewski M, Rothweiler U, Singh M, and Holak TA (2005) Monitoring the effects of antagonists on protein-protein interactions with NMR spectroscopy. *J. Amer. Chem. Soc.* 127:13220-13226.

Ducka AM, Joel P, Popowicz GM, Trybus KM, Schleicher M, Noegel AA, Huber R, Holak TA, and Sitar T (2010) Structures of actin-bound Wiskott-Aldrich

syndrome protein homology 2 (WH2) domains of Spire and the implication for filament nucleation. *Proc. Natl. Acad. Sci. U S A* 107:11757-11762.

Erdmann KS (2003) The protein tyrosine phosphatase PTP-Basophil/Basophil-like. Interacting proteins and molecular functions. *Eur. J. Biochem.* 270:4789-4798.

Evangelista M, Blundell K, Longtine M, Chow C, Adames N, Pringle J, Peter M, and Boone C (1997) Bni1p, a yeast formin linking Cdc42p and the actin cytoskeleton during polarized morphogenesis. *Science* 276:118-121.

Evangelista M, Pruyne D, Amberg DC, Boone C, and Bretscher A (2002) Formins direct Arp2/3-independent actin filament assembly to polarize cell growth in yeast. *Nat. Cell Biol.* 4:32-41.

Evangelista M, Zigmond S, and Boone C (2003) Formins: signaling effectors for assembly and polarization of actin filaments. *J. Cell Sci*. 116:2603-2611.

Firat-Karalar EN, and Welch MD (2011) New mechanisms and functions of actin nucleation. *Curr Opin Cell Biol*. 23:4-13.

Fletcher DA, and Mullins RD (2010) Cell mechanics and the cytoskeleton. *Nature* 463:485-492.

Franke D, and Svergun DI (2009) DAMMIF, a program for rapid ab-initio shape determination in small-angle scattering. *J. Appl. Crystallogr.* 42:342-346.

Fujii T, Iwane AH, Yanagida T, and Namba K (2010) Direct visualization of secondary structures of F-actin by electron cryomicroscopy. *Nature* 467:724-728.

Fujiwara I, Vavylonis D, and Pollard TD (2007) Polymerization kinetics of ADP-and ADP-Pi-actin determined by fluorescence microscopy. *Proc Natl Acad Sci USA* 104:8827-8832.

Galletta BJ, and Cooper JA (2009) Actin and endocytosis: mechanisms and phylogeny. *Curr. Opin. Cell Biol.* 21: 20-27.

Gill SC, and von Hippel PH (1989) Calculation of protein extinction coefficients from amino acid sequence data. *Anal. Biochem.* 182:319-326.

Gimona M, Kaverina I, Resch GP, Vignal E, and Burgstaller G (2003) Calponin repeats regulate actin filament stability and formation of podosomes in smooth muscle cells. *Mol. Biol. Cell* 14:2482-2491.

Goley ED, and Welch MD (2006) The ARP2/3 complex: an actin nucleator comes of age. *Nat Rev Mol Cell Biol.* 7:713-726.

Goode BL, and Eck MJ (2007) Mechanism and function of formins in the control of actin assembly. *Annu Rev Biochem* 76:593-627.

Graceffa P, and Dominguez R (2003) Crystal structure of monomeric actin in the ATP state. Structural basis of nucleotide-dependent actin dynamics. *J. Biol. Chem*. 278:34172-34180.

Hanson J, and Lowy J (1963) The structure of F-actin and of actin filaments isolated from muscle. *J. Mol. Biol.* 6:46-60.

Hertzog M, Heijenoort Cv, Didry D, Gaudier M, Coutant J, Gigant B, Didelot G, Preat T, Knossow M, Guittet E, and Carlier MF (2004) The β-thymosin/WH2 domain; structural basis for the switch from inhibition to promotion of actin assembly. *Cell* 117:611-623.

Higgs HN (2005) Formin proteins: a domain-based approach. *Trends Biochem. Sci.* 30:342-353.

Hodge T, and Cope MJA (2000) A myosin family tree. Journal of Cellular *Science* 113:3353-3354.

Holmes KC (2009) Actin in a twist. *Nature* 457:389-390.

Holmes KC (2010) 50 years of fiber diffraction. *J Struct Biol.* 170:184-191.

Holmes KC, Popp D, Gebhard W, and Kabsch W (1990) Atomic model of the actin filament. *Nature* 347:44-49.

Hotulainen P, and Hoogenraad CC (2010) Actin in dendritic spines: Connecting dynamics to function. *J Cell Biol* 189:619-629.

Hurley JH (1996) The sugar kinase/heat shock protein 70/actin superfamily: implications of conserved structure for mechanism. *Annu Rev Biophys Biomol Struct.* :25:137-162.

Hussey PJ, Hawkins TJ, Igarashi H, Kaloriti D, and Smertenko A (2002) The plant cytoskeleton: recent advances in the study of the plant microtubule-associated proteins MAP-65, MAP-190 and the Xenopus MAP215-like protein, MOR1. *Plant Mol. Biol.* 50:915-924.

Irobi E, Aguda AH, Larsson M, Guerin C, Yin HL, Burtnick LD, Blanchoin L, and Robinson RC (2004) Structural basis of actin sequestration by thymosin β4: implications for WH2 proteins. *EMBO J.* 23:3599-3608.

Isambert H, Venier P, Maggs AC, Fattoum A, Kassab R, Pantaloni D, and Carlier MF (1995) Flexibility of actin filaments derived from thermal fluctuations. Effect of bound nucleotide, phalloidin, and muscle regulatory proteins. *J Biol Chem.* 270:11437-11444.

Ito T, Narita A, Hirayama T, Taki M, Iyoshi S, Yamamoto Y, Maeda Y, and Oda T (2011) Human Spire Interacts with the Barbed End of the Actin Filament. *J. Mol. Biol.* 408:18-25.

Kabsch W (1993) Automatic processing of rotation diffraction data from crystals of initially unknown symmetry and cell constants. *J Appl Cryst*. 26:795-800.

Kabsch W, and Holmes KC (1995) Protein motifs 2. The actin fold. *FASEB J.* 9:167-174.

Kabsch W, Mannherz HG, Suck D, Pai EF, and Holmes KC (1990) Atomic structure of the actin: DNase I complex. *Nature* 347:37-44.

Kaksonen M, Toret CP, and Drubin DG (2006) Harnessing actin dynamics for clathrin-mediated endocytosis. *Nat. Rev. Mol. Cell Biol.* 7:404-414.

Kennedy SP, Warren SL, Forget BG, and Morrow JS (1991) Ankyrin binds to the 15th repetitive unit of erythroid and nonerythroid beta-spectrin. *J. Cell Biol.* 115:267-277.

Kerkhoff E (2006) Cellular functions of the Spir actin nucleation factors. *Trends Cell Biol.* 16:477-483.

Kerkhoff E (2010) Actin dynamics at intracellular membranes: The Spir/formin nucleator complex. *Eur. J. Cell Biol.* In press.

Kerkhoff E, Simpson JC, Leberfinger CB, Otto IM, Doerks T, Bork P, Rapp UR, Raabe T, and Pepperkok R (2001) The Spir actin organizers are involved in vesicle transport processes. *Curr. Biol.* 11:1963-1968.

Klenchin VA, Khaitlina SY, and Rayment I (2006) Crystal structure of polymerization-competent actin. *J. Mol. Biol.* 362:140-150.

Knight B, Laukaitis C, Akhtar N, Hotchin NA, Edlund M, and Horwitz AR (2000) Visualizing muscle cell migration in situ. *Curr. Biol.* 10:576-585.

Korn ED, Carlier MF, and Pantaloni D (1987) Actin polymerization and ATP hydrolysis. *Science* 238:638-644.

Kovar DR (2006) Molecular details of formin-mediated actin assembly. *Curr. Opin. Cell Biol*. 18:11-17.

Kovar DR, and Pollard TD (2004) Insertional assembly of actin filament barbed ends in association with formins produces piconewton forces. *Proc. Natl. Acad. Sci. USA* 101:14725-14730.

Krause M, Dent EW, Bear JE, Loureiro JJ, and Gertler FB (2003) Ena/VASP proteins: regulators of the actin cytoskeleton and cell migration. *Annu. Rev. Cell Dev. Biol*. 19:541-564.

Krause M, Leslie JD, Stewart M, Lafuente EM, Valderrama F, Jagannathan R, Strasser GA, Rubinson DA, Liu H, Way M, Yaffe MB, Boussiotis VA, and Gertler FB (2004) Lamellipodin, an Ena/VASP ligand, is implicated in the regulation of lamellipodial dynamics. *Dev. Cell* 7: 571-583.

Krishnan K, Holub O, Gratton E, Clayton AHA, Cody S, and Moens PDJ (2009) Profilin interaction with phosphatidylinositol (4,5)-bisphosphate destabilizes the membrane of giant unilamellar Vesicles. *Biophys. J.* 96:5112-5121.

Kuhnel K, Jarchau T, Wolf E, Schlichting I, Walter U, Wittinghofer A, and Strelkov SV (2004) The VASP tetramerization domain is a right-handed coiled coil based on a 15-residue repeat. *Proc. Natl. Acad. Sci. USA* 101:17027-17032.

Lai FP, Szczodrak M, Block J, Faix J, Breitsprecher D, Mannherz HG, Stradal TE, Dunn GA, Small JV, and Rottner K (2008) Arp2/3 complex interactions and actin network turnover in lamellipodia. *EMBO J.* 27:982-992.

Lappalainen P, Kessels MM, Cope, MJ, and Drubin DG (1998) The ADF homology (ADF-H) domain: a highly exploited actin-binding module. *Mol. Biol. Cell* 9:1951-1959.

Le Goff C, Laurent V, Le Bon K, Tanguy G, Couturier A, Le Goff X, and Le Guellec R (2006) pEg6, a SPIR family member, is a maternal gene encoding a vegetally localised mRNA in Xenopus embryos. *Biol. Cell* 98:697-708.

Leader B, Lim H, Carabatsos MJ, Harrington A, Ecsedy J, Pellman D, Maas R, and Leder P (2002) Formin-2, polyploidy, hypofertility and positioning of the meiotic spindle in mouse oocytes. *Nat. Cell Biol.* 4:921-928.

Lee SH, and Dominguez R (2010) Regulation of actin cytoskeleton dynamics in cells. *Mol. Cells* 29:311-325.

Lee SH, Kerff F, Chereau D, Ferron F, Klug A, and Dominguez R (2007) Structural basis for the actin-binding function of missing-in-metastasis. *Structure* 15:145-155.

Li F, and Higgs HN (2003) The mouse formin mDia1 is a potent actin nucleation factor regulated by autoinhibition. *Curr. Biol.* 13:1335-1340.

Li H, Guo F, Rubinstein B, and Li R (2008) Actin-driven chromosomal motility leads to symmetry breaking in mammalian meiotic oocytes. *Nature Cell Biol.* 10:1301-1308.

Liu R, Abreu-Blanco MT, Barry KC, Linardopoulou EV, Osborn GE, and Parkhurst SM (2009) Wash functions downstream of Rho and links linear and branched actin nucleation factors. *Development* 136:2849-2860.

Liverman AD, Cheng HC, Trosky JE, Leung DW, Yarbrough ML, Burdette DL, Rosen MK, and Orth K (2007) Arp2/3-independent assembly of actin by Vibrio type III effector VopL. *Proc. Natl. Acad. Sci. USA* 104:1711717122.

Lodish H, Berk A, Zipursky SL, Matsudaira P, Baltimore D, and Darnell JE (2000) Molecular Cell Biology. Section 18.1 The actin cytoskeleton. 4th ed. New York, WH Freeman and Co.

Makrides SC (1996) Strategies for achieving high-level expression of genes in *Escherichia coli*. *Microbiol. Rev.* 60:512-538.

Manor U, and Kachar B (2008) Dynamic length regulation of sensory stereocilia. *Semin. Cell Dev. Biol*. 19:502-510.

Manseau LJ, and Schupbach T (1989) Cappuccino and spire: two unique maternal-effect loci required for both the anteroposterior and dorsoventral patterns of the *Drosophila* embryo. *Genes Dev*. 3:1437-1452.

Mattila PK, and Lappalainen P (2008) Filopodia: molecular architecture and cellular functions. *Nat. Rev. Mol. Cell Biol*. 9:446-454.

McGough AM, Staiger CJ, Min JK, and Simonetti KD (2003) The gelsolin family of actin regulatory proteins: Modular structures, versatile functions. *FEBS Lett.* 552:75-81.

McRee DE (1999) XtalView/Xfit - A versatile program for manipulating atomic coordinates and electron density. *J. Struc. Biol.* 125:156-165.

Mees A, Rock R, Ciccarelli FD, Leberfinger CB, Borawski JM, Bork P, Wiese S, Gessler M, and Kerkhoff E (2005) Very-KIND is a novel nervous system specific guanine nucleotide exchange factor for Ras GTPases. *Gene Expr. Patterns* 6:79-85.

Meszaros B, Tompa P, Simon I, and Dosztanyi Z (2007) Molecular principles of the interactions of disordered proteins. *J. Mol. Biol.* 372:549-561.

Michie KA, and Löwe J (2006) Dynamic filaments of the bacterial cytoskeleton. *Annu. Rev. Biochem.* 75:467-492.

Misra S, and Hurley JH (1999) Crystal structure of a phosphatidylinositol 3-phosphate-specific membrane-targeting motif, the FYVE domain of Vps27p. *Cell* 97:657-666.

Morel E, Parton RG, and Gruenberg J (2009) Annexin A2-dependent polymerization of actin mediates endosome biogenesis. *Dev. Cell* 16:445-457.

Muller J, Oma Y, Vallar L, Friederich E, Poch O, and Winsor B (2005) Sequence and comparative genomic analysis of actin-related proteins. *Mol. Biol. Cell* 16:5736-5748.

Mullins RD, Heuser JA, and Pollard TD (1998) The interaction of Arp2/3 complex with actin: nucleation, high affinity pointed end capping, and formation of branching networks of filaments. Proc. Natl. Acad. Sci. USA 95:6181-6186.

Mullins RD, and Pollard TD (1999) Rho-family GTPases require the Arp2/3 complex to stimulate actin polymerization in *Acanthamoeba* extracts. *Curr. Biol*. 9:405-415.

Naumanen P, Lappalainen P, and Hotulainen P. (2008) Mechanisms of actin stress fiber assembly. *J. Microsc.* 231:446-454.

Nolen BJ, and Pollard TD (2007) Insights into the influence of nucleotides on actin family proteins from seven structures of Arp2/3 complex. *Mol. Cell* 26:449-457.

Oda T, Iwasa M, Aihara T, Maeda Y, and Narita A (2009) The nature of the globular- to fibrous-actin transition. *Nature* 457:441-445.

Okada K, Bartolini F, Deaconescu AM, Moseley JB, Dogic Z, Grigorieff N, Gundersen GG, and Goode BL (2010) Adenomatous polyposis coli protein nucleates actin assembly and synergizes with the formin mDia1. *J. Cell Biol.* 189:1087-1096.

Ostermeier C, and Brunger AT (1999) Structural basis of Rab effector specificity: crystal structure of the small G protein Rab3A complexed with the effector domain of rabphilin-3A. *Cell* 96:363-374.

Otomo T, Tomchick RR, Otomo C, Panchal SC, Machius M, and Rosen MK (2005) Structural Basis of Actin Filament Nucleation and Processive Capping by a Formin Homology 2 Domain. *Nature* 433:488-494.

Otterbein LR, Graceffa P, and Dominguez R (2001) The crystal structure of uncomplexed actin in the ADP state. *Science* 293:708-711.

Otto JJ (1994) Actin-bundling proteins. *Curr. Opin. Cell Biol.* 6:105-109.

Otto IM, Raabe T, Rennefahrt UE, Bork P, Rapp UR, and Kerkhoff E (2000) The p150-Spir protein provides a link between c-Jun N-terminal kinase function and actin reorganization. *Curr. Biol.* 10:345-348.

Pantaloni D, and Carlier MF (1993) How profilin promotes actin filament assembly in the presence of thymosin beta 4. *Cell* 75:1007-1014.

Parent CA (2004) Making all the right moves: chemotaxis in neutrophils and Dictyostelium. *Curr. Opin. Cell Biol.* 16:4-13.

Pascual J, Castresana J, and Saraste M (1997) Evolution of the spectrin repeat. *BioEssays* 19:811-817.

Paunola E, Mattila PK, and Lappalainen P (2002) WH2 domain: a small, versatile adapter for actin monomers. *FEBS Lett.* 513:92-97.

Pollard TD (1986) Rate constants for the reactions of ATP- and ADP-actin with the ends of actin filaments. J. Cell Biol. 103:2747-2754.

Pollard TD (2007) Regulation of Actin Filament Assembly by Arp2/3 Complex and Formins. *Annu. Rev. Biophys. Biomol. Struct.* 36:451-477.

Pollard TD, and Borisy GG (2003) Cellular motility driven by assembly and disassembly of actin filaments. *Cell* 112:453-465.

Pring M, Weber A, and Bubb M (1992) Profilin-actin complexes directly elongate actin filaments at the barbed end. *Biochemistry* 31:1827-1836.

Pruyne D, Evangelista M, Yang C, Bi E, Zigmond S, Bretscher A, and Boone C (2002) Role of formins in actin assembly: nucleation and barbed-end association. *Science* 297:612-615.

Qualmann B, and Kessels MM (2009) New players in actin polymerization-WH2-domain-containing actin nucleators. *Trends Cell Biol*. 19:276-285.

Quinlan ME, Heuser JE, Kerkhoff E, and Mullins RD (2005) *Drosophila* Spire is an actin nucleation factor. *Nature* 433:382-388.

Quinlan ME, Hilgert S, Bedrossian A, Mullins RD, and Kerkhoff E (2007) Regulatory interactions between two actin nucleators, Spire and Cappuccino. *J. Cell Biol.* 179:117-128.

Rafelski SM, and Theriot JA. (2004) Crawling toward a unified model of cell mobility: spatial and temporal regulation of actin dynamics. *Annu. Rev. Biochem.* 73:209-239.

Rando TA (2001) The dystrophin-glycoprotein complex, cellular signaling, and the regulation of cell survival in the muscular dystrophies. *Muscle Nerve* 24:1575-1594.

Rebowski G, Boczkowska M, Hayes DB, Guo L, Irving TC, and Dominguez R (2008) X-ray scattering study of actin polymerization nuclei assembled by tandem W domains. *Proc. Natl. Acad. Sci. USA* 105:10785-10790.

Rehm T, Huber R, and Holak TA (2002) Application of NMR in structural proteomics: screening for proteins amenable to structural analysis. *Structure* 10:1613-1618.

Reisler E, and Egelman EH (2007) Actin's structure and function: What we still do not understand. *J. Biol. Chem.* 282:36133-36137.

Renault L, Bugyi B, and Carlier MF (2008) Spire and Cordon-bleu: multifunctional regulators of actin dynamics. *Trends Cell Biol.* 18:494-504.

Ridley AJ, Schwartz MA, Burridge K, Firtel RA, Ginsberg M.H, Borisy G, Parsons JT, and Horwitz AR (2003) Cell Migration: Integrating signals from front to back. *Science* 302:1704-1709.

Robinson RC, Turbedsky K, Kaiser DA, Higgs H, Marchand JB, Choe S, and Pollard TD (2001) Crystal structure of Arp2/3 complex. *Science* 294:1679-1684.

Rosales-Nieves AE, Johndrow JE, Keller LC, Magie CR, Pinto-Santini DM, and Parkhurst SM (2006) Coordination of microtubule and microfilament dynamics by *Drosophila* Rho1, Spire and Cappuccino. *Nat. Cell Biol.* 8:367-376.

Rouiller I, Xu XP, Amann KJ, Egile C, Nickell S, Nicastro D, Li R, Pollard TD, Volkmann N, and Hanein D (2008) The structural basis of actin filament branching by the Arp2/3 complex. *J. Cell Biol.* 180:887-895.

Rould MA, Wan Q, Joel PB, Lowey S, and Trybus KM (2006) Crystal structures of expressed non-polymerizable monomeric actin in the ADP and ATP states. *J. Biol. Chem.* 281:31909-31919.

Sablin EP, Kull FJ, Cooke R, Vale RD, and Fletterick RJ (1996) Crystal structure of the motor domain of the kinesin-related motor ncd. *Nature* 380:555-559.

Sagot I, Rodal AA, Moseley J, Goode BL, and Pellman D (2002) An actin nucleation mechanism mediated by Bni1 and profilin. *Nat. Cell Biol.* 4:626-631.

Schagger H, and von Jagow G (1987) Tricine-sodium dodecyl sulfate-polyacrylamide gel electrophoresis for the separation of proteins in the range from 1 to 100 kDa. *Anal. Biochem.* 166:368-379.

Schuh M, and Ellenberg J (2008) A new model for asymmetric spindle positioning in mouse oocytes. *Curr. Biol.* 18:1986-1992.

Schumacher N, Borawski JM, Leberfinger CB, Gessler M, and Kerkhoff E (2004) Overlapping expression pattern of the actin organizers Spir-1 and formin-2 in the developing mouse nervous system and the adult brain. *Gene Expr. Patterns* 4:249-255.

Sellers JR (2000) Myosins: a diverse superfamily. *Biochim. Biophys. Acta* 1496:3-22.

Sept D, and McCammon JA (2001) Thermodynamics and kinetics of actin filament nucleation. *Biophys. J.* 81:667-674.

Shih YL, and Rothfield L (2006) The bacterial cytoskeleton. *Microbiol. Mol. Biol. Rev.* 70:729-754.

Sonnichsen B, De Renzis S, Nielsen E, Rietdorf J, and Zerial M (2000) Distinct membrane domains on endosomes in the recycling pathway visualized by multicolor imaging of Rab4, Rab5, and Rab11. *J. Cell Biol.* 149:901-914.

Stenzel N, Fetzer CP, Heumann R, and Erdmann KS (2009) PDZ-domain-directed basolateral targeting of the peripheral membrane protein FRMPD2 in epithelial cells. *J Cell Sci.* 122:3374-3384.

Straub FB (1942) in Studies Int med Chem Univ Szeged (ed Szent-Györgi). 2:3-15.

Svergun DI (1992) Determination of the regularization parameter in indirect-transform methods using perceptual criteria. *J. Appl. Crystallogr.* 25:495-503.

Svitkina TM, Verkhovsky AB, McQuade KM, and Borisy GG (1997) Analysis of the actin-myosin II system in fish epidermal keratocytes: mechanis of cell body translocation. *J. Cell Biol.* 139:397-415.

Tam VC, Serruto D, Dziejman M, Brieher W, and Mekalanos JJ (2007) A type III secretion system in Vibrio cholerae translocates a formin/spire hybridlike actin nucleator to promote intestinal colonization. *Cell Host Microbe*. 1:95-107.

Tilney LG, Bonder EM, Coluccio LM, and Mooseker MS (1983) Actin from Thyone sperm assembles on only one end of an actin filament: a behavior regulated by profilin. *J. Cell Biol.* 97:112-124.

Vale RD (1996) Switches, latches, and levers: common themes of G proteins and molecular motors. *J. Cell Biol.* 135:291-302.

van den Ent F, Amos LA, and Lowe J (2001) Prokaryotic origin of the actin cytoskeleton. *Nature* 413:39-44.

Wansink DG, Peters W, Schaafsma I, Sutmuller RP, Oerlemans F, Adema GJ, Wieringa B, van der Zee CE, and Hendriks W (2004) Mild impairment of motor nerve repair in mice lacking PTP-BL tyrosine phosphatase activity. *Physiol. Genomics* 19:50-60.

Watanabe N, Madaule P, Reid T, Ishizaki T, Watanabe G, Kakizuka A, Saito Y, Nakao K, Jockusch BM, and Narumiya S (1997) p140mDia, a mammalian homolog of *Drosophila* diaphanous, is a target protein for Rho small GTPase and is a ligand for profilin. *EMBO J.* 16:3044-3056.

Wegner A (1976) Head to tail polymerization of actin. *J. Mol. Biol.* 108:139-150.

Welch MD, and Mullins RD (2002) Cellular control of actin nucleation. *Annu. Rev. Cell Dev. Biol*. 18:247-288.

Wellington A, Emmons S, James B, Calley J, Grover M, Tolias P, and Manseau L (1999) Spire contains actin binding domains and is related to ascidian posterior end mark-5. *Development* 126:5267-5274.

Winder SJ (2003) Structural insights into actin binding, branching, and bundling proteins. *Curr. Opin. Cell Biol.* 15:14-22.

Winder SJ, and Ayscough KR (2005) Actin binding proteins. *J. Cell Sci.*118:651-654

Wüthrich K (1986) NMR of proteins and nucleic acids. *John Wiley & Sons, New York.*

Xu Y, Moseley J, Sagot I, Poy F, Pellman D, Goode BL, and Eck MJ (2004) Crystal Structures of a formin homology-2 domain reveal a tethered dimer architecture. *Cell* 116:711-723.

Zheng X, Diraviyam K, and Sept D (2007) Nucleotide effects on the structure and dynamics of actin. *Biophys J.* 93:1277-1283.

Zigmond SH (2004) Formin induced nucleation of actin filaments. *Curr. Opin. Cell Biol.* 16: 99-105.

Zuchero JB, Coutts AS, Quinlan ME, Thangue NB, and Mullins RD (2009) p53-cofactor JMY is a multifunctional actin nucleation factor. *Nat. Cell Biol.* 11:451-459.

Technische Universität München

Max-Planck-Institut für Biochemie

Abteilung Strukturforschung

Biologische NMR-Arbeitsgruppe

Molecular architecture of Spire-actin complexes and its implication for actin filament assembly

Anna Magdalena Ducka